5-1-2018

Fatigue Investigation of Slit Rib-to-floor Beam Connections in Steel Orthotropic Bridge Decks

Jayne Marks
Lehigh University, jayne.marks347@gmail.com

Fatigue Investigation of Slit Rib-to-floor Beam Connections in Steel Orthotropic Bridge Decks

by

Jayne Marks

A Thesis

Presented to the Graduate and Research Committee

of Lehigh University

in Candidacy for the Degree of

Master of Science

in

Structural Engineering

Lehigh University

May 2018

This thesis is accepted and approved in partial fulfillment of the requirements for the Master of Science.

_____
Date

_____
Dr. Richard Sause
Thesis Advisor

_____
Dr. Panayiotis Diplas
Chairperson of Department
Civil and Environmental Engineering

ACKNOWLEDGEMENTS

The author would like to express her sincere gratitude to her thesis advisor, Dr. Richard Sause, for his support, time, and knowledge which went into this research. The author thanks Mr. Ian Hodgson, Mr. Joe Saunders, and Ms. Yixin Chen for their numerous contributions throughout the course of her graduate education. The author would also like to thank Mr. Peter Bryan for his technical support, Mr. Darrick Fritchman for his guidance and assistance, and the ATLSS lab staff for their hard work. The author would like to acknowledge the contributions of Dr. Sougata Roy, Ms. Katie Kitner, and Mr. Soham Mukherjee to this project. The author gratefully acknowledges the funding provided by the sponsor of her research project, Lehigh University, and the FHWA. Finally, the author would like to thank her family and friends for their continued support.

TABLE OF CONTENTS

LIST OF TABLES

TABLE OF FIGURES

ABSTRACT

The steel orthotropic bridge deck (SOBD) is a bridge deck system which consists of longitudinal open or closed ribs that pass through transverse floor beams with a continuous steel deck plate on top. All of these components are joined using welded connections which can be costly to fabricate and prone to fatigue cracks. The rib-to-floor beam (RFB) connection in an SOBD is labor intensive and fatigue sensitive. In the past, the RFB connection has either been a fully fitted connection or a connection with an extended cut-out which is larger than the opening in the floor beam web for the rib to pass through. A third RFB detail that includes an additional opening below the rib bottom, which is not an extension of the rib opening, has been proposed and is studied herein. This connection, termed a "slit RFB connection," is similar to the fitted connection with closed, U-shaped ribs passing continuously through matching openings in the floor beam webs, but an additional opening contained entirely within the floor beam web allows for relatively unrestrained out-of-plane rib rotation. The slit RFB connection has not been used or studied previously, and shows potential for efficient, automated fabrication and good fatigue performance.

This study investigated the slit RFB connection potential for automated fabrication as well as fatigue performance under various fatigue loading scenarios and SOBD configurations. The slit RFB connection is amenable to automated fabrication since it does not include an extended cut-out with complex welded-joint preparation, weld terminations, or internal stiffening. The slit RFB connection studied uses only fillet welds for the connection which require no labor intensive joint preparation. Since the slit is located

entirely within the floor beam web, the RFB fillet weld is uninterrupted around the bottom of the rib and can be made robotically.

A finite element analysis study was performed to evaluate the stress response and fatigue performance of the slit RFB connection under multiple fatigue loading scenarios for two different floor beam restraint conditions: independent and restrained/supported. The study showed that the stress response of the connection is highly dependent on the in-plane shear carried by the floor beam. When the slit RFB connection was studied with an independent floor beam (which has no vertical or horizontal restraint) high tension stresses developed along the edges of the slit. These stresses can be lowered slightly by changing the slit geometry, floor beam depth, or floor beam thickness, however, an unreasonably deep floor beam may be needed to ensure good fatigue performance.

When an SOBD is used in a bridge deck replacement project, the floor beam bottom flange is usually restrained/supported by a transverse structural member such as a truss, and the shear force carried by the floor beam web is significantly reduced. This reduction in shear force reduces the large tension stresses that develop at the slit edge to levels that may fall below the constant amplitude fatigue limit. In this case, large tension and compression stress concentrations still exist at the edge of the slit due to local deformation of the slit from the reactions on the floor beam web from shear forces (shear flow) in the rib walls. The largest magnitude stresses are compression stresses which are expected to contribute to fatigue damage only if tension stresses develop at the same location under an alternate fatigue load position. The stresses that develop at the weld toes on the floor beam web face and the rib wall are low.

The stresses from floor beam web shear and from reacting the shear forces in the rib walls (known as in-plane behavior) are the dominating stresses for the slit RFB connection. The stresses from rib rotation (due to primary bending in the rib when wheel loads are in the span between floor beams, known as out-of-plane behavior) are not significant since the slit in the floor beam web allows the rib to rotate relatively freely. Behavior from in-plane floor beam shear and reaction rib wall shear forces are the main causes of stress at the edges of the slit, even when the loading is out-of-plane.

The conclusions of this study are:

(1) The slit RFB connection appears to be amenable to automated fabrication.

(2) For an independent floor beam (which has no vertical support within its span), the stress response of the slit RFB connection is highly dependent on the magnitude of the in-plane shear force carried by the floor beam; large tension stresses may develop along the slit edge, and the fatigue performance may not be acceptable.

(3) When the floor beam is supported by a transverse structural member, the stress response of the slit RFB connection is dominated by reaction forces on the floor beam web from shear forces in the rib walls; the resulting stresses along the slit edge are compressive, and are not excessive, and good fatigue performance is anticipated.

(4) The slit in the floor beam web allows the rib to rotate with relative freedom, resulting in small stresses in the slit RFB connection from out-of-plane deformation of the floor beam web; stresses at the fillet weld toes are relatively small.

(5) The slit RFB connection has the potential for good fatigue performance when used in deck replacement projects, when the floor beam is restrained/supported by existing transverse structural members of the bridge.

1. INTRODUCTION

1.1 Background

The steel orthotropic bridge deck (SOBD) is a bridge deck system that has been utilized in many modern bridges. An SOBD consists of longitudinal open or closed ribs that pass through transverse floor beams with a continuous steel deck plate on top. All of these components are joined using welded connections. The SOBD allows the bridge deck to be integral with the supporting bridge superstructure, resulting in increased rigidity and decreased material use. It also is a redundant bridge deck system made almost entirely of steel. An SOBD is often lighter, is easier to construct in the field due to its modular nature, and provides a longer service life than other traditional bridge deck systems. These features make it a popular choice for long-span, movable, temporary, cable-stayed, and suspension bridges. Time dependent deterioration of bridge decks is one of the challenges of maintaining the highway system in the United States; if adequately designed and fabricated, the SOBD is the only bridge deck system likely to provide a service life exceeding 100 years (Fisher and Roy 2010).

Despite the potential advantages of the SOBD, one of the major challenges to increased use of SOBDs in the United States has been the relatively high initial cost of fabrication. This is due, in part, to the requirements that are necessary to achieve the desired fatigue resistance of the various welded connections in the deck. The most labor intensive and fatigue sensitive connection of an SOBD is the rib-to-floor beam (RFB) connection. In the past, the RFB connection has either been a fully fitted connection as seen in Figure 1 or a connection with an extended cut-out located below the rib bottom as seen in Figure 2.

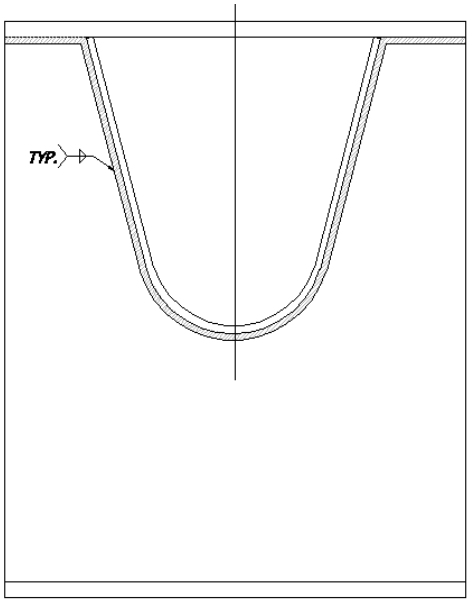

Figure 1. Illustration. Fitted RFB connection.

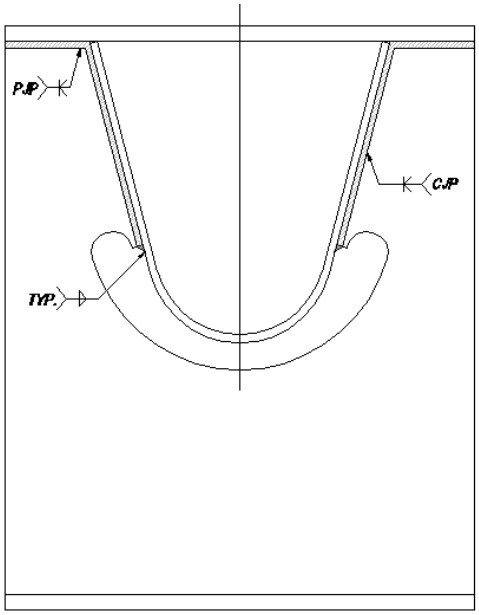

Figure 2. Illustration. Extended cut-out RFB connection.

The decision to use either a fitted RFB connection or an extended cut-out RFB connection often depends on the demand for rotation of the rib relative to the floor beam, which causes out-of-plane deformation of the floor beam web. The relative rotational demand on the RFB connection depends on the rib span (distance between the floor beams), rib depth, and restraint of the floor beam web from the floor beam bottom flange which may be restrained by the bridge superstructure (see Figure 3). The stresses in the RFB connection from out-of-plane deformation of the floor beam web are affected by the floor beam web thickness, the floor beam depth, and the floor beam support/restraint conditions. An RFB connection with an extended cut-out below the rib accommodates relative rib rotation much more freely than a fully fitted RFB connection due to the significantly increased flexibility of the connection at the cut-out. For this reason, RFB connections with cut-outs are often used for floor beams that are supported/restrained; for example, when the SOBD is used as a replacement deck for a bridge with existing transverse superstructure members (such as trusses), and the SOBD floor beam is essentially a diaphragm attached to the top of the existing member (Figure 3). The increased flexibility of an RFB connection with a cut-out makes up for the reduced flexibility of the SOBD floor beam due to the restraint from the attached transverse superstructure member.

Figure 3. Photo. SOBD floor beam attached to transverse truss. Source: Joseph Saunders.

To achieve acceptable fatigue performance, the extended cut-out is often designed with complex geometry and a tangential termination on the rib wall (see Figure 4). The extended cut-out termination often requires expensive fabrication, including: significant joint preparation; complete joint penetration welds near the cut-out termination; inspection; grinding of the cut-out to fit the as-fabricated rib geometry; and significant grinding of the cut-out termination after welding to achieve a smooth termination (Marks, et al. 2018).

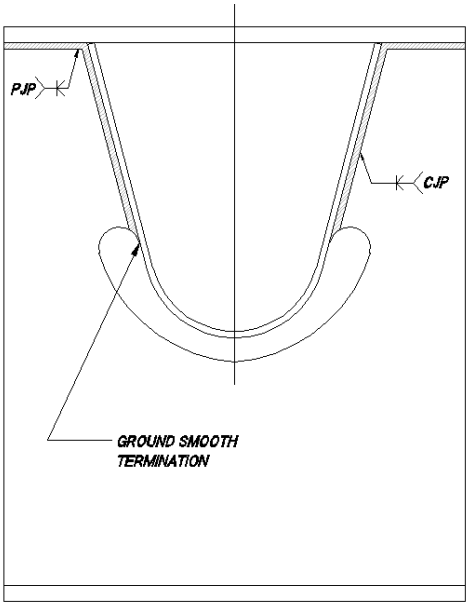

Figure 4. Illustration. RFB connection with an extended cut-out and ground smooth weld termination.

If the termination of the extended cut-out is designed as a fillet welded connection, a perpendicular termination on the rib wall is used, and an internal bulkhead or stiffeners may be needed to achieve adequate fatigue performance (Figure 5). Including this internal stiffening adds another step to the fabrication process, which is difficult to automate. An extended cut-out also eliminates the potential for continuous, automated fillet-welding of the RFB connection, because the extended cut-out interrupts the RFB weld near the bottom of the rib. In summary, the fabrication requirements for an RFB with an extended cut-out are labor intensive and less amenable to automated fabrication.

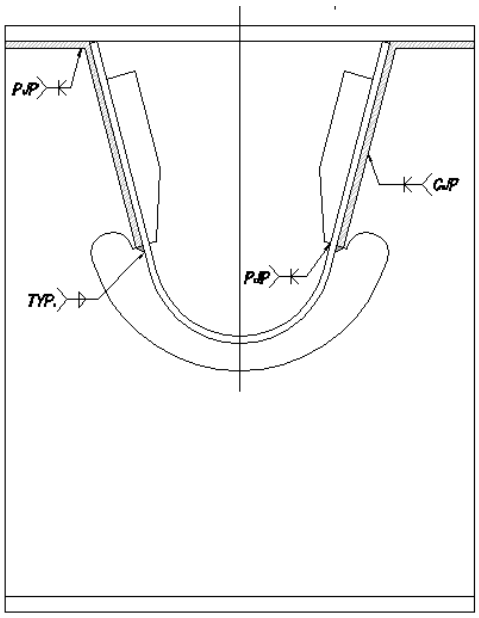

Figure 5. Illustration. RFB connection with an extended cut-out and internal stiffener.

To provide the potential for efficient, automated fabrication of an RFB connection that can accommodate relative rib rotation when conditions do not permit use of the fitted RFB connection, an RFB connection has been studied that includes an additional opening below the rib bottom, which is not an extension of the rib opening in the floor beam web (see Figure 6). This type of RFB connection has not been used previously and is based on an RFB connection suggested in the HNTB report titled "Cost-Effective Orthotropic Bridge Decks (An Evaluation of Optional Welding Processes)" (HNTB 2015). Termed a "slit RFB connection", this connection is similar to the fitted connection with closed, U-shaped ribs passing continuously through matching openings in the floor beam web. The only difference from the fitted connection is the additional slit which is located entirely within the floor beam web below the rib.

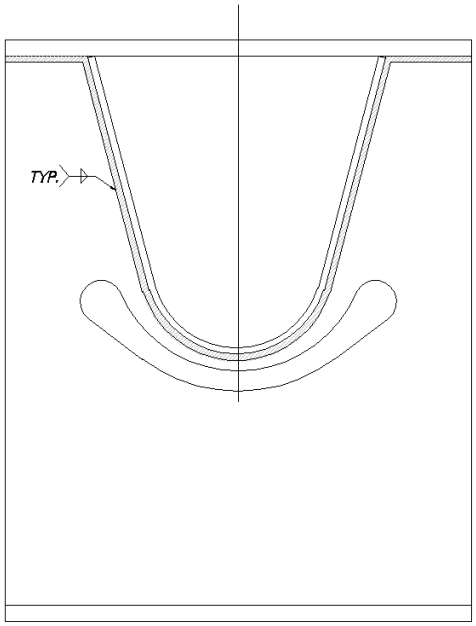

Figure 6. Illustration. Slit RFB connection.

The slit RFB connection studied has fillet welds for the entire connection which do not require labor intensive joint preparation. Because the slit is located entirely within the floor beam web, the RFB fillet weld is uninterrupted around the bottom of the rib and can be made robotically while the deck panel is in the inverted position as shown in Figure 7 and Figure 8. Since the ribs are welded to the deck plate in the inverted position, welding the RFB connection in this position reduces the number of times the panel needs to be rotated during fabrication.

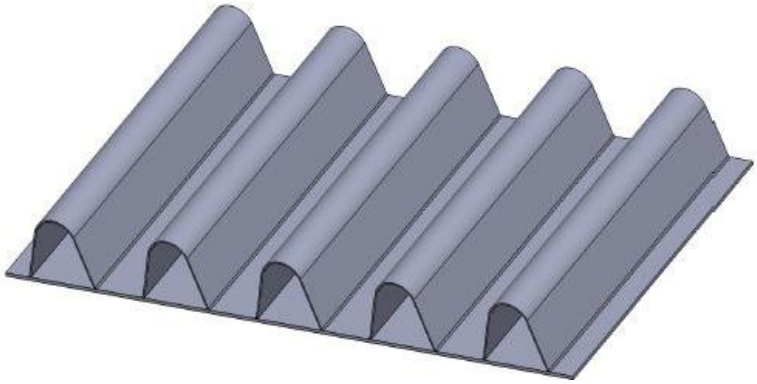

Figure 7. Illustration. Assembled rib-deck panel in the inverted position.

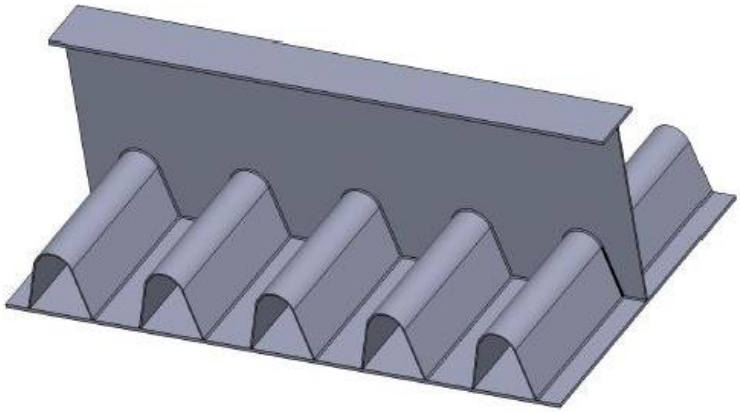

Figure 8. Illustration. Fitting of the floor beam to the assembled rib-deck panel in the inverted position.

Good fit-up between the assembled rib-deck panel and the floor beam web is necessary for the robotic welding of both the fitted RFB connection and the slit RFB connection and to ensure good fatigue performance. The fillet welds leave a small strip of the rib wall plate surface along the RFB connection unfused by the weld process (see Figure 9). The depth of this lack-of-fusion (LOF) strip is controlled by the fit-up gap between the rib and the floor beam web. The width of this LOF strip is controlled by the penetration of the weld process. At the edge of the LOF area, where it meets the weld root, weld root discontinuities or inclusions will occur, which may lead to cracking from the weld root.

The characteristics of these weld root discontinuities may depend on the fit-up gap and/or the width of the LOF strip.

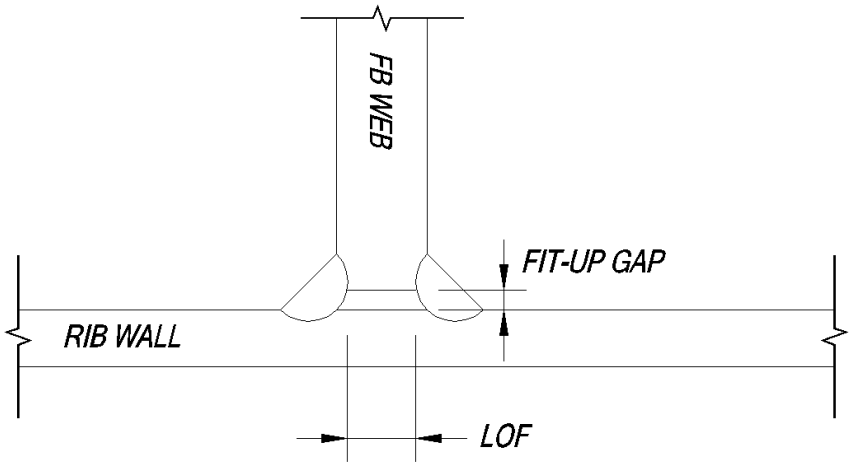

Figure 9. Illustration. Fit-up gap and lack-of-fusion (LOF) at RFB connection.

In the past, tight fit-up (i.e., a small fit-up gap) was difficult to achieve because the as-fabricated profile of the assembled rib-deck panel may differ significantly from the design drawings due to the process used to form the ribs, the fit-up and placement of the ribs on the deck plate, and/or any distortion of the assembled rib-deck panel due to welding of the ribs to the deck plate. However, using automated measuring techniques, the as-fabricated profile of the assembled rib-deck panel can be measured and automatically exchanged with an automated cutting machine, which can match cut the floor beam web to fit the measured rib-deck profile. The same cutting machine can also be used to cut the slits into the floor beam web. This automated process eliminates significant grinding that would be otherwise needed to ensure tight fit-up of the floor beam web to the rib-deck panel. The slit RFB connection has no internal bulkheads or stiffeners, further increasing the potential for automated fabrication of the slit RFB connection.

Fatigue cracks can initiate at the edge of the slit, as the cut-out geometry creates stress concentrations in the floor beam web. The stresses from the concentrations due to the slit geometry should be assessed using the relevant fatigue category. To achieve AASHTO Fatigue Category A, some grinding of the slit edge is necessary to reach a ground "smooth" condition based on AWS D1.5 as specified in the seventh edition of the AASHTO LRFD Bridge Design Specifications (henceforth referred to as the AASHTO BDS) (AASHTO 2016). If the edge of the slit is not ground "smooth", micro-discontinuities at the cut-out edge can have an adverse effect on the fatigue resistance.

Under live load, fatigue-critical stresses can develop in the slit RFB connection at the weld toes along the rib wall and the floor beam web where the critical stresses are the stresses perpendicular to the weld toes. In addition, stresses tangent to the weld root are of concern, although they may not be fatigue-critical. According to the AASHTO BDS, the weld toes are classified as a Fatigue Category C detail with a constant amplitude fatigue limit (CAFL) of 10 ksi (AASHTO 2016). The weld root under stresses tangent to the root appears to be consistent with an AASHTO Category B fatigue detail with a CAFL of 16 ksi, similar to the root of the web-to-flange weld of a steel plate girder (AASHTO 2016).

Results from this study, given in this thesis, show that the slit RFB connection, with appropriate geometry, floor beam web thickness, floor beam depth, and floor beam support/restraint conditions, can achieve adequate fatigue resistance using the appropriate AASHTO fatigue category described above. The slit RFB connection is amenable to automated fabrication since it does not include an extended cut-out with complex welded-

joint preparation or internal stiffening, and it has potential for continuous, automated fillet-welding.

1.2 Objectives

The objectives of this work are:

(1) Determine stress response of slit RFB connections for various fatigue loading scenarios and various SOBD configurations using finite element analysis (FEA);

(2) Study how various slit geometries affect the stress response and expected fatigue performance of slit RFB connections using FEA;

(3) Assess expected fatigue performance of slit RFB connections using the appropriate AASHTO fatigue categories;

1.3 Approach

Initial slit geometries were developed to study the behavior of the slit RFB connection. Multi-level three dimensional (3D) linear elastic parametric FEA were conducted on a simple steel bridge superstructure sub-assembly with an SOBD which has the slit RFB connections. The models of the SOBD were subjected to fatigue loading scenarios based on the AASHTO BDS. The fatigue load takes the form of the rear tandem axle of the fatigue truck (AASHTO 2016). The stress response of the slit RFB connection was studied under different longitudinal and transverse positions of the tandem axle for various SOBD configurations and slit geometries. The most critically stressed locations in the slit RFB connection were determined for critical load locations, and the stresses were used to evaluate the connection fatigue performance.

2. FINITE ELEMENT ANALYSIS PROCEDURE

2.1 Purpose of Finite Element Analysis

To evaluate the stresses and associated fatigue performance of the slit RFB connection, three-dimensional (3D) linear elastic finite element analyses (FEA) were performed using ABAQUS, a commercially available software produced by Dassault Systèmes (Dassault Systemes Simulia Corp. 2016). These analyses were performed to better understand the stress and deformation response, to evaluate the potential for favorable fatigue performance, and to identify critical loading conditions and fatigue-critical stress locations for the slit RFB connection.

2.2 Plate Girder Model

The FEA were performed using a model of an SOBD known as the Plate Girder (PG) model. The PG model was developed based on an existing FEA model of a movable lift bridge with an SOBD to ensure that the SOBD had reasonable properties. The existing FEA model of the SOBD and movable lift bridge was significantly simplified in developing the PG model to reduce the modeling effort as SOBD design parameters were changed and to decrease computation time.

2.2.1 Movable Lift Bridge

In previous studies of RFB connections in SOBDs (Mukherjee 2016, Kitner 2016), three levels of FEA models of an existing movable lift bridge with an SOBD, consisting of one global model and two submodels, were created as shown in Figure 10. The global model spanned 324 feet, and included three box girders, twenty-seven floor beams with

uniform depth, thickness, and spacing, and forty-six U-shaped ribs with fitted RFB connections. The dimensions of the ribs and RFB connections are shown in Figure 11, which were the dimensions used in the moveable lift bridge. The center-to-center spacing of the floor beams was 11 feet, 9 inches. This model was used to determine the most critically stressed RFB connection in the lift bridge SOBD and to determine a critical position of the rear tandem axle of the AASHTO fatigue truck that would produce fatigue-critical stresses in the critical RFB connection. A critical position of the load was defined as a longitudinal and transverse location of the tandem axle which resulted in large stresses normal to the weld toe of the critical RFB connection in the center floor beam of the SOBD; the stresses normal to the weld toe on the web and the weld toe on the rib wall were considered. This load position (defined as L1-T29 by Mukherjee 2016) has the rear tandem axle centered in the longitudinal direction on the center floor beam and positioned transversely near the box girder web as shown in Figure 12 and Figure 13.

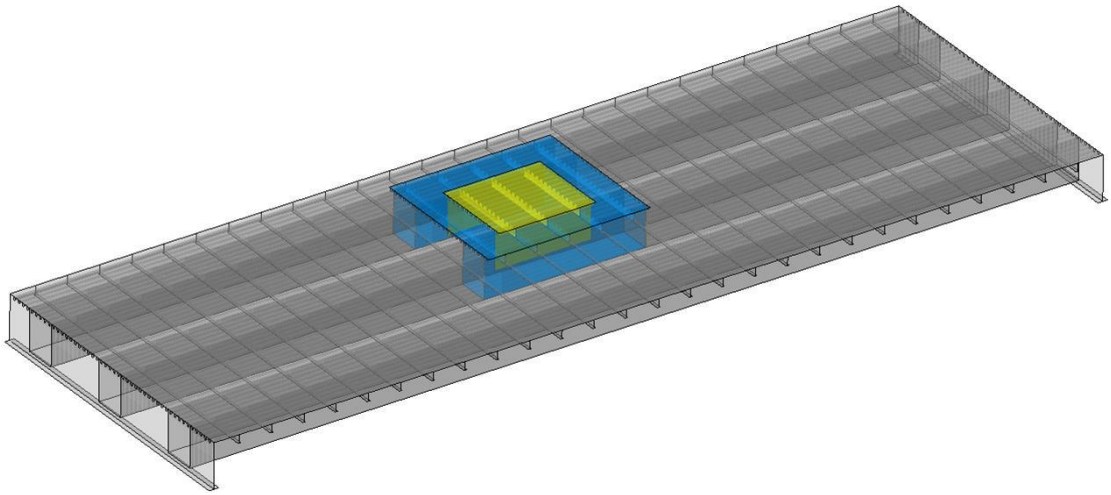

Figure 10. Illustration. Global model (grey), larger submodel (blue) and smaller submodel (yellow) of movable lift bridge (adapted from Kitner 2016).

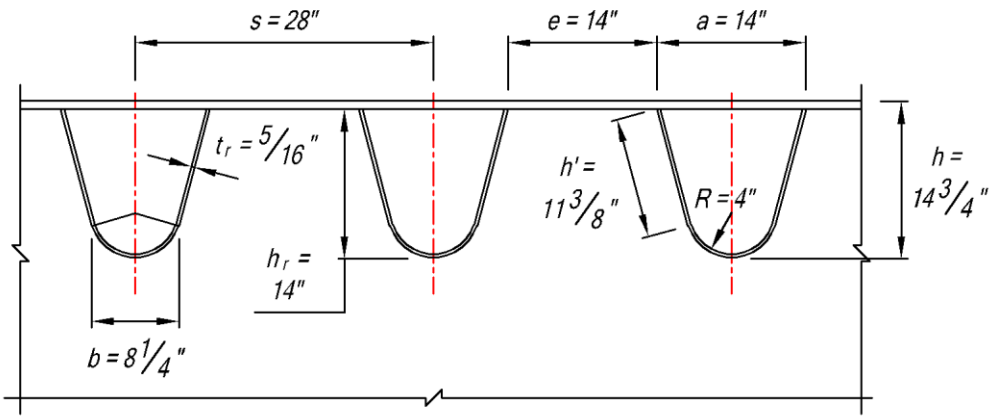

Figure 11. Illustration. Dimensions of rib-to-floor beam connection of movable lift bridge (adapted from Kitner 2016).

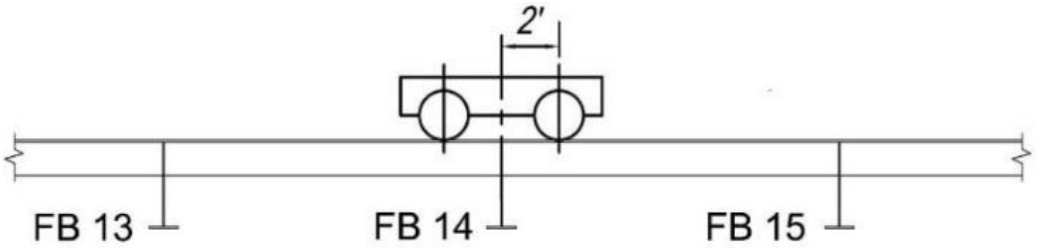

Figure 12. Illustration. Longitudinal location of rear tandem axle, known as L1, which produced critical stresses in movable lift bridge SOBD model (adapted from Mukherjee 2016).

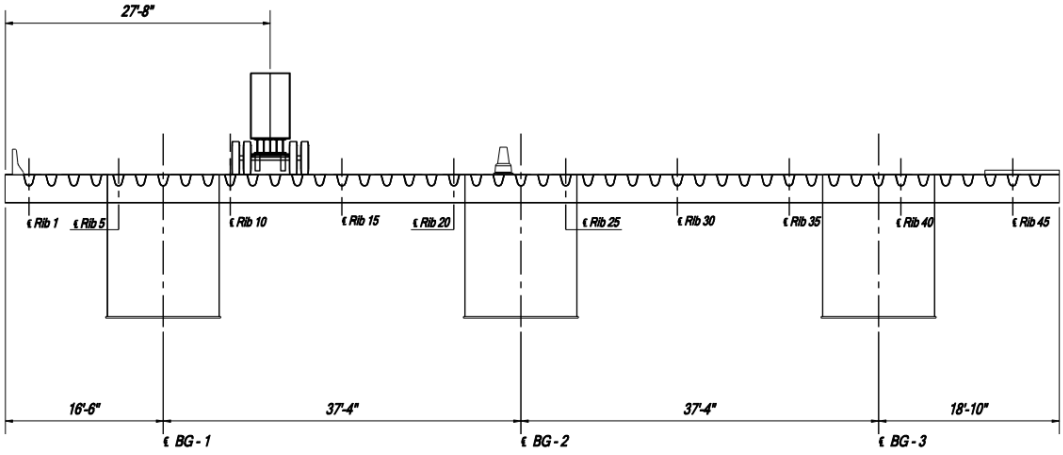

Figure 13. Illustration. Transverse location of rear tandem axle, known as T29, which produced critical stresses in movable lift bridge SOBD model (adapted from Mukherjee 2016).

The FEA model of the movable lift bridge was modified to produce a new global model, the Plate Girder model (the PG model), which was used for all further FEA of the slit RFB connection. The SOBD geometry shown in Figure 11 formed the basis for the PG model to ensure that the FEA model used to study the RFB connections was representative of an actual SOBD that was designed according to appropriate requirements for an existing bridge (e.g., AASHTO 2016).

For FEA that focused on critical in-plane response at the RFB connection, a longitudinal position of the rear tandem axle, similar to the L1 position, was used in the PG model with the tandem centered on the middle floor beam. A transverse position of the rear tandem axle, similar to the T29 position, was often used with one half of the tandem centered between the ribs nearest the plate girder. For FEA that focused on out-of-plane response at the RFB connection, the longitudinal and transverse load positions were varied. The plate girder model is discussed further below.

2.2.2 Plate Girder Model Details

As noted above, the existing global FEA model of the moveable lift bridge was modified substantially to simplify the global analysis of the bridge, to reduce the modeling effort as SOBD design parameters were varied, and to decrease computation time. This new PG model enabled efficient FEA of SOBDs as variations in the floor beam depth, thickness, and spacing, were introduced. The PG model consists of five floor beams, two I-shaped edge plate girders (one on either side of the deck), and eleven U-shaped ribs as shown in Figure 14.

In the base version of the PG model used in this study, the ribs and floor beams have the same dimensions as in the lift bridge model (Figure 11). To study the slit RFB connection, the slit was introduced into the model. As noted above, in some FEA models, described later, the floor beam web depth, thickness, and spacing were varied from those of the base PG model, and the geometry of the slit was changed. The PG model has plate girders instead of box girders as the primary elements of the bridge superstructure. Full height stiffeners, $^1/_2$ inch thick, stiffen the edge plate girder webs at the floor beam locations.

The floor beams span 25 feet, 8 inches between the edge plate girders. For the base model, the floor beam spacing is 11 feet, 9 inches, as in the lift bridge model, and this floor beam spacing is used for studies that focused on in-plane response of the RFB connection. In a modified version of the PG model, the floor beam spacing is extended to 20 feet, which is the maximum recommended limit in FHWA's "Manual for Design, Construction, and Maintenance of Orthotropic Steel Deck Bridges" (Connor et al. 2012). This floor beam spacing is used for studies focused on out-of-plane response of RFB connections.

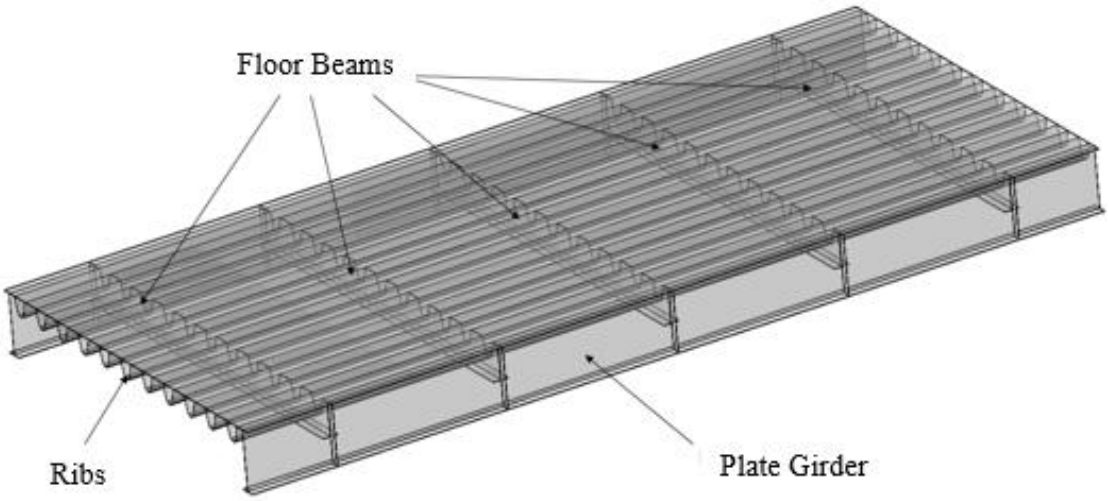

Figure 14. Illustration. Overview of the plate girder model. Shown are the edge plate girders, ribs, floor beams and deck plate.

The rib and floor beam identifiers as well as the orientation of the PG model are shown in Figure 15 and Figure 16. Ribs were numbered from one to eleven, with the south-most rib identified as Rib 1. Floor beams were numbered from one to five, with the east-most floor beam identified as Floor Beam 1. The FEA focused on the center floor beam, Floor Beam 3, and on Rib 1 and Rib 6. As discussed later, loads were placed on the SOBD to maximize stresses at the RFB connections for these ribs.

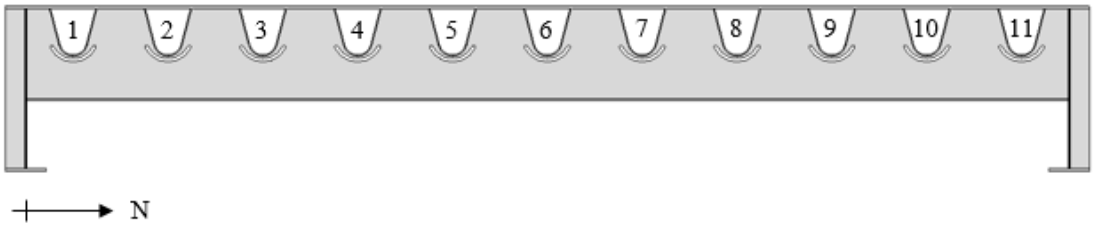

Figure 15. Illustration. Rib identifiers for plate girder model with Rib 1 on the south side of the deck.

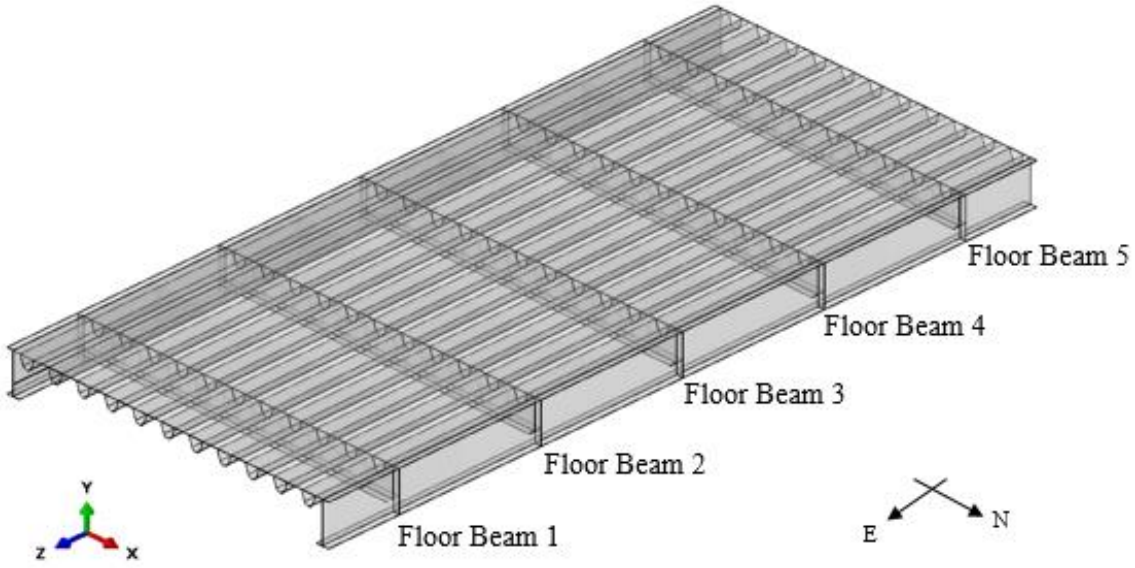

Figure 16. Illustration. Naming convention for the plate girder model floor beams with Floor Beam 1 on the east side of the deck.

2.2.3 Calibration of the PG Model

Calibration of the PG model relative to the existing global FEA model of the movable lift bridge was performed by comparing the stress results of the two models under the same load condition. This load position was the critical position discussed previously (defined as L1-T29 by Mukherjee 2016) and has the rear tandem axle centered in the longitudinal direction on the center floor beam and positioned transversely near the box girder web as shown in Figure 12 and Figure 13. Since the FEA model for the moveable lift bridge SOBD had fitted RFB connections, the calibration of the PG model was done using fitted RFB connections. The stresses normal to the weld toes of the RFB connection at Rib 1 and Floor Beam 3 from the moveable lift bridge model were compared to the stresses normal to the weld toes at the same location in the PG model. The stresses in both

the rib wall and floor beam web were compared. Comparisons of the rib wall stresses and the floor beam web stresses are shown in Figure 17 and Figure 18, respectively. The stresses match well which demonstrates that the global PG model develops stresses at Floor Beam 3 that are similar to the stresses that develop in the SOBD for a large bridge, such as the existing movable lift bridge.

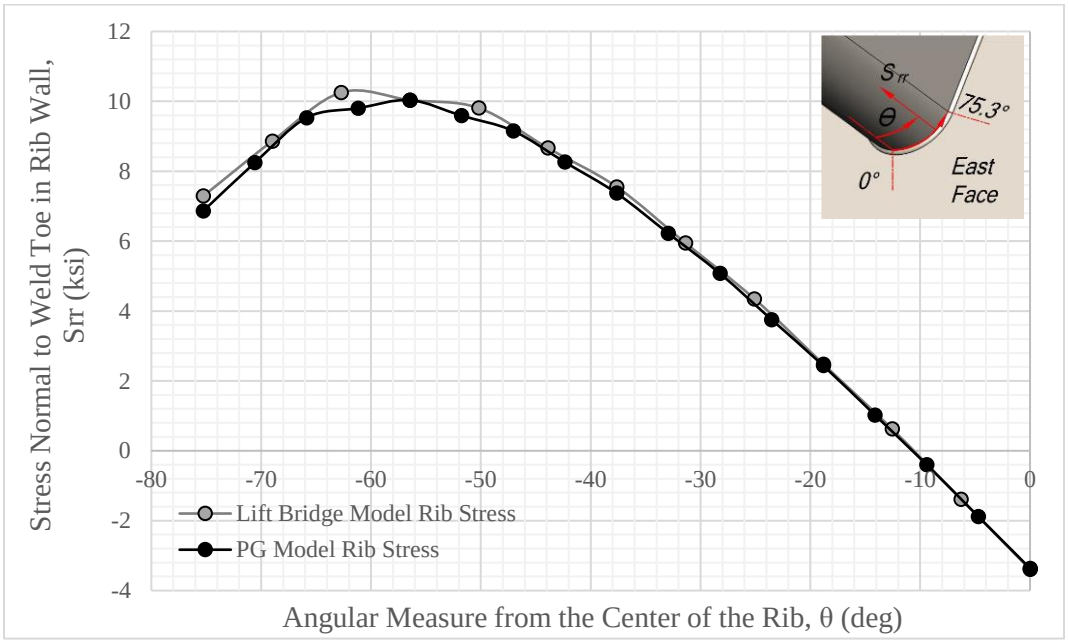

Figure 17. Graph. Comparison of FEA stress normal to the weld toe on the wall of Rib 1 in the east direction.

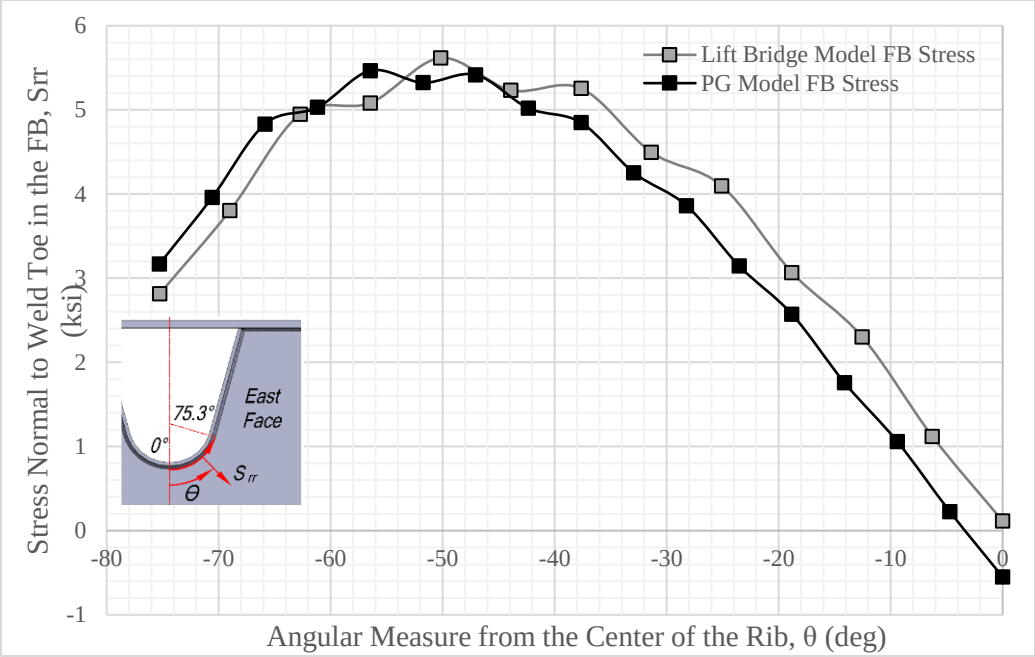

Figure 18. Graph. Comparison of FEA stress normal to the weld toe on the east face of Floor Beam 3 at Rib 1 connection.

2.3 Modeling Details

An analysis technique termed "submodeling" was extensively used throughout the FEA study. Submodeling uses a more refined FEA model of a local region of a larger, coarser FEA model to generate more accurate stress results. The submodel with the more refined mesh is loaded using displacement input at the boundaries that are based on interpolated displacements from the larger FEA model with the coarser mesh. In applying the submodeling technique to SOBDs, the FEA results for the global model of a bridge are used to drive a smaller, more refined model of an SOBD panel. Further submodels can be created with refined meshes of details within the SOBD panel. The benefits of the

submodeling technique are reduced modeling effort (i.e., by creating a refined mesh for only a part of the larger model) and decreased computation time.

In total, five levels of modeling were used in the FEA study, where the mesh size of the models was progressively reduced at each level. These levels are the global PG model, denoted Model A (MA) which was discussed earlier, and four refined submodels, with an increasingly smaller part of the SOBD in the model and a finer mesh size. These models are denoted Submodel B (SMB), Submodel C (SMC), Submodel D (SMD), and Submodel E (SME). Each of these models is described in further detail below.

2.3.1 Element Type and Meshing

Three-dimensional meshes for all models and submodels were generated automatically by ABAQUS using a structured meshing algorithm with a defined target element size (Dassault Systemes Simulia Corp. 2016). The meshes were created using hexahedral elements, which are preferred over the tetrahedral elements created by other algorithms. All models and submodels were meshed using elastic 3D continuum solid hexahedron elements. Other model-specific elements that were needed for certain FEA models are discussed later within this chapter. Each solid hexahedral element has twenty nodes and uses a second order interpolation function with reduced integration. Each node has three translational degrees of freedom. In the ABAQUS element library, this solid hexahedral element is identified as the C3D20R element and is shown in Figure 19.

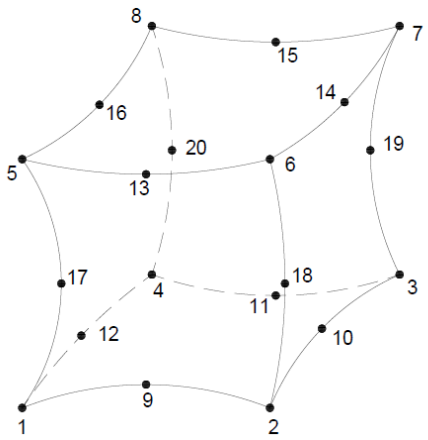

Figure 19. Illustration. C3D20R solid element (adapted from ABAQUS Dassault Systemes Simulia Corp. 2016).

2.3.2 Loading

The FEA models were usually loaded with the rear tandem axle of the fatigue design truck from the AASHTO BDS, as shown in the red box in Figure 20 (AASHTO 2016). The rear tandem axle consists of four 8-kip wheels spaced 4 feet longitudinally and 6 feet transversely. In some situations, only half of the tandem was used to enable the FEA to focus on isolated loading and response. To do this, the full tandem rear axle was split in half longitudinally to include only two load pads spaced four feet apart longitudinally, as shown in the blue box in Figure 20.

Critical fatigue-sensitive details of SOBDs respond to individual truck axles instead of the entire truck, so the number of loading cycles experienced by these details during the bridge service life is large. As a result, these details should be designed for infinite fatigue life, so the AAHSTO Fatigue I load combination was considered for all of the analyses. For SOBDs, the AASHTO BDS specifies a load factor for the Fatigue I load combination

of 2.25, which is applied to loads shown in Figure 20 after they have been increased by 15% for the impact factor. The resulting total factored tandem axle load is (32 kips x 1.15) x 2.25 = 82.8 kips (AASHTO 2016).

The SOBD Fatigue I total factored tandem axle load corresponds to a factored wheel load of 20.7 kips which is distributed uniformly over a rectangular tire contact area with a width of 20 inches and a length of 10 inches, with the shorter dimension parallel to the traffic direction. The resulting uniformly distributed pressure load is 0.104 ksi over each patch. Each tire contact area was modeled in the FEA models as a solid rectangular load pad which is $^{5}/_{8}$ inch thick. The load pad was discretized using C3D20R elements and tied to the deck plate elements using node-based tie constraints. The load pads allowed the loads to be easily moved to various positions on the SOBD deck plate. Specific load positions and configurations are discussed in further detail below.

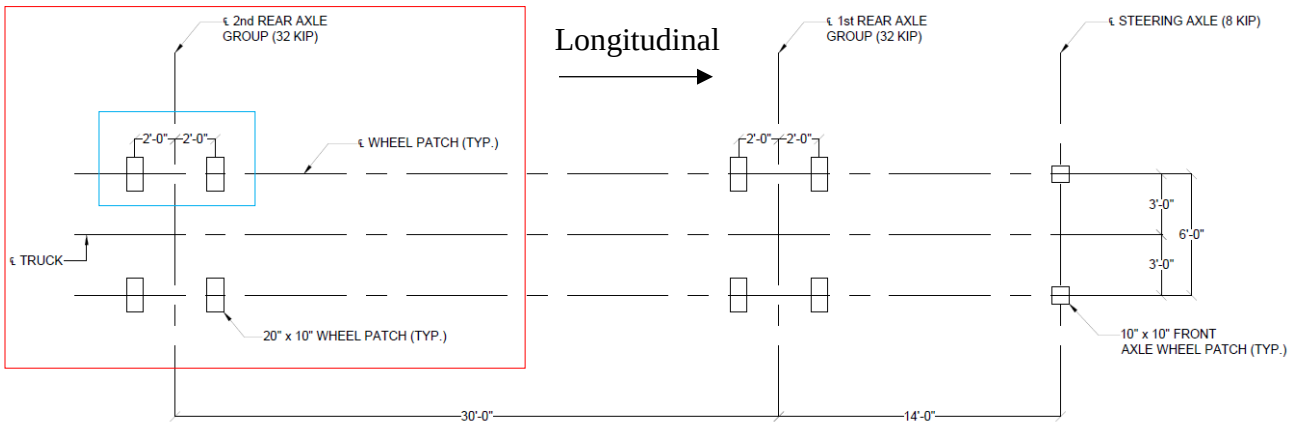

Figure 20. Illustration. Fatigue load for SOBDs (adapted from AASHTO 2016).

2.3.3 Material Properties

General linear elastic material properties for steel were used in the FEA models. The modulus of elasticity and Poisson's ratio for steel were assumed to be 29,000 ksi and 0.3, respectively. The modulus of elasticity and Poisson's ratio for the load pads were assumed as 300 ksi and 0.48, respectively, which made the load pads both flexible and incompressible to avoid adding stiffness to the SOBD deck plate.

2.3.4 Boundary Conditions

The boundary conditions applied to selected nodes of the global PG model restrained all three translational displacement degrees of freedom of the nodes. These boundary conditions were applied in Model A (MA) to the edge plate girder bottom flange at the end of each edge plate girder. Specifically, the boundary conditions were applied to all nodes across the entire width of the bottom flange, and over approximately seven inches of the bottom flange on either side of the center lines of Floor Beam 1 and Floor Beam 5.

2.3.5 Restrained Floor Beam Truss Details

The vertical support and transverse restraint of the bottom flange of an SOBD floor beam may affect the deformations and stresses of RFB connections at the floor beam. As mentioned earlier, the floor beams of the SOBDs used in deck replacement projects may be supported vertically and restrained transversely by the bridge superstructure elements. The global PG model, as described earlier, has independent floor beams with no bottom flange support or restraint (except where the floor beams are supported by the edge plate girders). To study the effect of floor beam restraint on the stress response of the slit RFB

connection, a support/restraint system was developed to restrain the floor beams of a modified PG model.

The support/restraint system was derived from an existing large-size, full-scale SOBD test specimen. In this test specimen, the SOBD floor beams are supported on transverse floor trusses which span between the longitudinal trusses of the bridge superstructure (Figure 3). The geometry of these floor trusses is the basis for floor trusses included in the modified PG model. In addition, the longitudinal trusses of the test specimen are included in the modified PG model. Due to the difference in height between the bottom flange of the edge plate girders and the bottom flange of the floor beams of the PG model (see Figure 15), the edge plate girder bottom flange was removed and the height of the web was reduced, so the bottom of the web was level with the bottom flange of the floor beam. This change allowed the truss system to be continuously tied to the bottom of the SOBD at the same elevation.

The cross section properties of the truss system are the same as the cross sectional properties of the large-size, full-scale SOBD test specimen (without scaling) to provide a stiff support for the floor beam. The increased support of the SOBD floor beam, which decreases deformations and stresses in the floor beam web from in-plane shear, also increases the transverse restraint of the SOBD bottom flange, which increases deformations and stresses at the RFB connection from out-of-plane rotation due to rib rotation. The cross section properties of the transverse trusses in the truss system are listed in Table 1 and the longitudinal truss properties are listed in Table 2. The truss system can be seen in Figure

21. The depth of the longitudinal trusses is 8 feet, 9 inches, and the depth of the transverse trusses is 4 feet, 9 inches.

Table 1. Properties of transverse trusses in truss system.

	Area (inches^2)	Iz, In-plane of Truss (inches^4)	Iy, Out-of-plane of Truss (inches^4)
Top Chord	50.00	2320.00	2680.00
Diagonals	11.60	308.00	44.00
Bottom Chord	15.20	312.00	868.00

Table 2. Properties of longitudinal trusses in truss system.

	Area (inches^2)	Iz, In-plane of Truss (inches^4)	Iy, Out-of-plane of Truss (inches^4)
Top Chord	11.70	308.04	44.64
Diagonals	11.70	308.04	44.64
Bottom Chord	11.70	308.04	44.64

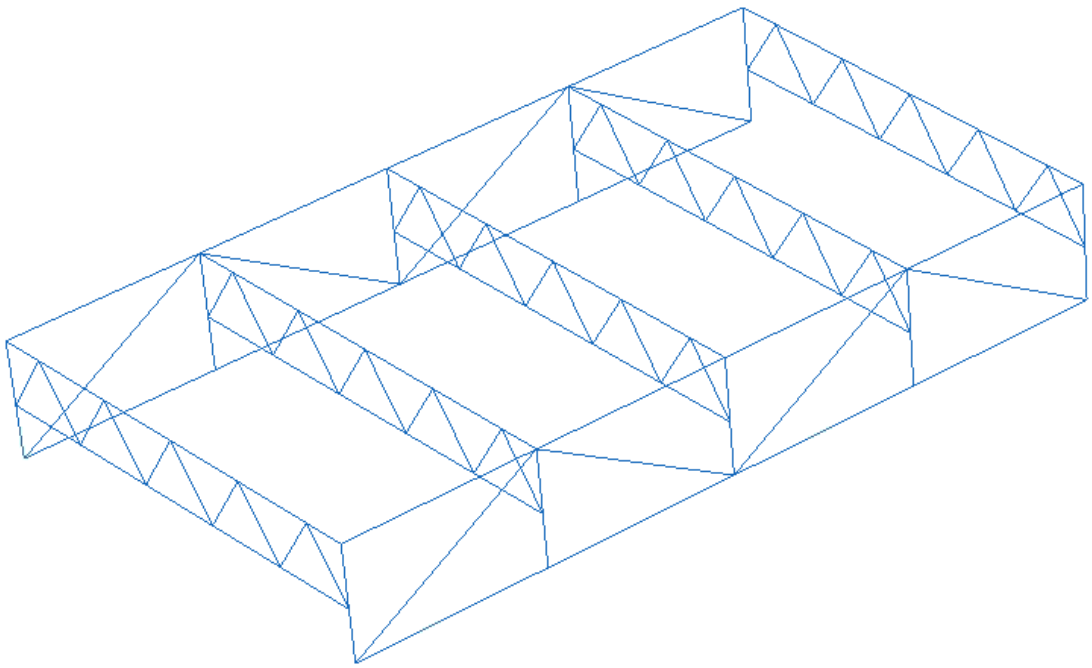

Figure 21. Illustration. Support truss system with five transverse trusses and two longitudinal trusses.

In the modified PG model, the truss members are modeled with B31 beam elements from the ABAQUS element library. These elements are 3D Timoshenko beams with two nodes and linear interpolation functions. Stress results for the truss members were considered to be unimportant, so beam elements as opposed to solid elements were utilized. The beam elements represent the global stiffness of the truss members without much modeling effort or computational time compared to solid elements. The average element length for the truss member model is 1 inch.

General linear elastic material properties for steel were used for the truss member elements, with a modulus of elasticity and Poisson's ratio equal to 29,000 ksi and 0.3, respectively.

The modified PG model with trusses had boundary conditions similar to the PG model without trusses. At the bottom corner nodes of each longitudinal truss adjacent to Floor Beam 1 and Floor Beam 5, the translational displacement degrees of freedom were restrained.

For the modified PG model, a fully rigid connection between the top chord of the transverse truss and the bottom flange of the SOBD floor beam was implemented. ABAQUS surface-to-surface tie constraints were used to attach the bottom flange of each floor beam to the top chord of the adjacent truss. A tie constraint ensures that the nodes on each surface have the same values for each displacement degree of freedom. Similar tie constraints were used to attach the bottom surface of the shortened edge plate girder webs to the adjacent longitudinal truss.

2.4 Submodel Details

As previously mentioned, as many as five levels of submodeling were used to determine the stresses in the SOBD models. The submodels were used to determine accurate stresses to assess the slit RFB connection. The very refined submodels were necessary to determine if the FEA submodels were sufficiently refined and the stresses had converged. The following is a description of the five levels of models, including their purpose, model size, and mesh size.

2.4.1 Model A

The purpose of the first level model, which is a global bridge model, referred to as MA, is to enable efficient FEA of SOBDs as parameter variations, such as variations in the floor beam dimensions, slit geometry, loading, and floor beam support conditions, are introduced. Relative to the more refined models, MA level models require less effort to revise as parameters change. The results from MA models provide an overall understanding of stresses in the SOBD and help to identify locations and amplitudes of critical stress responses. MA models include the entire PG model (or any modified versions of the PG model), including both edge plate girders and longitudinal trusses (if present), five floor beams and transverse trusses (if present), and eleven ribs. The welds of the RFB connections and the rib-to-deck plate (RDP) welds are not included in MA models.

MA models use C3D20R solid elements for the SOBD components. The average element size is 3.5 inches, and a representative MA mesh is shown in Figure 22.

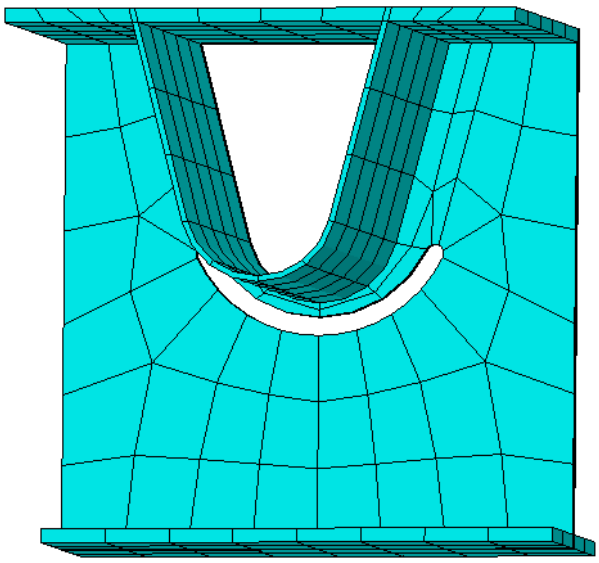

Figure 22. Illustration. Model A mesh at RFB connection. Average mesh size is 3.5 inches.

2.4.2 Submodel B

The second level model, referred to as SMB, is used to study the local behavior of the RFB connection. SMB level submodels include one floor beam, all eleven ribs, and no portion of the edge plate girders. The submodel contained a portion of the SOBD which was 308 inches wide and 141 inches long. The floor beam that is included in a SMB is the most critically stressed floor beam as determined from FEA results from MA, which is usually Floor Beam 3 of the PG model. Floor Beam 3 is usually most critical because the position of the tandem axle load (described earlier) is usually centered over Floor Beam 3 or located between Floor Beam 3 and Floor Beam 4. The welds in SMB were modeled with

a simple model, which has a $^{5}/_{16}$ inch fillet and a zero-radius notch at the weld toes, and has no lack of fusion or root gap at the weld root.

SMB meshes were generated automatically by ABAQUS using a structured meshing algorithm and were inspected to ensure adequate element quality according to ABAQUS recommendations. Elements with an aspect ratio greater than 10, with small face angles less than 10 degrees or large face angles greater than 160 degrees were avoided as much as possible in the region near the RFB connection. The average element size for SMB is 1 inch and a representative SMB mesh is shown in Figure 23.

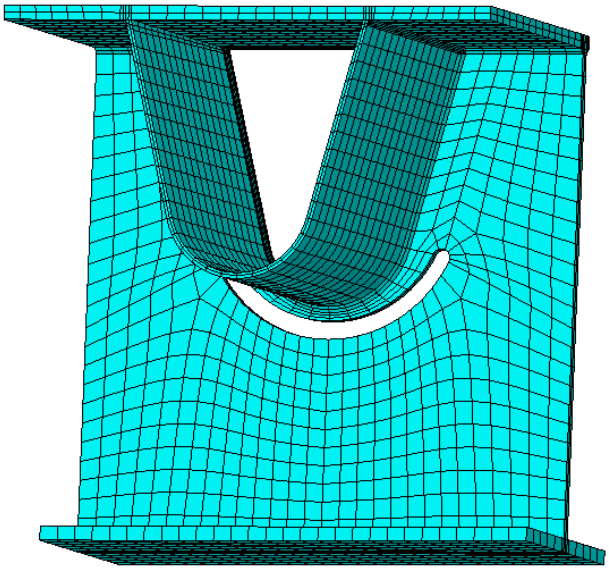

Figure 23. Illustration. Submodel B mesh at RFB connection. Average mesh size is 1 inch.

2.4.3 Submodel C

The third level model, referred to as SMC, has a mesh density that is sufficiently fine for a local structural stress (LSS) approach to be applied to the RFB connection weld toes. The LSS approach from FHWA's "Manual for Design, Construction, and Maintenance of Orthotropic Steel Deck Bridges" (Connor et al. 2012) uses a refined FEA model to evaluate (by extrapolation) local fatigue-critical stresses at welds, particularly at welds in locations with complex stress fields, for which a nominal stress approach is not applicable. The LSS approach uses the surface stresses at reference points at specified distances from the weld toe, where the stress concentration effects due to the geometry of the connection and of the weld are present; at these distances, the stress concentration effect due to the notch at the weld toe is not present. These surface stresses are linearly extrapolated to the weld toe, and this extrapolated stress is referred to as the local structural stress. The reference points for the surface stresses are shown in Figure 24 (IIW 2007). As specified in (IIW 2007, Connor et al. 2012), surface stresses are determined at the 0.4t and 1.0t reference points, which are nodal points, and extrapolated to determine the local structural stress.

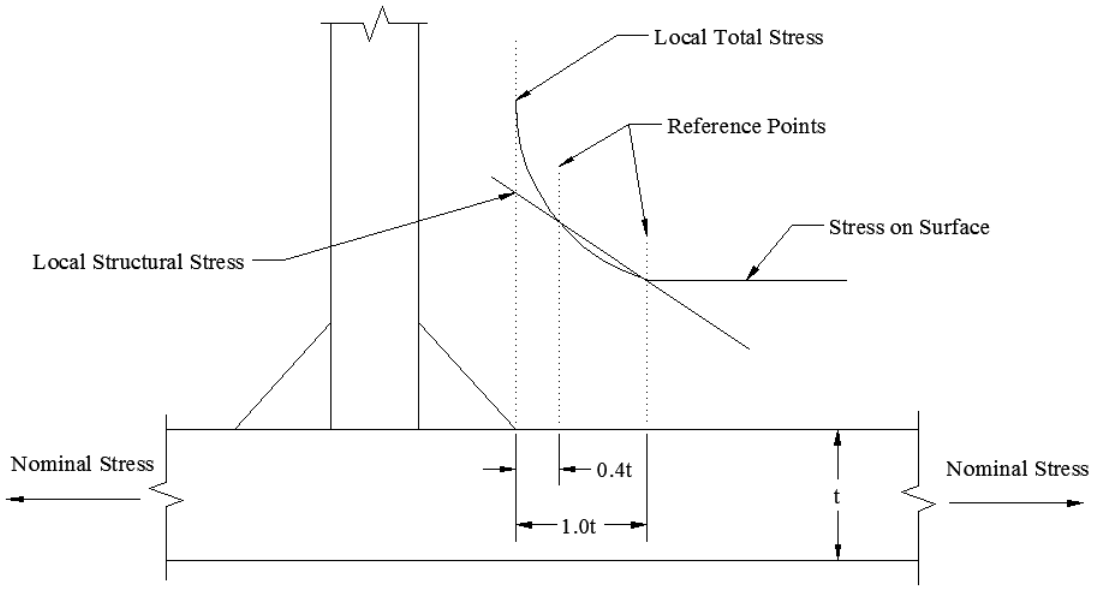

Figure 24. Illustration. Reference points at distances of 0.4 times the plate thickness and 1.0 times the plate thickness for stress extrapolation using the local structural stress approach (adapted from IIW 2007).

(Connor et al. 2012) states that a fatigue assessment of SOBD RFB connection welds should use the local structural stress normal to the weld toe and compare this stress to AASHTO Fatigue Category C. More detail on the LSS approach can be found in (IIW 2007, Connor et al. 2012). For the present study of the slit RFB connection, weld toe stresses were not critical (due to the effectiveness of the slit), however, SMC was sufficiently refined so that the LSS approach could be implemented.

The SMC level submodels include one rib that is 141 inches long, no deck plate, and a 28 inch long portion of the floor beam which begins and ends halfway between adjacent ribs. The rib selected for FEA using SMC is associated with a slit RFB connection

of interest as determined from SMB. The welds in SMC were modeled with the same simple model used in SMB.

As for SMB, SMC meshes were generated using the ABAQUS structured meshing algorithm, and then inspected to ensure adequate element quality according to ABAQUS recommendations. As specified in (IIW 2007, Connor et al. 2012), element sizes for relatively fine meshes are 0.4t by 1.0t where t is the thickness of the part where the surface stress is being determined. Elements outside the region of interest have an average size of $^1/_4$ inch. A representative SMC mesh for the LSS approach is shown in Figure 25.

Figure 25. Illustration. Submodel C mesh at RFB connection. Average mesh size is $^1/_4$ inch.

2.4.4 Submodel D

Submodel D (SMD) has an average element size of $^{1}/_{16}$ inch, and was developed for only the north side or the south side of a single slit RFB connection, eliminating most of the rib and floor beam. Because one SMD contained only one side of the RFB connection, a north SMD and a south SMD were created to observe the stresses on either side of the RFB connection. A representative SMD is shown in Figure 26.

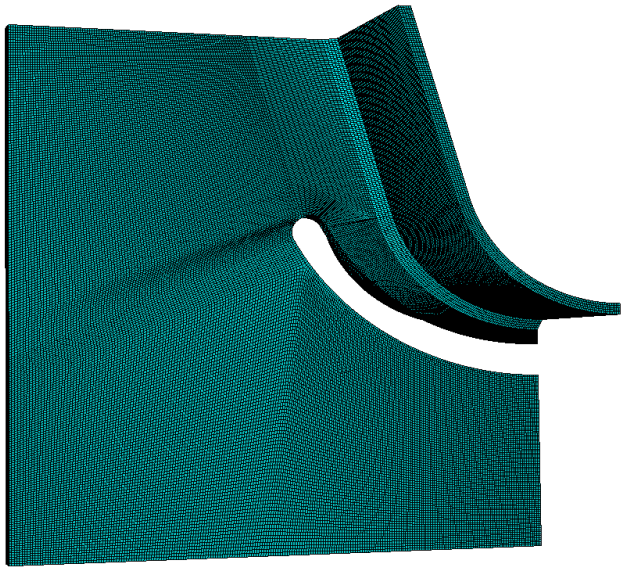

Figure 26. Illustration. Rib-to-floor beam connection Submodel D mesh. Average mesh size is $^{1}/_{16}$ inch.

2.4.5 Submodel E

Submodel E (SME) has an average element size of $^{1}/_{32}$ inch. Owing to this very small element size, SME included only a portion of the floor beam web which contained either the north side or the south side of the slit. Similar to SMD, a north SME and a south

SME were created to observe the stresses on either side of the RFB connection. A representative SME mesh can be seen in Figure 27, which shows SME included only a rectangular portion of the web with the slit and RFB weld.

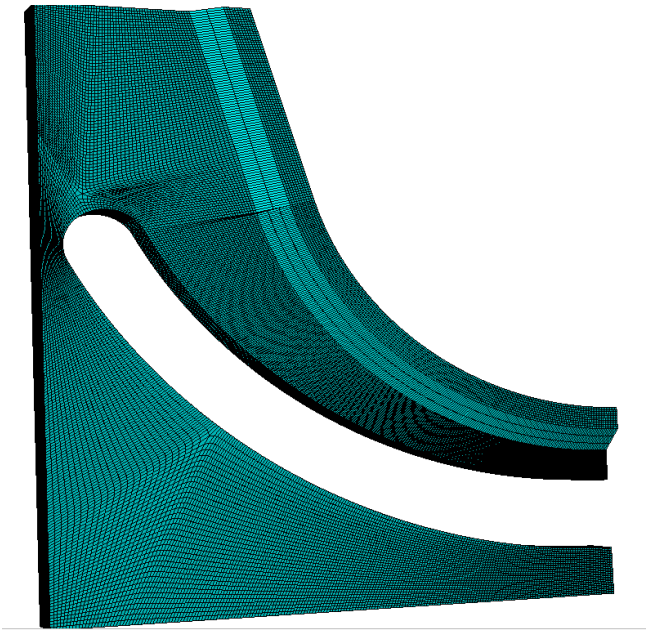

Figure 27. Illustration. Rib-to-floor beam connection Submodel E mesh. Average mesh size is 1/32 inch.

3. FINITE ELEMENT ANALYSIS STUDY

The slit rib-to-floor beam (RFB) connection was studied using FEA to better understand the stress and deformation response, to evaluate the potential for favorable fatigue performance, and to identify the critical loading conditions and fatigue-critical stress locations for the connection. As noted earlier, the slit RFB connection has a stress relieving opening in the floor beam web located below the rib. However, unlike the extended cut-out RFB connection, the opening in the slit RFB connection is located entirely within the web of the floor beam and does not terminate on the rib wall, thereby eliminating the stress concentrations caused by the welds at the cut-out terminations. The slit RFB connection is fillet welded all around with the rib passing continuously through a matching opening in the floor beam, similar to the fitted RFB connection, which makes it more amenable to automated fabrication than the extended cut-out RFB connection.

The slit RFB connection has not been studied previously, so the initial FEA focused on understanding the behavior of the connection and determining favorable geometries for the slit that reduce stresses and improve fatigue performance. A representative slit RFB connection is shown in Figure 28 along with notation for the components of the slit geometry. Thirteen different slit geometries were investigated and results from these studies will be discussed in more detail below. The slit geometry shown in Figure 28, termed Slit 3, was used in the in-plane loading FEA studies as the base case to investigate the behavior. Later in this chapter, results for other slit geometries are discussed.

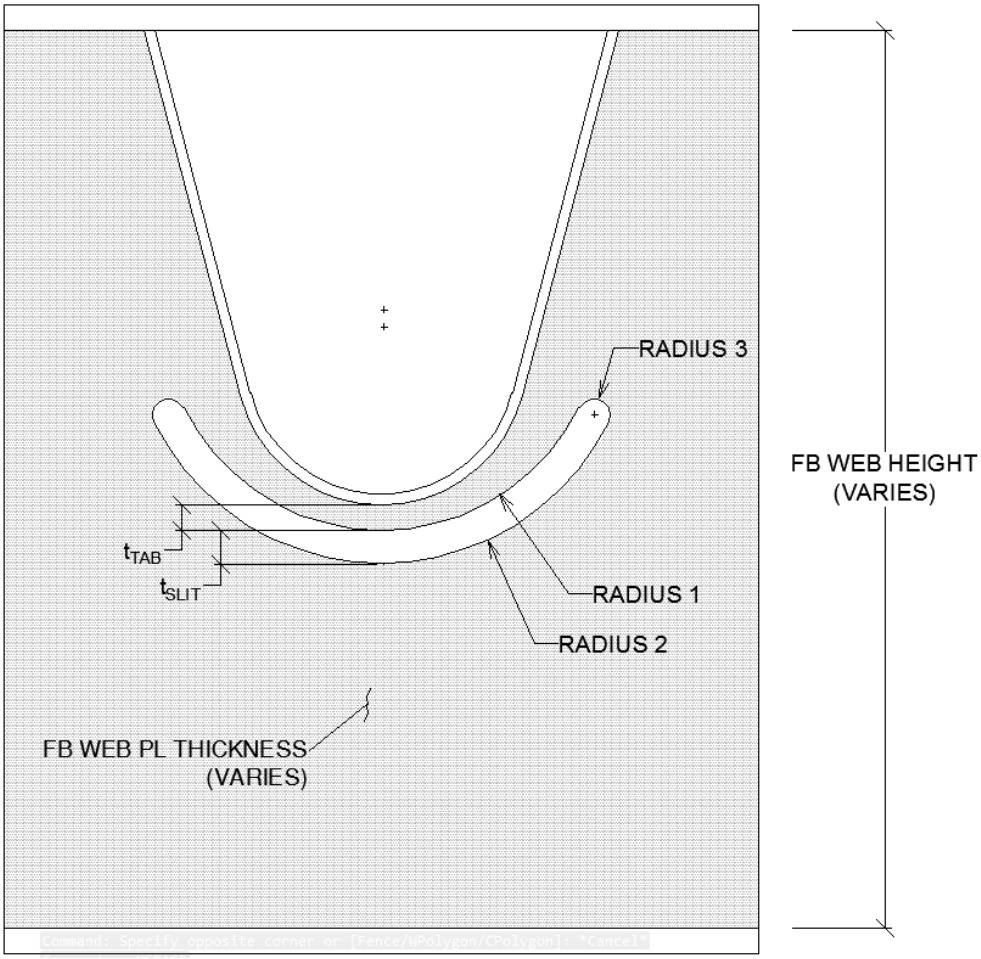

Figure 28. Illustration. Slit rib-to-floor beam connection with components labeled.

3.1 In-plane Loading with an Independent Floor Beam

The slit RFB connection was studied for an independent floor beam under in-plane loading. The previous analysis of the movable lift bridge (Mukherjee 2016) showed high stresses at the weld toes of the fitted RFB connection near the location where the floor beam is supported by the box girder of the bridge superstructure. These stresses were high at the weld toe on the floor beam web and the weld toe on the rib wall. The slit RFB connection under in-plane loading was investigated using the same load configuration as

used for the movable lift bridge (Mukherjee 2016): the full rear tandem axle was placed concentrically at Floor Beam 3 with one half of the full tandem (two load pads) centered between Rib 1 and Rib 2, as shown in Figure 29. The floor beam section had a floor beam web depth of 34.5 inches and a web thickness of $^{1}/_{2}$ inch. This floor beam section (FBS) was termed FBS1. The deck plate and floor beam flange were both $^{3}/_{4}$ inch thick, resulting in a total SOBD depth of 36 inches.

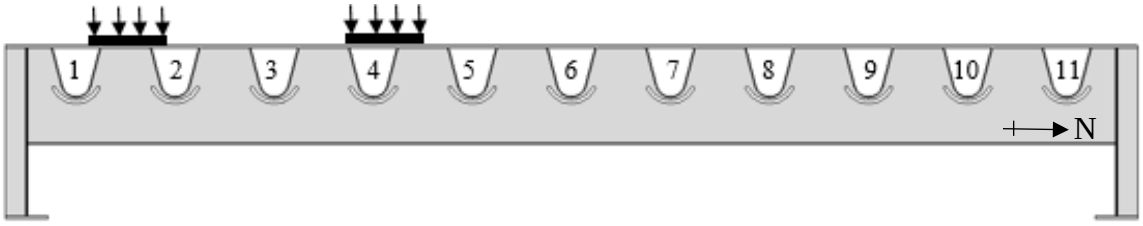

Figure 29. Illustration. Transverse load position of full tandem for independent floor beam under in-plane loading.

For an independent floor beam, the shear force carried by the floor beam web is relatively large compared to the shear force carried by a restrained floor beam, which has vertical support to prevent in-plane deformation of the floor beam. The shear force diagram in Figure 30 shows large values near Rib 1, especially, which is adjacent to the reaction provided by the edge plate girder.

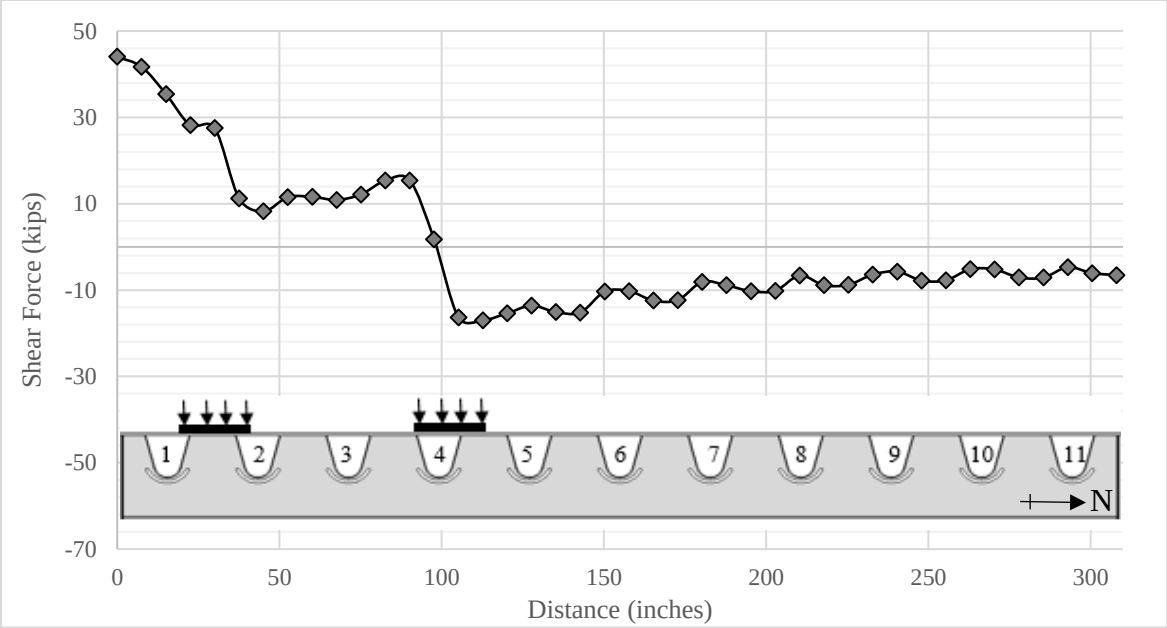

Figure 30. Graph. Shear force in independent floor beam with slit RFB connection under full tandem in-plane loading (SMB).

3.1.1 Full Tandem Loading Near Rib 1

The FEA results for the slit RFB connection with an independent floor beam show high maximum principal stresses around the slit edges of the Rib 1 connection, as shown in the stress contour plot of Figure 31. A large tension stress of 27.12 ksi can be seen on the lower south edge of the slit for the slit RFB connection of Rib 1 which is adjacent to the edge plate girder. A plot of these stresses along the bottom of the slit is shown in Figure 32. The large stress along the lower south edge of the slit is a result of a diagonal tension stress field in the floor beam web which is driven by shear force in the floor beam under in-plane loading.

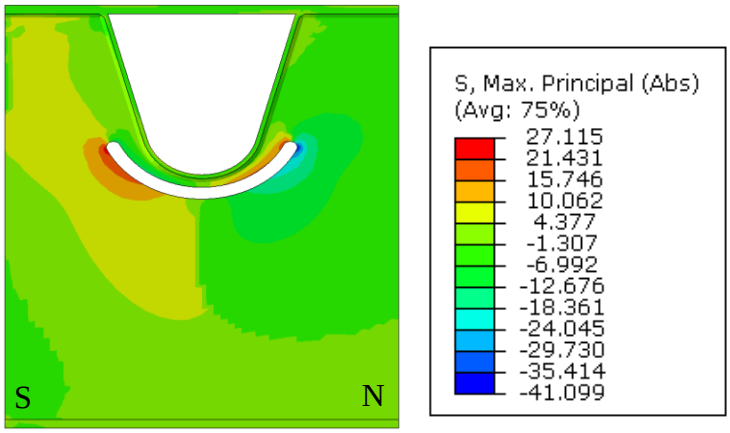

Figure 31. Illustration. Contour plot of maximum principal stresses (ksi) near slit RFB connection (Slit 3) of Rib 1 to independent floor beam (FBS1) under in-plane loading (SMB).

A plot of the stresses along the top of the slit is shown in Figure 33. This figure and Figure 32, show large stresses on the upper north edge of the slit where Radius 1 and Radius 2 transition into the smaller, upper Radius 3 (see Figure 28 for the notation). The figures show a large tension principal stress of 22.74 ksi on upper north edge of the slit closest to the rib, as well as a large (in magnitude) compression principal stress of -41.10 ksi on lower north edge of the slit. Further FEA results discussed below suggest that these stresses are mostly from local deformation of the slit from reaction forces on the floor beam web which are reactions to shear forces in the rib walls.

Figure 34 and Figure 35 show that stresses normal to the weld toes of the fillet weld of the slit RFB connection, both on the rib wall and the floor beam web, are small. These stresses are well below the 10 ksi CAFL for AASHTO Fatigue Category C.

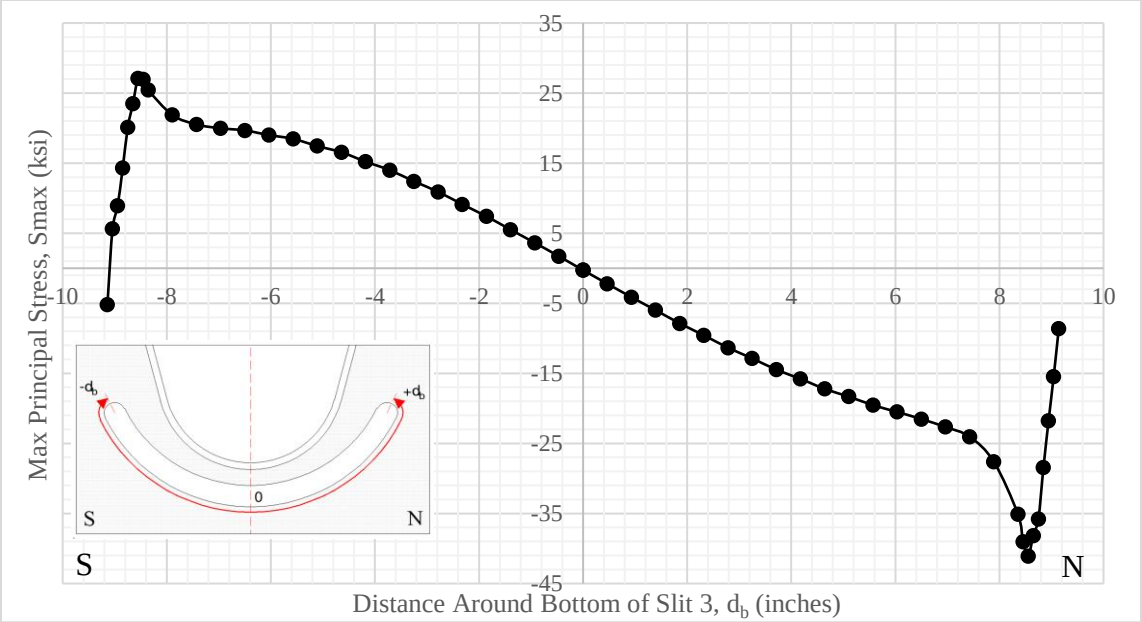

Figure 32. Graph. Variation in maximum principal stresses along bottom of slit RFB connection (Slit 3) of Rib 1 to independent floor beam (FBS1) under in-plane loading (SMB).

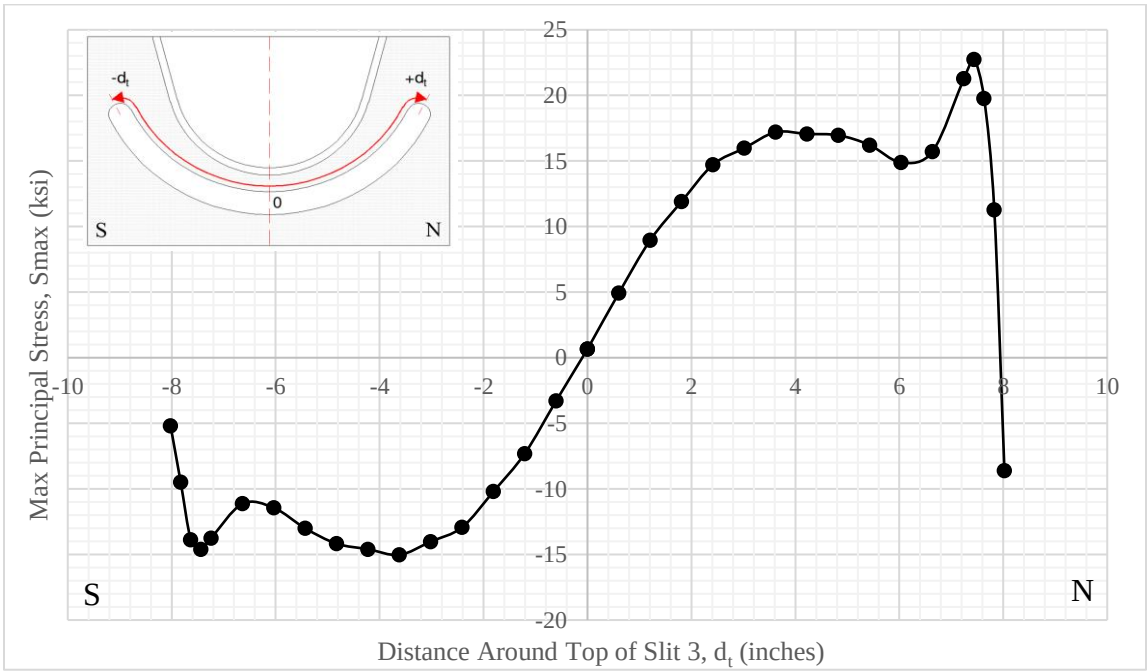

Figure 33. Graph. Variation in maximum principal stresses along top of slit RFB connection (Slit 3) of Rib 1 to independent floor beam (FBS1) under in-plane loading (SMB).

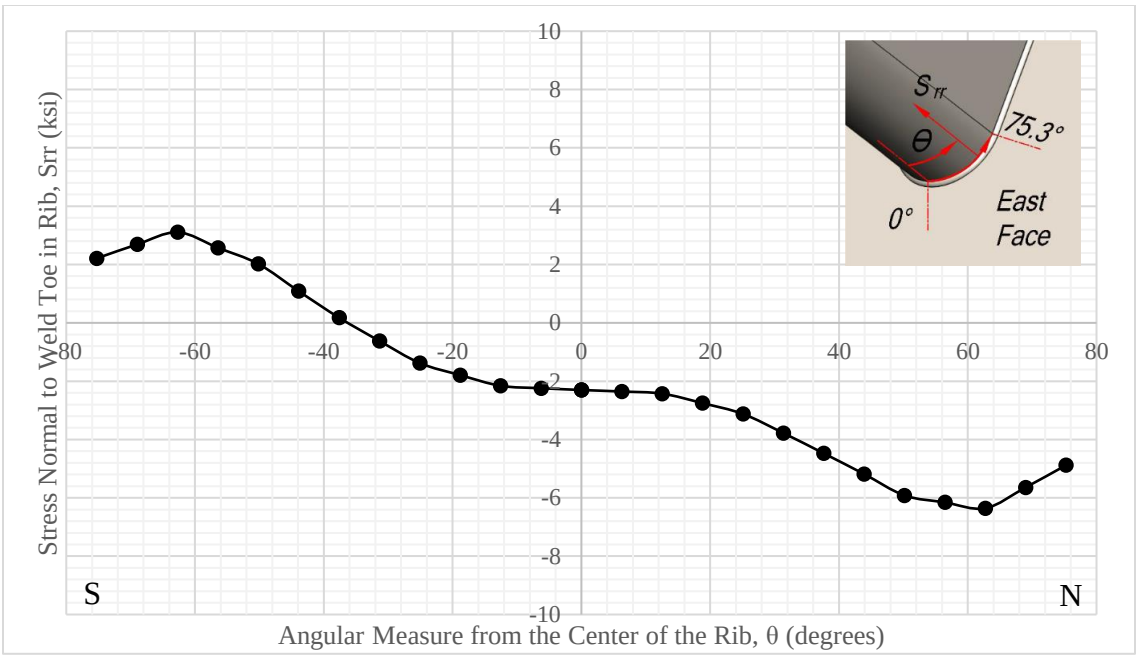

Figure 34. Graph. Variation in rib wall weld toe stress around rib bottom of slit RFB connection (Slit 3) of Rib 1 to independent floor beam (FBS1) under in-plane loading (SMB).

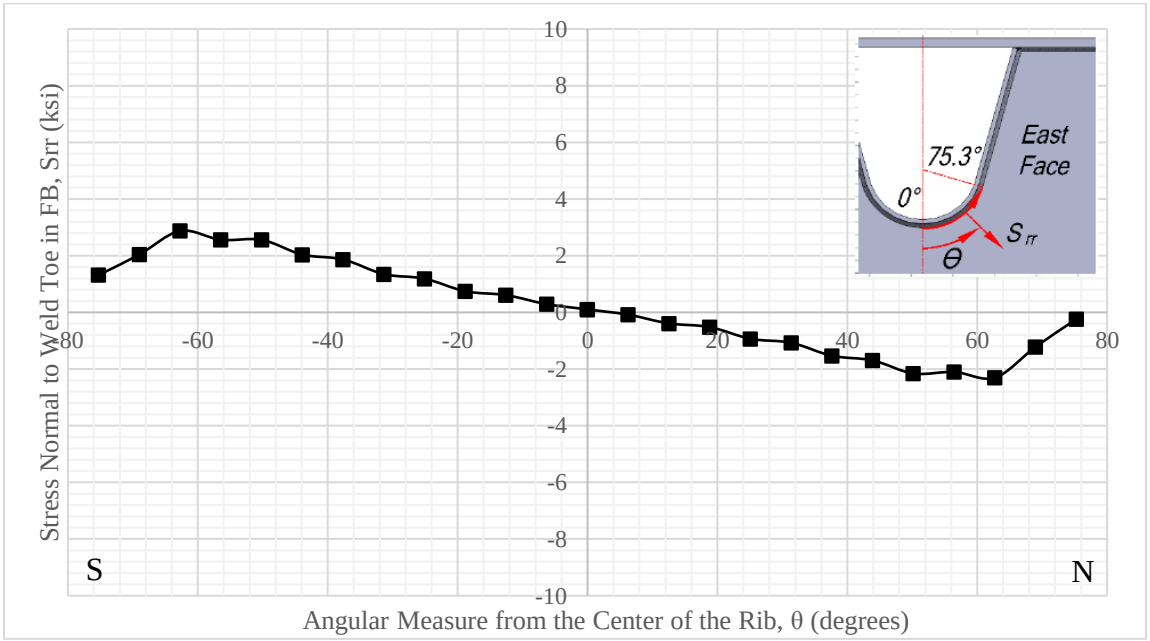

Figure 35. Graph. Variation in floor beam web weld toe stress around rib bottom of slit RFB connection (Slit 3) of Rib 1 to independent floor beam (FBS1) under in-plane loading (SMB).

3.1.2 Mesh Refinement Study

The results discussed above are from models with a SMB finite element mesh. More refined FEA submodels were created to study how FEA model mesh refinement affects the stresses observed around the slit edge. Figure 36 compares the largest tension principal stress on the bottom south edge of the Slit 3 RFB connection of Rib 1 as the FEA model mesh is refined from MA through SME where the convergence is clearly visible. A summary of the changes in the largest tension principal stress is given in Table 3. Results from this mesh refinement study show the stresses around the slit edge converge to values close to the stresses from SMD. However, the computing run time needed to perform a parametric study of various slit RFB connections using SMD (or a more refined submodel) was excessive. Therefore, most of the FEA used SMB with the knowledge that the largest observed stresses may increase by roughly 43 percent for a more refined submodel.

It is also important to consider the stresses that should be compared to the fatigue resistance for a fatigue-critical detail, in this case AASHTO Category A for the edge of the slit. Past FEA studies of SOBD RFB connections do not appear to have used a consistent mesh size. The results in Figure 36 show that the stresses at the edges of a slit RFB connection can vary widely with the FEA model mesh refinement, relative to the applicable 24 ksi CAFL for AASHTO Category A. The paper "Consistent Approach to Calculating Stresses for Fatigue Design of Welded Rib-to-Web Connections in Steel Orthotropic Bridge Decks" (Connor and Fisher 2006) discusses how to properly quantify the fatigue performance of the base metal at a cut-out edge in a RFB connection. It states that Category A can be used conservatively to evaluate stresses on cut-out edges if a "sufficiently refined

mesh" is used. For this reason, any predictions of fatigue life of a slit edge using Category A should be done with stress values from a SMD size mesh. Regardless of the mesh refinement that may be needed to accurately assess the fatigue performance of the edge of the slit, in this study to understand how various parameters affect the stress response of the slit RFB connection, SMB was used to keep the computing run time to a practical level.

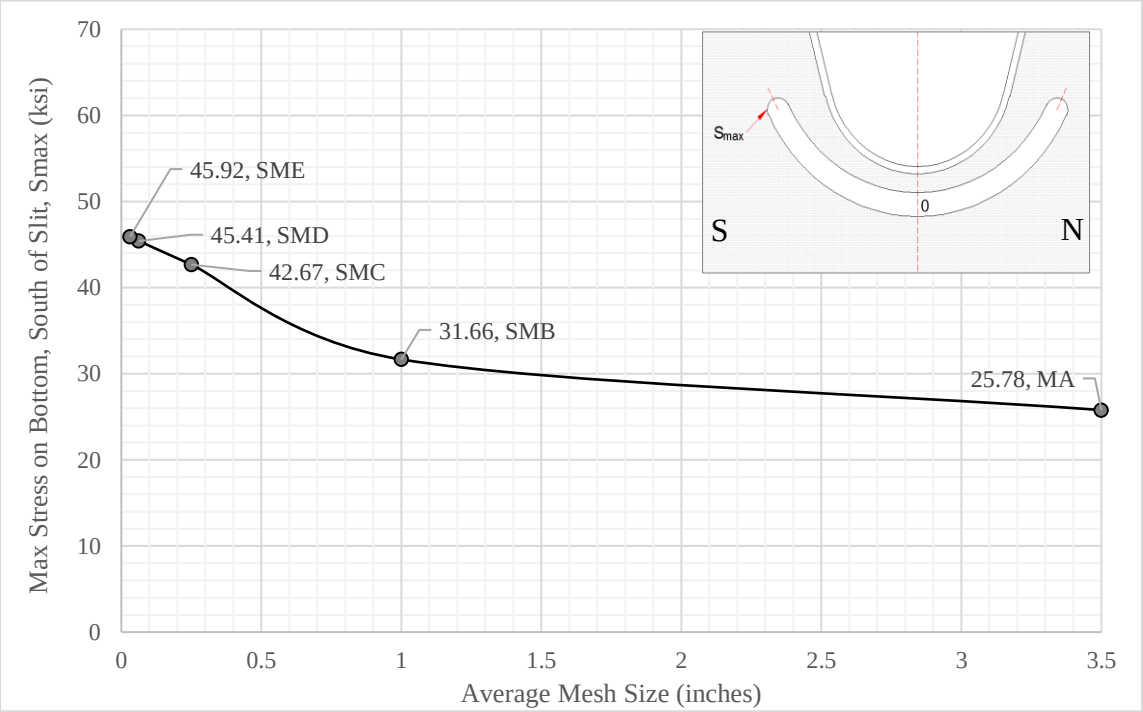

Figure 36. Graph. Comparison of largest tension principal stress from MA to SME on the bottom south edge of slit RFB connection (Slit 3) of Rib 1 to independent floor beam (FBS1) under in-plane loading.

Table 3. Variation in largest tension principal stress with mesh refinement.

Model	Mesh Size (inches)	Largest Tension Principal Stress (ksi)	Percent Increase in Stress from MA (%)
MA	$3\ ^{1}/_{2}$	25.78 ksi	0 %
SMB	1	31.66 ksi	22.8%
SMC	1/4	42.67 ksi	65.5%
SMD	1/16	45.41 ksi	76.1%
SME	1/32	45.92 ksi	78.1%

3.1.3 Floor Beam Shear Area Study

The effects of variation in the floor beam web depth and thickness for the slit RFB connection with independent floor beam were studied using FEA. Six different floor beam section geometries were investigated to see if the critical stresses at the slit edge (Slit 3) of the Rib 1 slit RFB connection could be significantly decreased. The dimensions of the various floor beam web sections, and the resulting maximum and minimum slit edge stresses from FEA (SMB), can be seen in Table 4. The largest tension principal stress on the north side and the south side of the slit edge is plotted against the area of the floor beam web below the rib (to resist the shear force) for each floor beam web geometry in Figure 37 and Figure 38, respectively. Note that the web area below the rib is calculated as the floor beam web depth minus the depth of the rib multiplied by the thickness of the floor beam web.

Figure 37 shows that the large tension stress on the south side of the slit RFB connection (see Figure 31), which is associated with the in-plane tension field from the

shear force in this area (near Rib 1), can be reduced by increasing the floor beam web depth or thickness. However, even with the largest web (FBS8, shown in Table 4), the largest tension principal stress is still 25.61 ksi, which is above the 24 ksi CAFL for AASHTO Category A; as shown earlier, the stress at the slit edge will increase with a more refined FEA model mesh.

Figure 38 shows that on the north side of the slit RFB connection, the largest tension principal stress at the slit edge does not have a clear relationship with the area of floor beam web below the rib, as seen from the dispersion of the 6 data points. However, as the floor beam web depth increases, the stress decreases, as shown by the results for floor beam sections FBS1, FBS2, and FBS3 which have the same web thickness ($^1/_2$ inch), but different web depths. Similarly, as the floor beam web thickness increases, the stress decreases, as shown by the results for floor beam sections FBS3, FBS6, and FBS7, which have the same web depth (26.5 inches), but different varying web thicknesses. For all cases considered (listed in Table 4), the floor beam sections have the same deck plate thickness ($^3/_4$ inch) and floor beam flange thickness ($^3/_4$ inch). As the web thickness increases, the stress decrease is more pronounced than the stress decrease as the web depth increases, suggesting that the stress at the north side of the Rib 1 slit is more sensitive to changes in web thickness than changes in web depth.

Table 4. Largest principal stresses on north and south sides of slit RFB connection (Slit 3) of Rib 1 to independent floor beam with different floor beam webs under in-plane loading (SMB).

Floor Beam Section Name	Floor Beam Web Depth (inches)	Floor Beam Web Thickness (inches)	Web Area Below Rib (inches^2)	South Tension Principal Stress (ksi)	South Comp. Principal Stress (ksi)	North Tension Principal Stress (ksi)	North Comp. Principal Stress (ksi)
FBS1	34.5	0.5	10.25	27.12	-15.03	22.74	-41.10
FBS2	30	0.5	8.00	30.83	-16.84	24.36	-43.61
FBS3	26.5	0.5	6.25	31.66	-19.59	28.85	-42.41
FBS6	26.5	0.625	7.8125	30.64	-16.00	21.84	-39.87
FBS7	26.5	0.75	9.375	28.14	-14.07	18.86	-35.64
FBS8	30	0.75	12.00	25.61	-12.64	17.51	-33.82

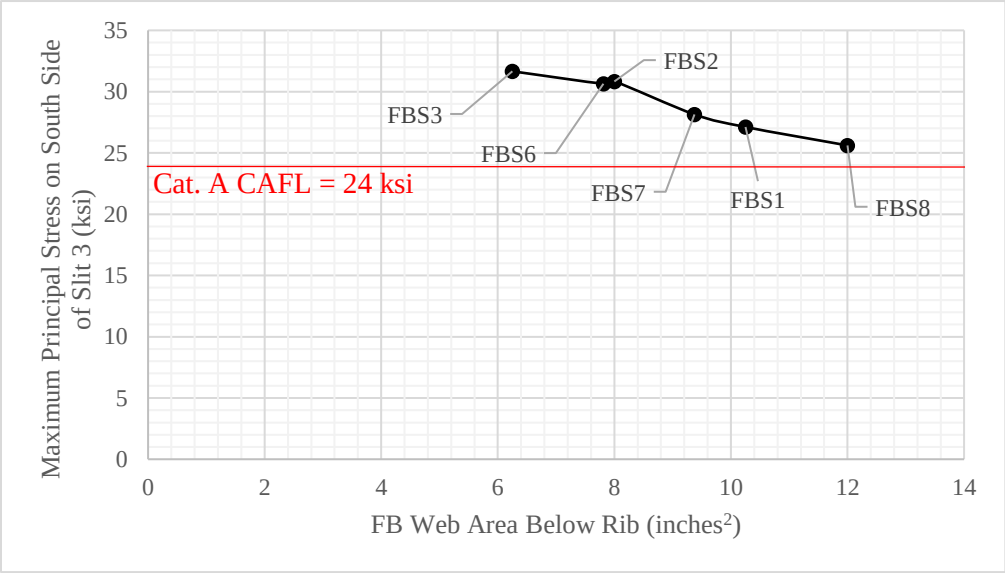

Figure 37. Graph. Largest tension principal stress on south side of slit RFB connection (Slit 3) of Rib 1 to independent floor beam with different floor beam webs under in-plane loading (SMB).

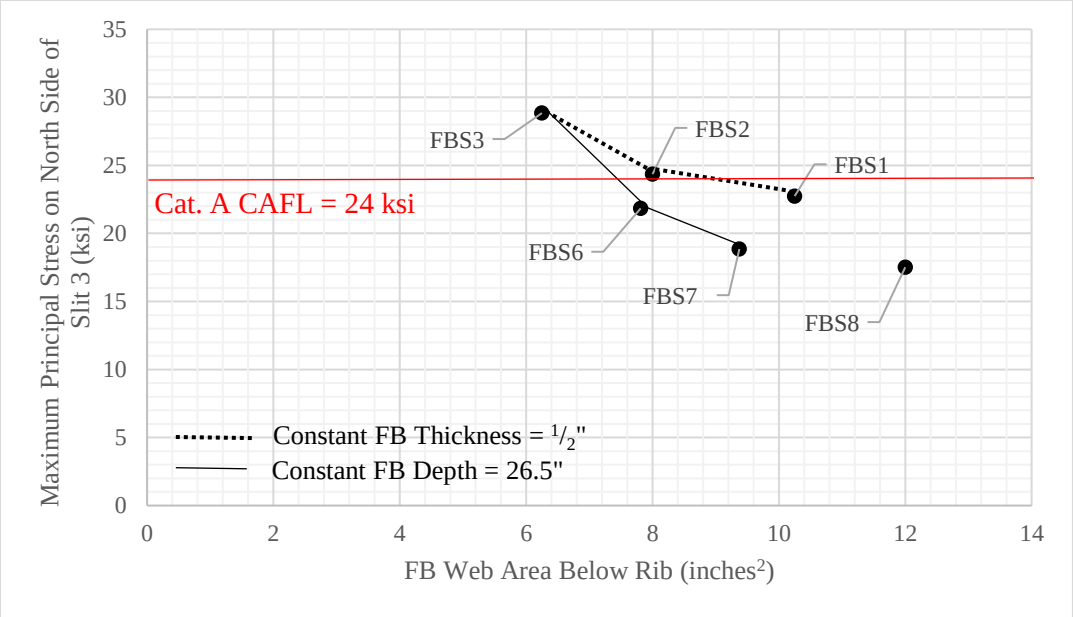

Figure 38. Graph. Largest tension principal stress on north side of slit RFB connection (Slit 3) of Rib 1 to independent floor beam with different floor beam webs under in-plane loading (SMB).

The results of FEA studies of the slit RFB connection with an independent floor beam show that the shear force carried by the floor beam web creates large tension principal stresses at the edge of the slit. As the floor beam web size is varied, these large tension stresses at the slit edge vary, but these stresses were not reduced below the 24 ksi CAFL for AASHTO Category A for any of the cases that were studied. Furthermore, the critical stresses used to assess the fatigue performance were from SMB and the FEA model mesh refinement study showed that these stresses will increase as the mesh is refined. Therefore, it appears that using the slit RFB connection with an independent floor beam will not lead to good fatigue performance under in-plane loading, especially if the depth of the floor beam is limited by an existing bridge superstructure geometry. This result is consistent

with the notion that RFB connections with cut-outs are better suited for restrained floor beams. For this reason, further FEA studies of the slit RFB connection with an independent floor beam, including under out-of-plane loading, were not considered. The additional FEA studies of the slit RFB connection focus on the slit RFB connection with a restrained floor beam.

Furthermore, the parameter study of the slit RFB connection with an independent floor beam, presented above, shows that critical in-plane stresses at the edge of the slit of slit RFB connections can be decreased by increasing the depth or thickness of the floor beam web thereby increasing the web area below the rib. Therefore, the floor beam section FBS3, with the smallest web area below the rib, was chosen as the floor beam section geometry for subsequent FEA studies, to maintain the worst-case condition for in-plane loading, with the understanding that the floor beam web area can be increased to decrease the critical stresses.

3.2 In-plane Loading with a Restrained Floor Beam

Next, the slit RFB connection was studied for in-plane loading with a restrained floor beam. For a restrained floor beam, the bottom flange of the SOBD floor beam is positively connected to a larger transverse member of the bridge superstructure, as discussed in Section 1.1, which restrains the flange against out-of-plane deflection and rotation and also supports the SOBD floor beam against in-plane deflection. The support against in-plane deflection decreases the in-plane shear force carried by the floor beam web, which was shown to create large tension principal stresses on the bottom south edge

of the slit of the RFB connection of Rib1 near the edge plate girder. In the FEA studies, different types of restraint/support of the floor beam were considered.

3.2.1 Half Tandem Loading Near Rib 1

To study the effects on the stress response of a slit RFB connection from reducing the in-plane shear carried by the floor beam, an FEA model with very stiff (supporting and restraining) springs along the bottom flange of the floor beam was created, with the purpose of significantly decreasing the shear force carried by the floor beam. The springs had a spring constant k_z = 10 kip/in in the longitudinal direction (which is transverse to the floor beam) and k_y = 100 kip/in in the vertical direction. One spring with k_z = 10 kip/in and one spring with k_y = 100 kip/in were attached to each of the 1,761 nodes along the bottom flange of the floor beam. In the total, these springs are too stiff to represent realistic conditions. The purpose of this spring-restrained floor beam model was to significantly reduce the floor beam shear force, to understand the other mechanisms creating stresses in the slit RFB connection.

In addition, to further simplify the conditions producing stresses in the slit RFB connection, only one half of the rear tandem axle loading was used in the FEA study, which placed the load pads close to the area of interest and isolated the effects of the loading. The study used the half tandem in two different transverse load positions. The first position was an eccentric transverse load position relative to Rib 1, shown in Figure 39(a), with the half tandem centered between Rib 1 and Rib 2. This position is similar to the load position shown in Figure 29 for the independent floor beam study (although this previous study used the full rear tandem axle). The second, symmetric transverse load position, shown in

Figure 39(b), has the half tandem centered on Rib 1, significantly reducing the torsion in Rib 1.

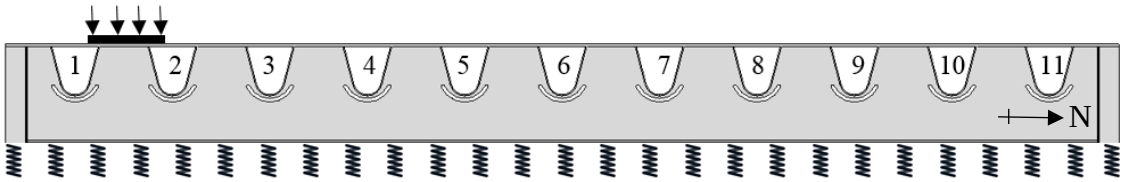

(a) Eccentric transverse load position with half tandem centered between Rib 1 and Rib 2 for spring-restrained FB

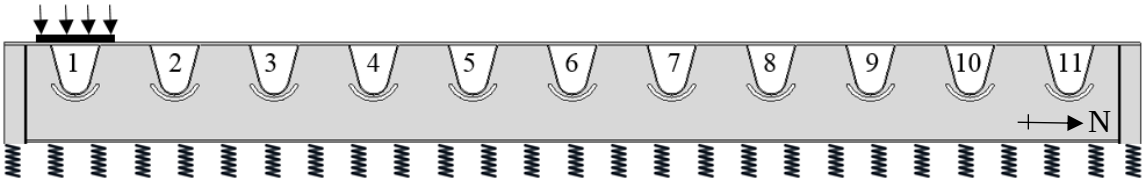

(b) Symmetric transverse load position with half tandem centered on Rib 1 for spring-restrained FB

Figure 39. Illustrations. Compound figure showing transverse load position of half tandem for spring-restrained floor beam under in-plane loading.

The eccentric transverse load position was studied first. The shear force diagram in Figure 40 shows a significant reduction of shear force near Rib 1, adjacent to the edge plate girder, when the floor beam is restrained by springs. Figure 41 and Figure 42 show that the reduction of floor beam shear force causes a reduction in stresses along the slit edge. The reduction in stresses is significant on both the top and bottom of the south side of the slit, which is closest to the edge plate girder. These results confirm that the stresses along the bottom of the slit on the south side are significantly affected by the shear in the floor beam

web. The reduction in stresses on the north side of the slit is not as significant as that on the south side, suggesting that mechanisms other than floor beam shear force dominate the stresses on the north side of the slit for this load position.

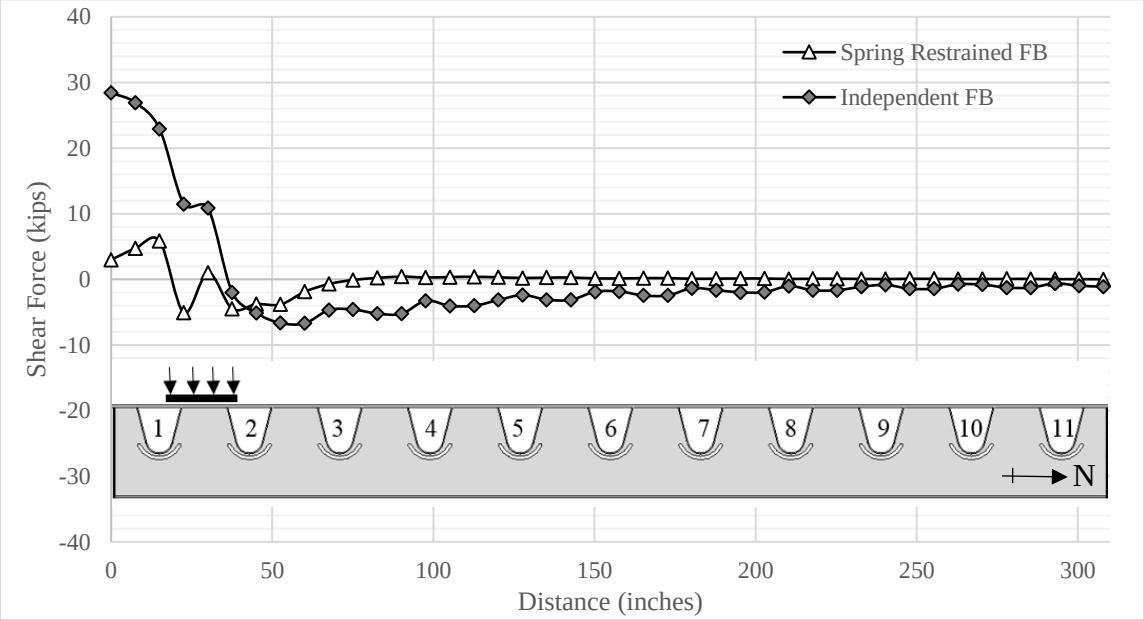

Figure 40. Graph. Shear force in floor beam with slit RFB connection under half tandem in-plane loading with eccentric transverse load position (Rib 1) for independent and spring-restrained floor beams (SMB).

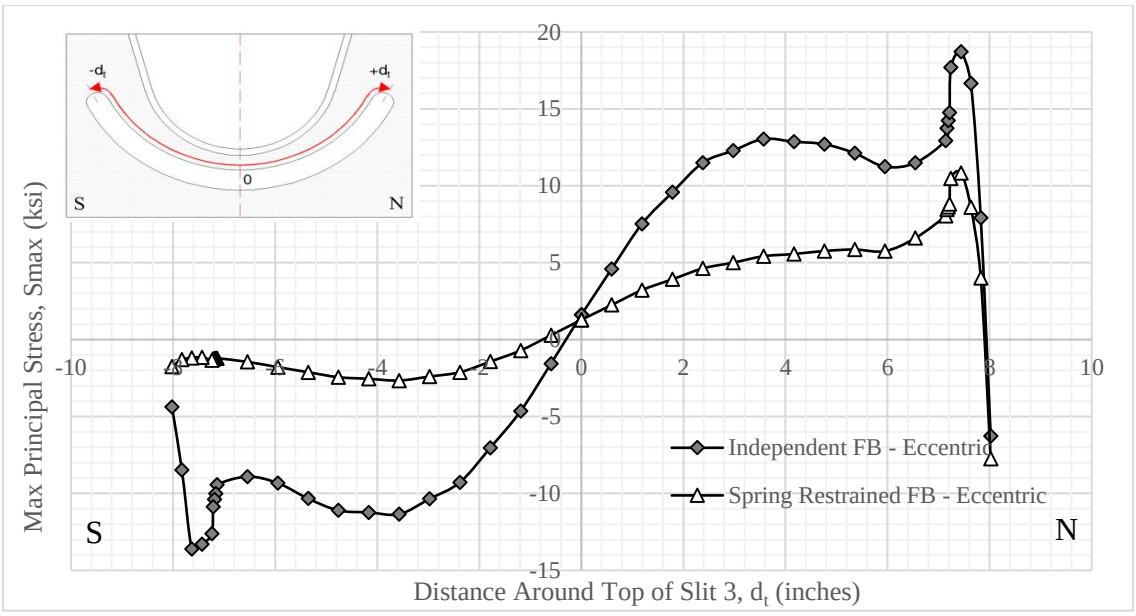

Figure 41. Graph. Variation in maximum principal stresses along top of slit RFB connection (Slit 3) of Rib 1 to independent floor beam and spring-restrained floor beam (FBS3) under half tandem in-plane loading with eccentric transverse load position (SMB).

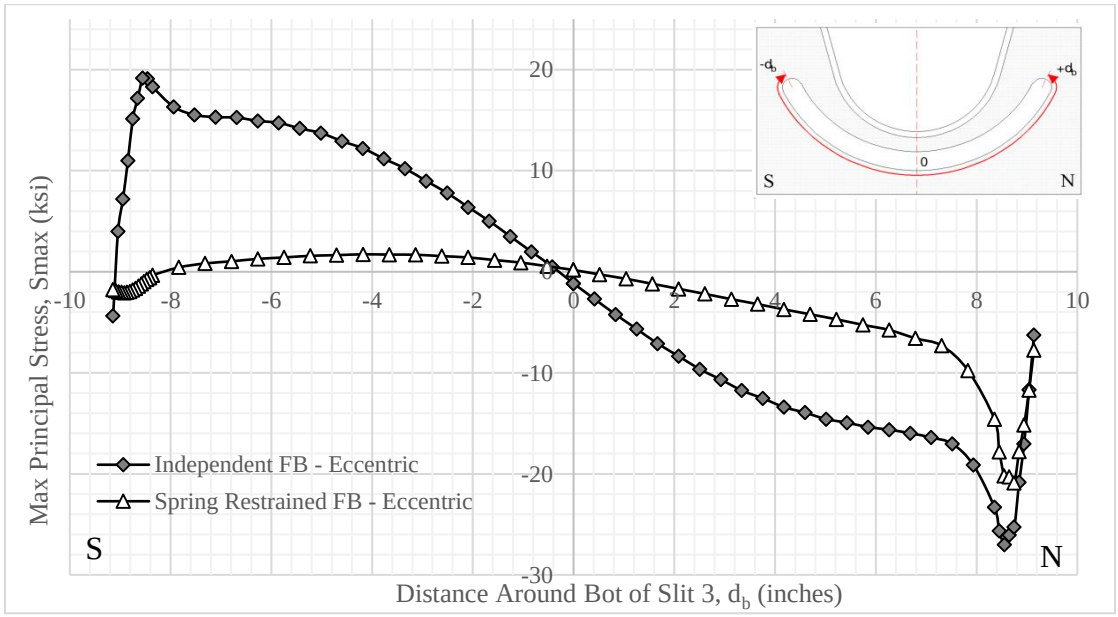

Figure 42. Graph. Variation in maximum principal stresses along bottom of slit RFB connection (Slit 3) of Rib 1 to independent floor beam and spring-restrained floor beam (FBS3) under half tandem in-plane loading with eccentric transverse load position (SMB).

To study the mechanism that dominates the high stresses on the north side of the slit, FEA was conducted with the symmetric transverse load position for Rib 1. This load position significantly reduces the torsion in Rib 1, and reaction forces on the floor beam web from the shear forces in the rib walls are similar on the north and south sides of the slit RFB connection since the north and south rib walls carry similar shear forces. Figure 43 shows the floor beam shear force near Rib 1 adjacent to the edge plate girder is significantly reduced for the spring-restrained floor beam, compared to the independent floor beam.

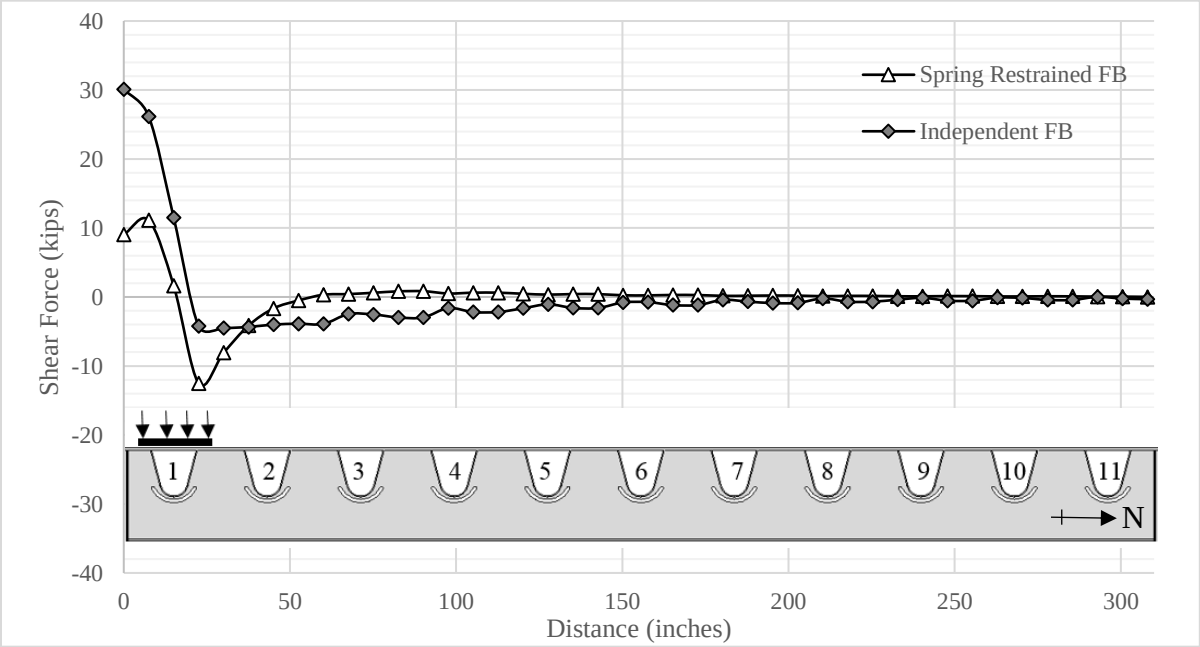

Figure 43. Graph. Shear force in floor beam with slit RFB connection under half tandem in-plane loading with symmetric transverse load position (Rib 1) for independent and spring-restrained floor beams (SMB).

Figure 44 and Figure 45 show the maximum principal stresses along the top and bottom edges of the slit under the half tandem in-plane loading with the symmetric

transverse load position. The variation of these stresses along the slit edge is very different from the variation of stresses for the eccentric transverse load position. The region with the most significant change is on the south side of the slit, where the stress is mostly compression on the bottom and mostly tension on the top. This pattern of stresses is opposite to the stresses observed for the eccentric transverse load position. It was shown previously that the large tension stresses along the bottom, south side of the slit RFB connection for an independent floor beam are from in-plane floor beam shear forces, and that these tension stresses are reduced for a restrained floor beam because the in-plane shear forces are reduced. Here, for the spring-restrained floor beam and the symmetric transverse load position, even though there is still a small shear force on the south side of Rib 1, the stresses on the south side have changed sign and are almost symmetric with those on the north side. This result suggests that when the large tension stresses from the floor beam shear force are reduced (by restraining the floor beam), the reaction forces on the floor beam web from shear forces in the rib walls are the important mechanism causing local deformations and stresses along the slit.

Maximum principal stress contours for the independent and the spring-restrained floor beams with the two transverse load positions can be seen in Figure 46. The tension field from shear force in the floor beam web on the south side near the edge plate girder is clearly visible for the independent floor beam. When this tension field is eliminated for the spring-restrained floor beam, the locations of high stress around the edge of the slit are where the reaction forces on the floor beam web from shear and torsion in the rib are largest.

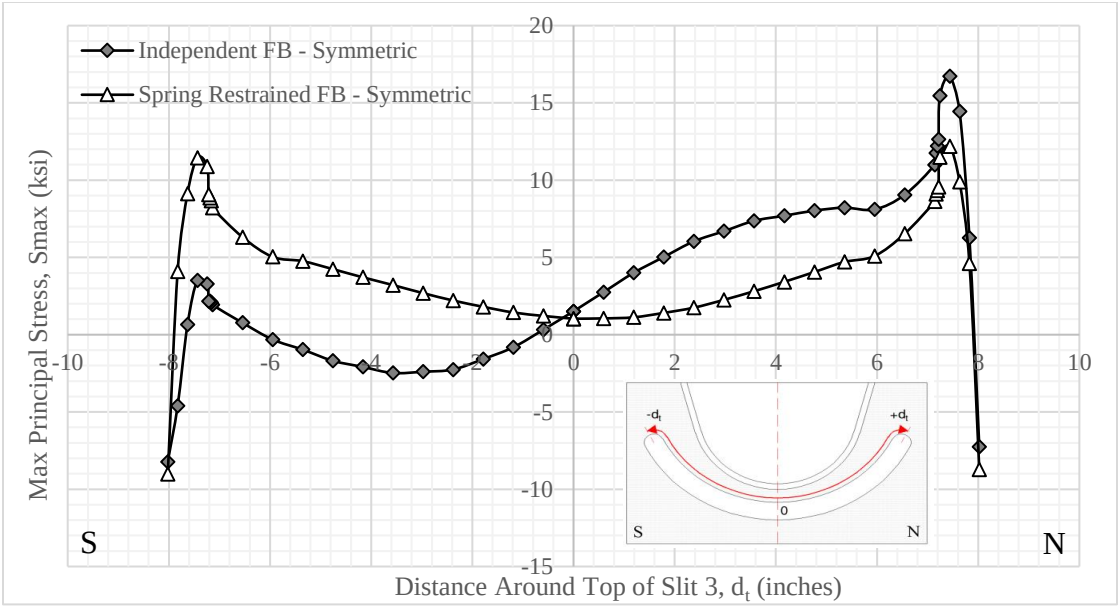

Figure 44. Graph. Variation in maximum principal stresses along top of slit RFB connection (Slit 3) of Rib 1 to independent floor beam and spring-restrained floor beam (FBS3) under half tandem in-plane loading with symmetric transverse load position (SMB).

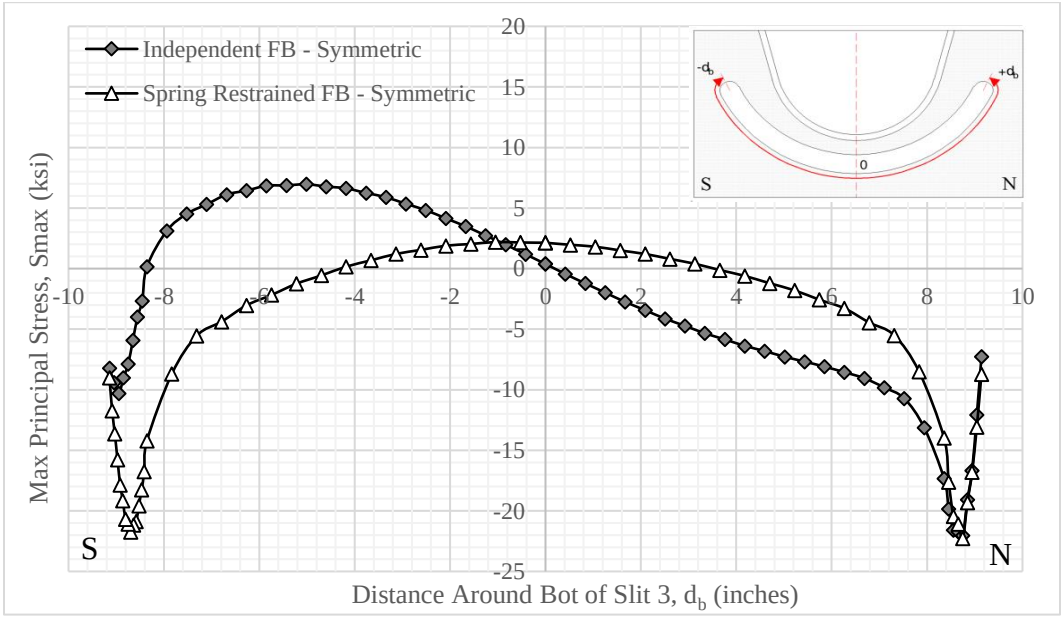

Figure 45. Graph. Variation in maximum principal stresses along bottom of slit RFB connection (Slit 3) of Rib 1 to independent floor beam and spring-restrained floor beam (FBS3) under half tandem in-plane loading with symmetric transverse load position (SMB).

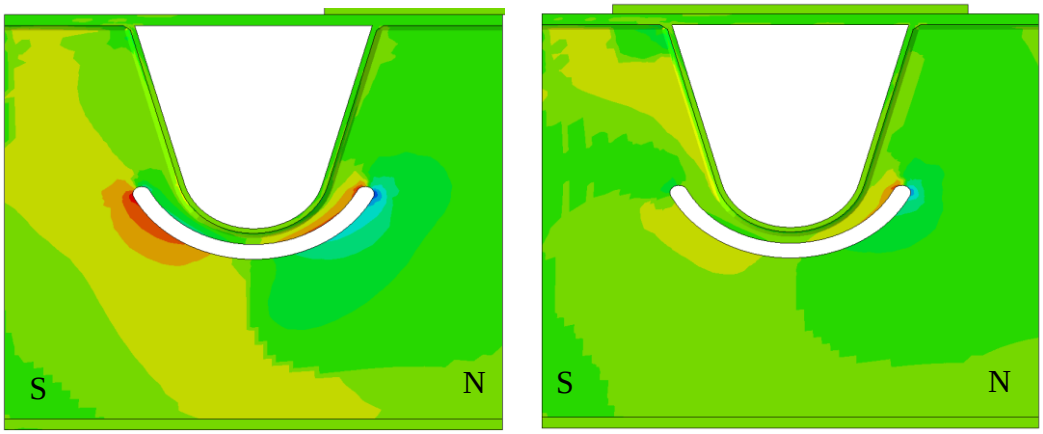

(a) Independent FB, Eccentric **(b) Independent FB, Symmetric**

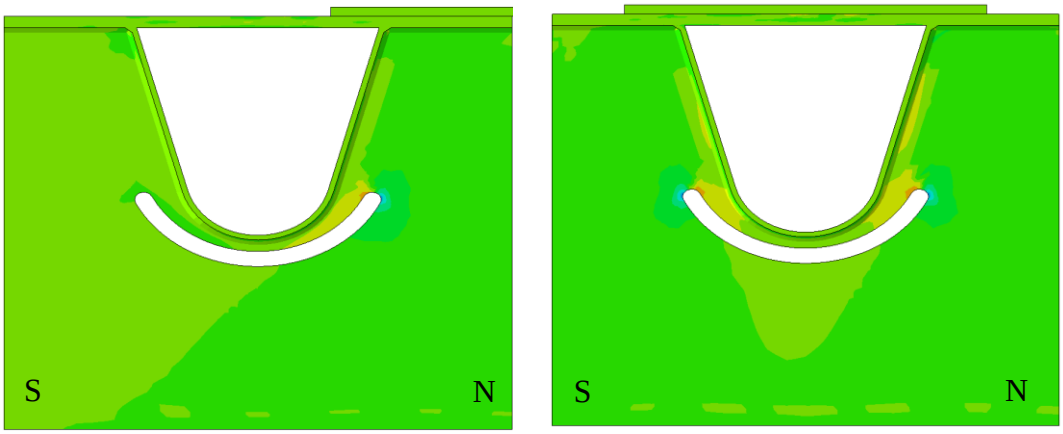

(c) Spring-restrained FB, Eccentric **(d) Spring-restrained FB, Symmetric**

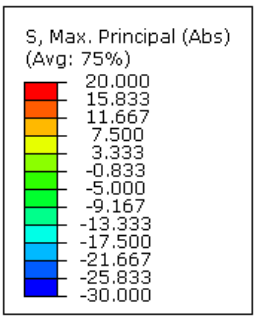

(e) Max Principal Stress Contour Plot Legend

Figure 46. Illustrations. Compound figure with contour plots of maximum principal stresses (ksi) near slit RFB connection (Slit 3) of Rib 1 to independent or spring-restrained floor beam (FBS3) under half tandem in-plane loading with symmetric or eccentric load position (SMB).

3.2.2 Full Tandem Loading Near Rib 1

The FEA studies described above provided understanding of mechanisms which affect the stresses at the slit RFB connection for Rib 1, adjacent to the edge plate girder. Further FEA studies were conducted using the truss system described in Section 2.3.5 to restrain the floor beam while simulating more realistic conditions. The slit RFB connection with the truss-restrained floor beam was studied using the same transverse load position of the full rear tandem axle loading as the slit RFB connection with the independent floor beam, as shown in Figure 47. Figure 48 shows the floor beam shear force which is decreased significantly at Rib 1 for the truss-restrained floor beam compared to the independent floor beam. The decrease is not as significant as for the spring-restrained floor beam.

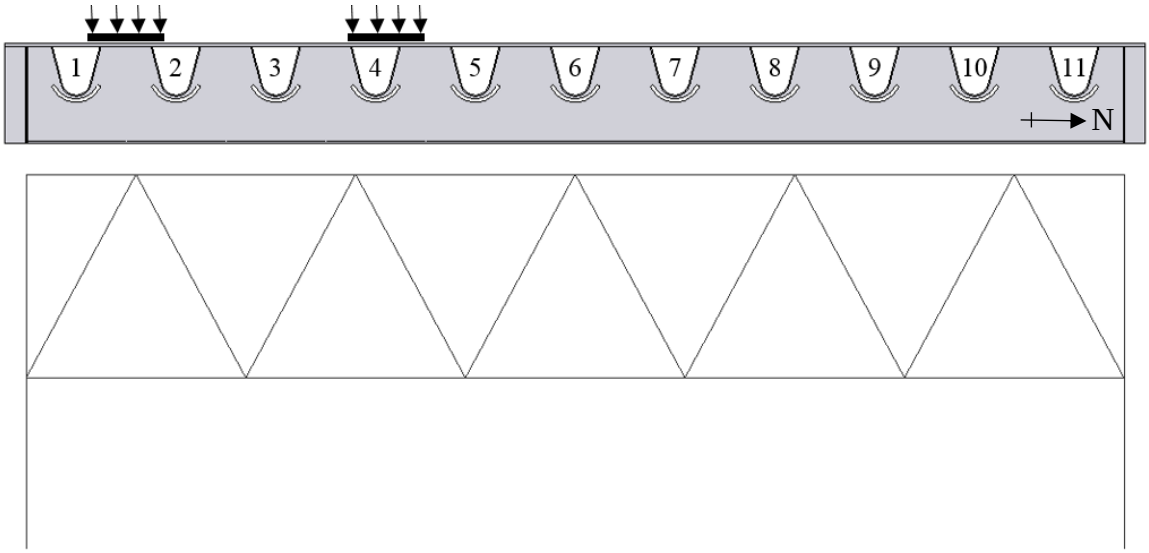

Figure 47. Illustration. Transverse load position of full tandem for truss-restrained floor beam under in-plane loading.

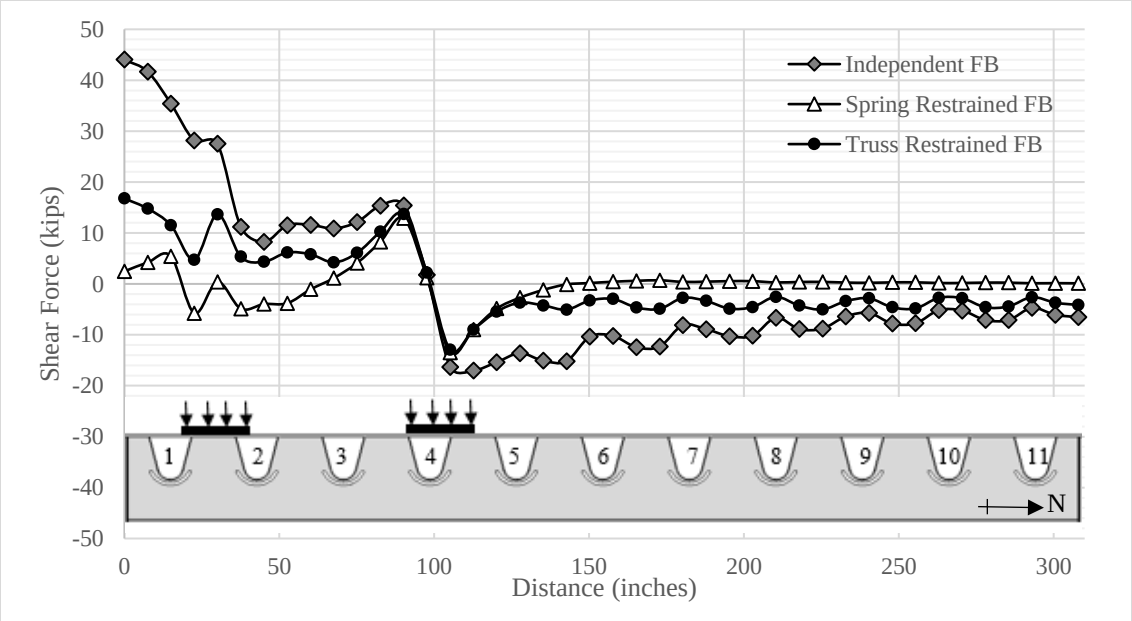

Figure 48. Graph. Floor beam shear force under full tandem in-plane loading for slit RFB connection to independent, spring-restrained, and truss-restrained floor beams (SMB).

The maximum principal stresses along the top and bottom edges of the slit RFB connection of Rib 1 under the loading shown in Figure 47 can be seen in Figure 49 and Figure 50. The tension principal stresses (from SMB) are far below the 24 ksi CAFL for AASHTO Category A. The largest tension principal stress is 15.54 ksi at the top of the north side of the slit, and even with a 43% increase which is expected with further mesh refinement, this stress is below 24 ksi. The largest (in magnitude) compression principal stress is -29.66 ksi at the bottom of the slit on the north side. These critical stress values are much lower than those observed for an independent floor beam, which were 22.74 ksi and -41.10 ksi, respectively.

As noted earlier, compression stresses are considered to contribute to fatigue damage if the tension stresses develop at the same locations under a different fatigue load

position. However, locations which remain in compression under all fatigue load conditions (in combination with dead load stress) are not usually considered when assessing fatigue performance (AASHTO 2016). Since the residual stress pattern at the edge from plasma-cutting the slit into the floor beam web is unknown, and the full range of stresses that may occur at the slit edge from different fatigue load conditions may include tension stresses, the large compression stresses could be critical. Limited research exists on the fatigue resistance of plasma-cut edges, especially when the dominant stress is in compression. For this reason, the large compression stresses at the slit edge are considered to be critical stresses since the stress amplitude exceeds the 24 ksi CAFL for AASHTO Category A and this stress amplitude will increase as the FEA model mesh is refined.

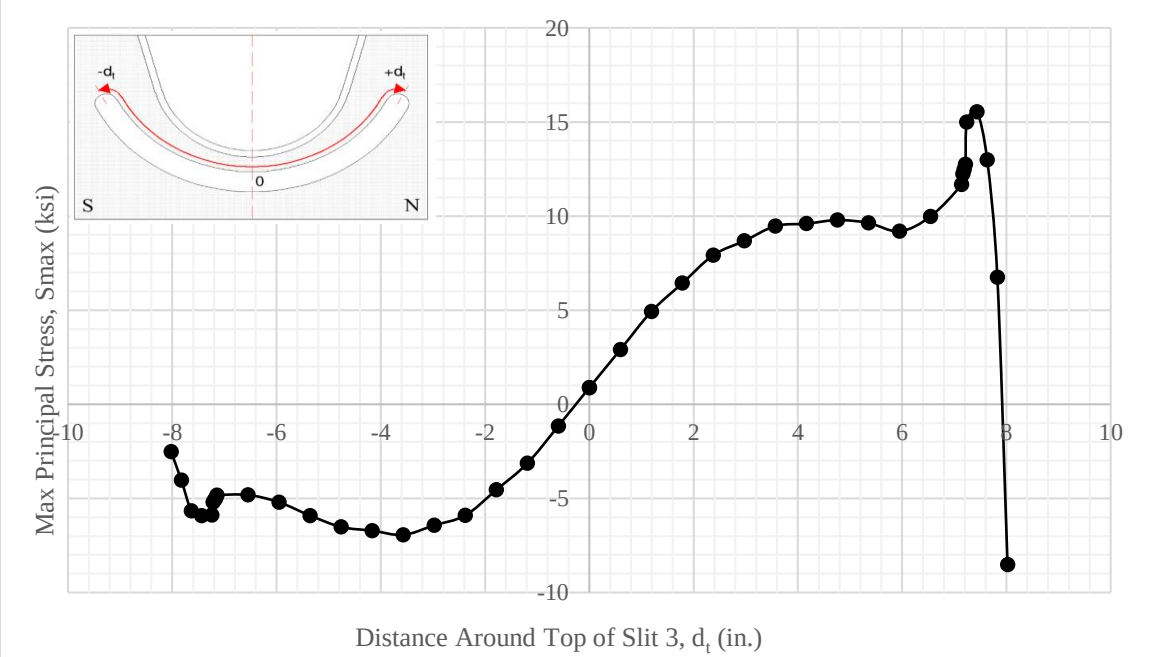

Figure 49. Graph. Variation in maximum principal stresses along top of slit RFB connection (Slit 3) of Rib 1 to truss-restrained floor beam (FBS3) under full tandem in-plane loading (SMB).

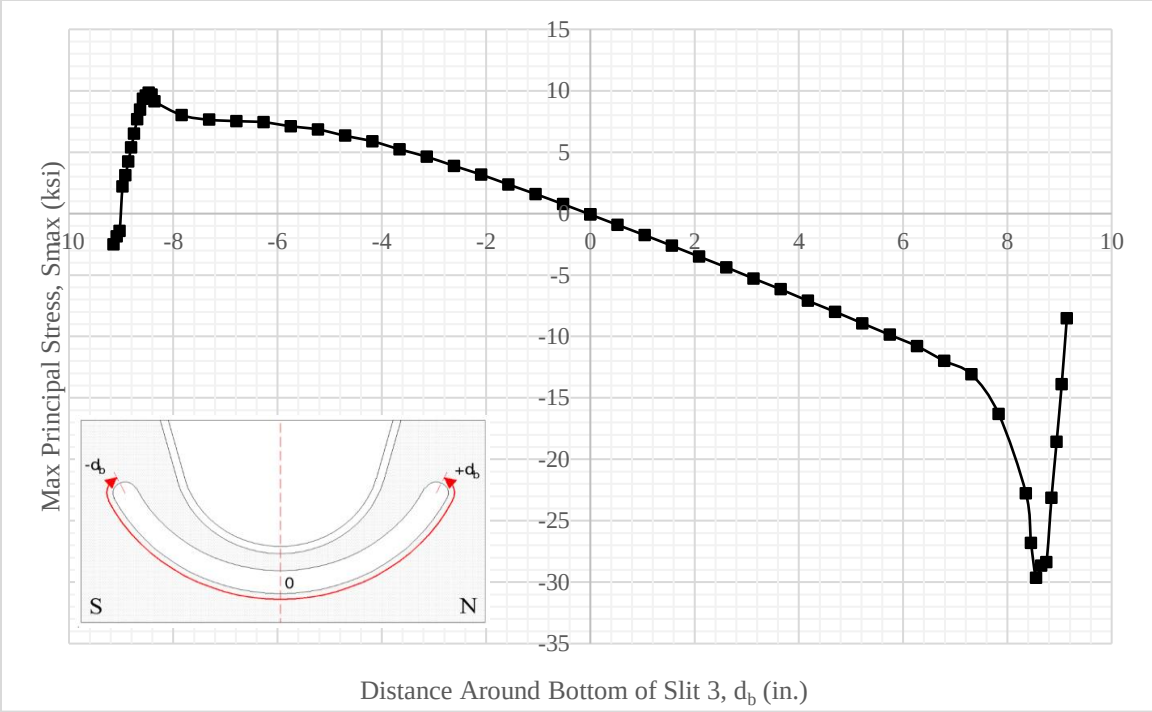

Figure 50. Graph. Variation in maximum principal stresses along bottom of slit RFB connection (Slit 3) of Rib 1 to truss-restrained floor beam (FBS3) under full tandem in-plane loading (SMB).

3.2.3 Full Tandem Loading Away From Rib 1

FEA were performed that focused on a slit RFB connection which is unaffected by the conditions at Rib 1 which is adjacent to the reaction point for the floor beam shear at the edge plate girder. Rib 6, the rib at midspan of the floor beam, was the focus of the FEA study. Half of the rear tandem axle loading was used to focus the study on the effects of the transverse position of the two load pads and to eliminate the floor beam shear force response from the additional two load pads that are included in the full tandem axle loading. Similar to the previous studies of loading at Rib 1, two transverse positions were studied, namely the symmetric transverse load position in Figure 51(a), with the load pads centered

on Rib 6, and the eccentric transverse load position in Figure 51(b), with half tandem centered between Rib 6 and Rib 7.

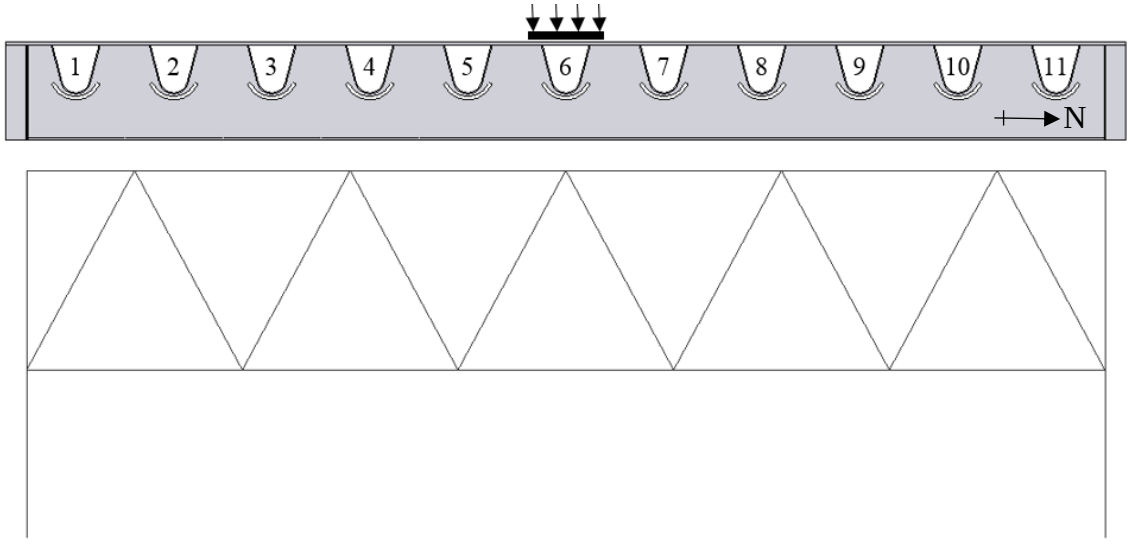

(a) Symmetric transverse load position with half tandem centered on Rib 6

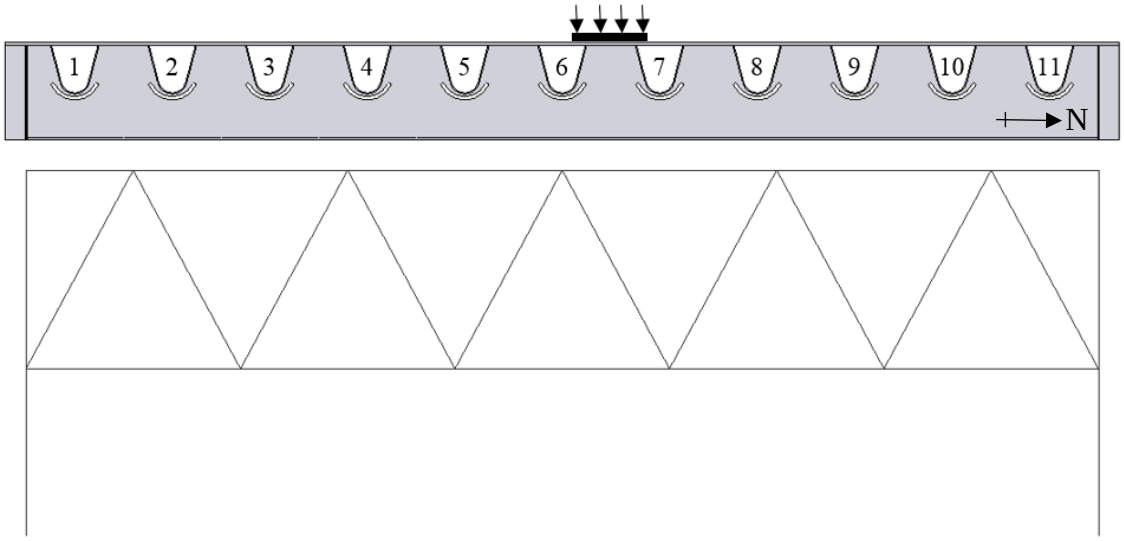

(b) Eccentric transverse load position with half tandem centered between Rib 6 and Rib 7

Figure 51. Illustrations. Compound figure showing transverse load positions for slit RFB connection (Slit 3) of Rib 6 to truss-restrained floor beam (FBS3) under in-plane loading.

Maximum principal stress contour plots for the symmetric and eccentric transverse load positions are shown in Figure 52. The largest stresses along the edges of the slits are at locations closest to the load pads. The stress responses tend to be symmetric about the longitudinal centerline of the load pads (transverse to the floor beam) for both the symmetric and eccentric transverse load positions.

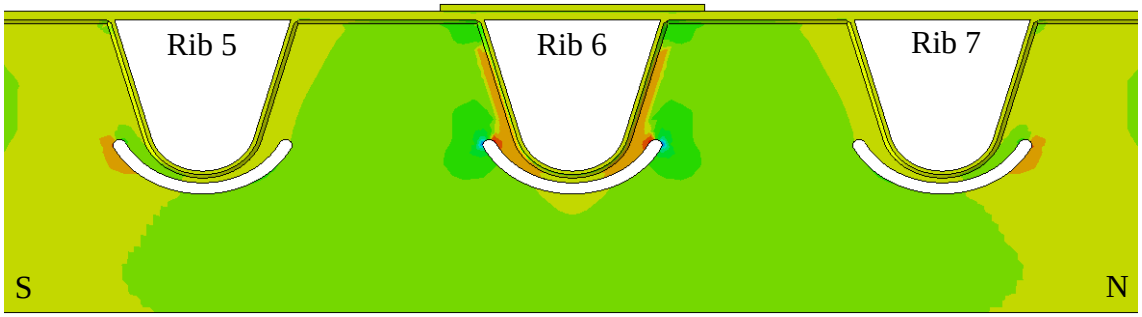

(a) Symmetric Transverse Load Position

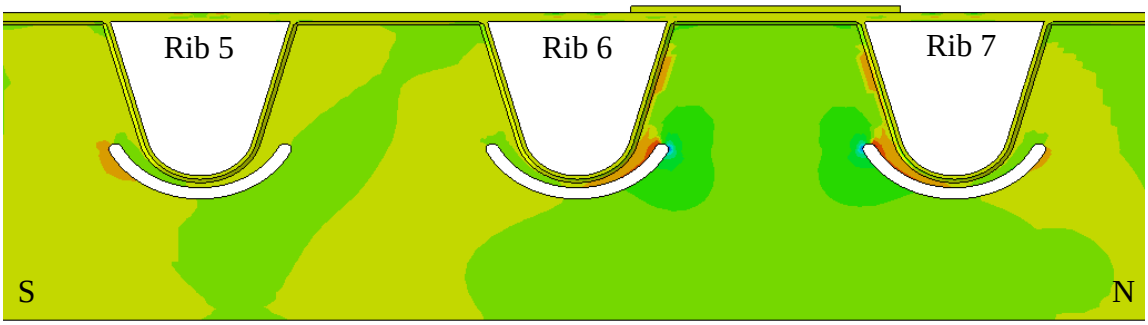

(b) Eccentric Transverse Load Position

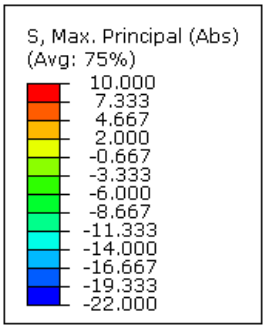

(c) Max Principal Stress Contour Plot Legend

Figure 52. Illustrations. Compound figure with contour plots of maximum principal stresses (ksi) near slit RFB connection (Slit 3) of Rib 6 to truss-restrained floor beam (FBS3) under half tandem in-plane loading with symmetric or eccentric load position (SMB).

For the symmetric transverse load position, the largest tension principal stress is 8.96 ksi at the top of each side of the slit beneath Rib 6. The largest compression principal stress is -19.79 ksi at the bottom of each side of this slit. These stress values from SMB are significantly below the 24 ksi CAFL for AASHTO Category A. The maximum tension principal stresses at the slits of adjacent Rib 5 and Rib 7 have a value of only 5.81 ksi.

For the eccentric transverse load position, a large tension principal stress of 9.06 ksi is at the top north edge of the slit beneath Rib 6 and a large tension principal stress of 8.79 ksi is at the top south edge of the slit beneath Rib 7. A large compression principal stress of -19.88 ksi is at the bottom north edge of the slit beneath Rib 6 and a large compression principal stress of -19.54 ksi is at the bottom south edge of the slit beneath Rib 7. Again, these stress values from SMB are below the 24 ksi CAFL for AASHTO Category A. Also noteworthy from the stress values is the sharp stress gradient at the top, south edge of the Rib 6 slit and the top south edge of the Rib 7 slit where the stress varies from about 9 ksi in tension to about -20 ksi in compression over a short distance. These stresses have an approximately symmetric distribution about the centerline of the load pads. The stresses for the eccentric transverse load position are slightly larger than those for the symmetric load position as a result of torsion in the ribs from the eccentric load position.

For both transverse load positions near Rib 6, the pattern of tension stresses at the top edge of the slit and compression stresses at the bottom edge of the slit, are similar to the stress pattern for the north edge of the slit at Rib 1 when the load pads were eccentric (transversely, between Rib1 and Rib 2) for both independent and restrained floor beams. This pattern of stresses is caused by reaction forces on the floor beam web from shear and

torsion in the rib which produce local deformation and stress at the top edge of the slit. These stresses do not appear to be most critical for the slit RFB connection since the stresses on the south edge of the slit at Rib 1 (adjacent to the edge plate girder) from in-plane floor beam shear forces appear to be the most critical stresses for the slit RFB conneciton. Therefore, the subsequent FEA studies focus on the slit RFB connection at Rib 1 near the edge plate girder.

3.2.4 Slit Geometry Parameter Study

Various slit geometries for the slit RFB connection with the truss-restrained floor beam were investigated using FEA to study the effect of slit geometry on the largest stresses at the Rib 1 RFB connection. Certain geometric parameters of the slit, defined in Figure 28, were varied as described below. The full rear tandem axle loading was used in the study, and the load position was the transverse position used previously, shown in Figure 29 and Figure 47, because this position produced critical stresses at the slit edge. The floor beam depth and thickness was 26.5 inches and $^1/_2$ inch, respectively. This floor beam section was termed FBS3, above. The deck plate and floor beam flange were both $^3/_4$ inch thick, resulting in a total SOBD depth of 28 inches.

Radius 1 and Radius 2

The first slit geometric parameters that were studied were the radii of the larger arcs which make up the slit, Radius 1 and Radius 2. Dimensioned drawings of the relevant slit geometries can be found in Figure 53. The geometry with the smallest Radius 1 and Radius 2, Slit 1, uses arcs which are concentric with the arc of the rib bottom. Slit 3, Slit 4, and Slit 5 gradually increase the radii of these arcs to "flatten" the geometry of the slit. All four

geometries have the same Radius 3, tab width, and slit width: $^{1}/_{2}$ inch, $^{3}/_{4}$ inch, and 1 inch, respectively.

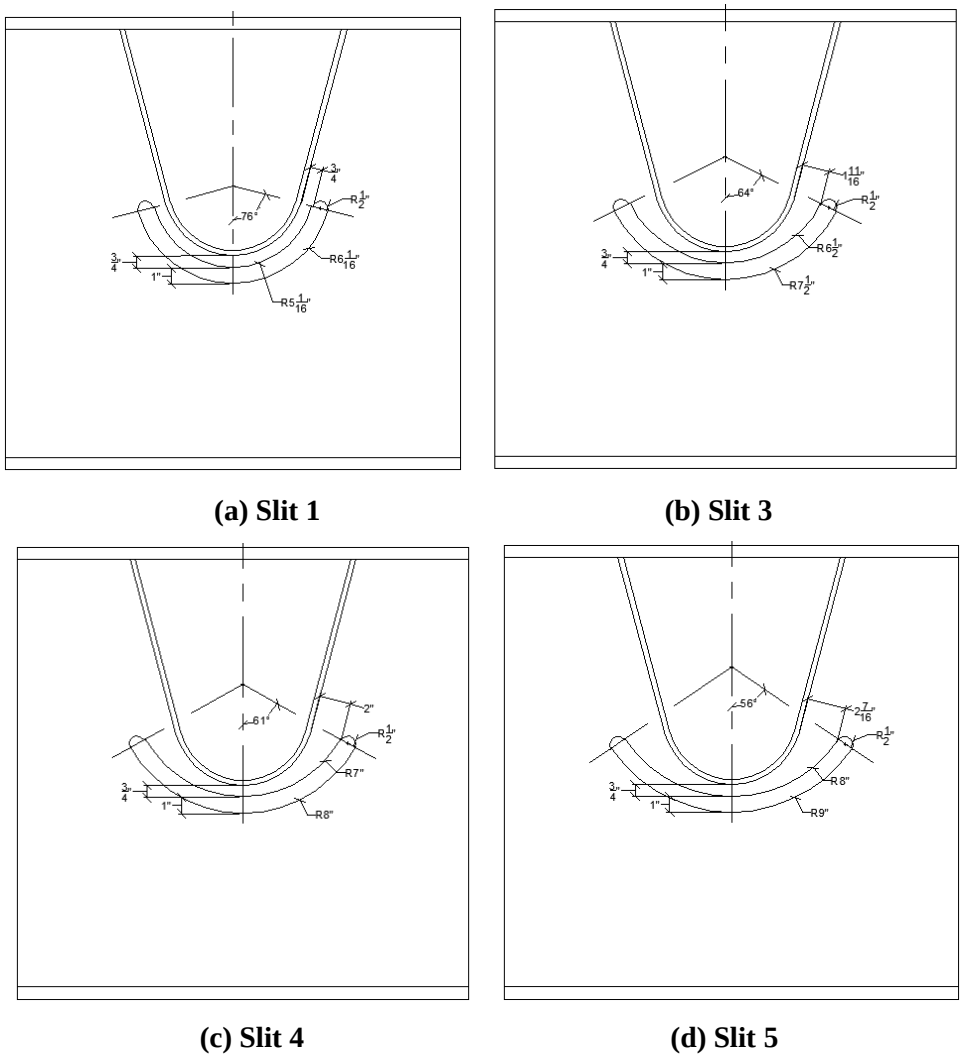

(a) Slit 1 **(b) Slit 3**

(c) Slit 4 **(d) Slit 5**

Figure 53. Illustrations. Compound figure showing four slit geometries with varying Radius 1 and Radius 2.

Principal stress results from FEA using SMB for the slit edges on the north and south sides of the slit RFB connection are given in Table 5. The stresses on the north side

of the slit RFB connection (away from the diagonal tension stress field on the south side), which were previously shown to be caused by reaction forces on the floor beam web from shear and torsion in the rib, have a clear pattern as Radius 1 and Radius 2 are increased and the slit is "flattened". "Flattening" the slit decreases the tension stress on the top of the slit, but increases the compression stress at the bottom of the slit. The reduction in tension on the top, north side of the slit could be due to the additional material between the slit edge and the rib-to-floor beam weld where the reaction forces are transferred. The tension stresses on the south side of the slit (adjacent to or within the diagonal tension stress field from shear in the floor beam web) also demonstrate a trend. As the slit geometry is "flattened" the tension stresses on the south side of the connection generally increase. Theses stresses were previously shown to be dominated by the diagonal tension stress field in the floor beam web due to shear. As the slit is flattened, the opening dips further into this tension field, creating larger tension stresses at the slit edge.

Table 5. Largest principal stresses on north and south sides of slit RFB connection of Rib 1 to truss-restrained floor beam (FBS3) under in-plane loading for slit geometries with varying Radius 1 and Radius 2 (SMB).

Slit Geometry Name	Radius No. 1 (inches)	Radius No. 2 (inches)	Radius No. 3 (inches)	South Tension Principal Stress (ksi)	South Comp. Principal Stress (ksi)	North Tension Principal Stress (ksi)	North Comp. Principal Stress (ksi)
Slit 1	5 1/16	6 1/16	1/2	8.04	-8.47	20.23	-25.37
Slit 3	6 1/2	7 1/2	1/2	9.84	-6.94	15.54	-29.66
Slit 4	7	8	1/2	9.81	-7.56	14.27	-30.56
Slit 5	8	9	1/2	10.95	-8.80	12.02	-33.04

Radius 3

The next slit geometric parameter that was studied was the radius of the small, upper arc of the slit, Radius 3. Dimensioned drawings of the relevant slit geometries can be found in Figure 57. Slit 1, Slit 2, and Slit 6 all have the same Radius 1 value of 5 $^{1}/_{16}$ inches. Slit 1 is the base case with an upper Radius 3 of $^{1}/_{2}$ inch, Slit 2 utilizes a keyhole shape to increase the radius to $^{3}/_{4}$ inch, and Slit 6 gradually increases the slit opening to achieve a Radius 3 of $^{13}/_{16}$ inch. Slit 3, Slit 7, and Slit 8 all have the same Radius 2 value of 7 $^{1}/_{2}$ inches with increasing values of Radius 3. All six slit geometries have the same tab width and slit width: $^{3}/_{4}$ inch and 1 inch, respectively.

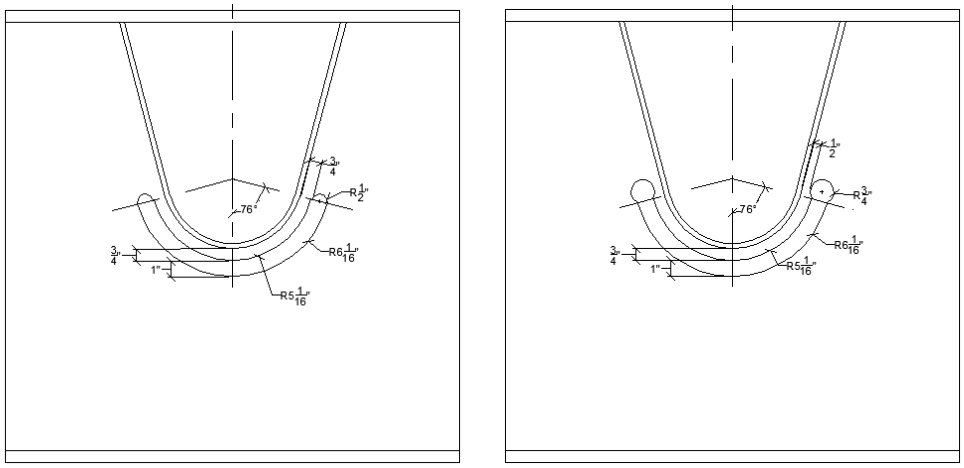

(a) Slit 1 **(b) Slit 2**

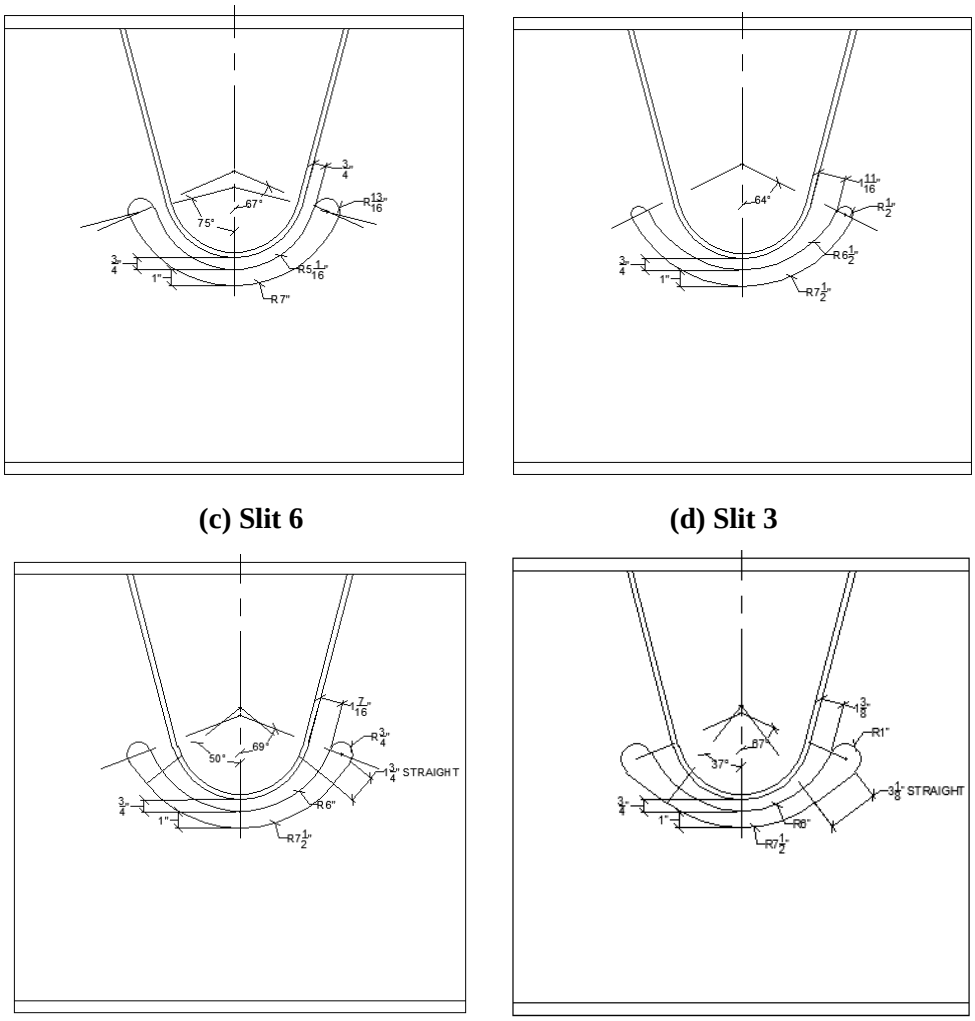

(c) Slit 6 **(d) Slit 3**

(e) Slit 7 **(f) Slit 8**

Figure 54. Illustrations. Compound figure showing three slit geometries with varying Radius 3.

Principal stress results from FEA using SMB for the slit edges on the north and south sides of the slit RFB connection are given in Table 6. One observation from these results is that the addition of a keyhole at the top of the slit (Slit 2), instead of a gradual change in radius (Slit 6), creates higher stresses along the slit edge. This is true for both tension and compression stresses on both the north and south sides of the slit. The stress

concentrations at the edge of the slit from the keyhole (Slit 2) are above the Category A CAFL of 24 ksi for SMB.

It can also be seen that increasing Radius 3 increases the tension stresses on the south side of the Rib 1 slit RFB connection. These stresses are dominated by the diagonal tension stress field from shear in the floor beam web deviating around the south side of the slit. When Radius 3 is increased, the slit is pushed further into this tension field, which increases the tension stress on the slit edge. Since the floor beam is supported by a truss, most tension stresses (excluding those for Slit 2) are still below the AASHTO Category A CAFL.

Table 6. Largest principal stresses on north and south sides of slit RFB connection of Rib 1 to truss-restrained floor beam (FBS3) under in-plane loading for slit geometries with varying Radius 3 (SMB).

Slit Geometry Name	Radius No. 1 (inches)	Radius No. 2 (inches)	Radius No. 3 (inches)	South Tension Principal Stress (ksi)	South Comp. Principal Stress (ksi)	North Tension Principal Stress (ksi)	North Comp. Principal Stress (ksi)
Slit 1	5 1/16	6 1/16	1/2	8.04	-8.47	20.23	-25.37
Slit 2	5 1/16	6 1/16	3/4	11.44	-10.74	26.15	-31.74
Slit 6	5 1/16	7	13/16	8.98	-8.11	18.35	-26.10
Slit 3	6 1/2	7 1/2	1/2	9.84	-6.94	15.54	-29.66
Slit 7	6	7 1/2	3/4	11.44	-6.24	15.52	-32.34
Slit 8	6	7 1/2	1	12.10	-6.56	14.87	-28.43

Tab Width

The width of the tab between the bottom of the rib and the top edge of the slit was varied for two separate slit geometries, Slit 1 and Slit 3, to study the effect on the stresses

around the slit edge. The tab width varies around the connection for many of the slit geometries (when the arc defined by Radius 1 is not concentric with the arc of the rib bottom), so the tab width, t_{tab}, is defined by the width at the centerline of the rib (see Figure 28). The original geometries for Slit 1 and Slit 3 can be seen in Figure 53(a) and Figure 53(b) where the tab width, t_{tab}, is $^3/_4$ inch. The tab width was decreased to $^1/_2$ inch (denoted with a "b" e.g. Slit 1b) and increased to 1 $^1/_2$ inches (denoted with a "c" e.g. Slit 1c). The width of the slit was kept the same at 1 inch.

Principal stress results from FEA using SMB for the slit edges on the north and south sides of the slit RFB connection are given in Table 7. There does not appear to be any clear effect associated with changing the tab width. In some locations, such as the location of maximum compression stress on the south side of the connection, increasing the tab width causes the stresses to increase in magnitude. In other locations, such as the north side of the Slit 1 connection, there is no significant change in the stresses.

Table 7. Largest principal stresses on north and south sides of slit RFB connection of Rib 1 to truss-restrained floor beam under in-plane loading for slit geometries with varying tab width (SMB).

Slit Geometry Name	Tab Width t_{tab} (inches)	South Tension Principal Stress (ksi)	South Comp. Principal Stress (ksi)	North Tension Principal Stress (ksi)	North Comp. Principal Stress (ksi)
Slit 1b	$^1/_2$	8.07	-7.36	20.23	-25.51
Slit 1	$^3/_4$	8.04	-8.47	20.23	-25.37
Slit 1c	1 $^1/_2$	8.50	-8.67	20.67	-25.82
Slit 3b	$^1/_2$	9.15	-6.80	16.36	-26.76
Slit 3	$^3/_4$	9.84	-6.94	15.54	-29.66
Slit 3c	1 $^1/_2$	8.56	-12.06	22.37	-27.64

Slit Width

The width of the slit was also studied. Similar to the tab width, the slit width, t_{slit}, is defined by the width at the centerline of the rib (see Figure 28). The slit width was typically 1 inch for the slit geometries studied, however, for Slit 9, the width was decreased to $^1/_2$ inch. The rest of the slit geometry is similar to the geometry for Slit 1. Dimensioned drawings of the Slit 1 and Slit 9 geometries can be seen in Figure 58. The tab width was $^3/_4$ inch.

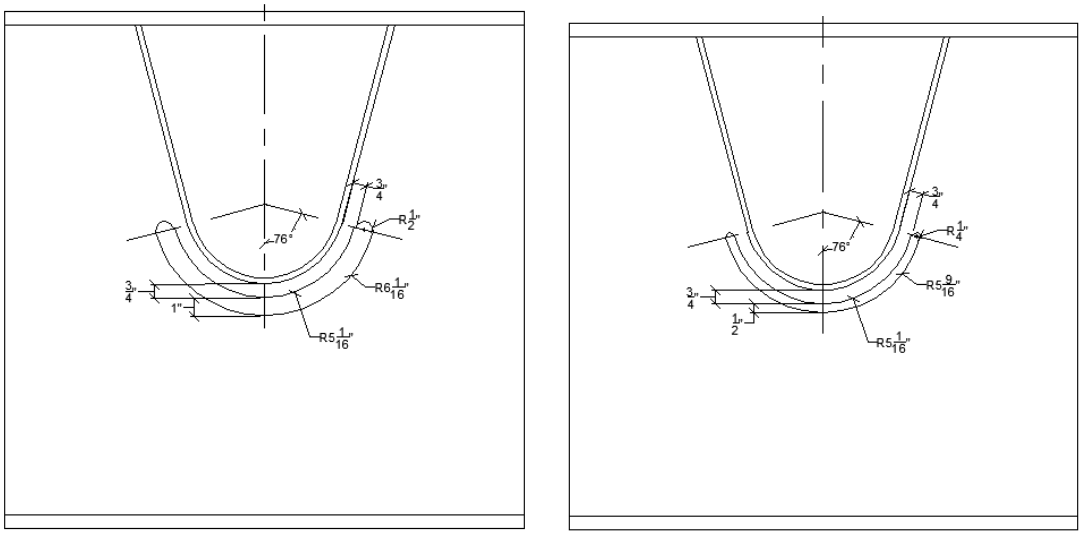

(a) Slit 1 **(b) Slit 9**

Figure 55. Illustrations. Compound figure showing two slit geometries with varying slit width, t_{slit}.

Principal stress results from FEA using SMB for the slit edges on the north and south sides of the slit RFB connection are given in Table 8. Decreasing the size of the slit increased the magnitude of all the critical stresses along the slit edge. The thinner opening

requires a smaller upper Radius 3. The critical stresses that develop at the top of the slit are inversely proportional to Radius 3, and the smaller radius for Slit 9 (resulting from the smaller slit width) compared to Slit 1 creates higher stresses.

Table 8. Largest principal stresses on north and south sides of slit RFB connection of Rib 1 to truss-restrained floor beam under in-plane loading for slit geometries with varying slit width (SMB).

Slit Geometry Name	Radius No. 1 (inches)	Radius No. 2 (inches)	Radius No. 3 (inches)	Slit Width t_{slit} (inches)	South Tension Principal Stress (ksi)	South Comp. Principal Stress (ksi)	North Tension Principal Stress (ksi)	North Comp. Principal Stress (ksi)
Slit 1	5 1/16	6 1/16	1/2	1	8.04	-8.47	20.23	-25.37
Slit 9	5 1/16	5 9/16	1/4	1/2	8.66	-9.30	23.78	-28.33

3.3 Out-of-plane Loading with a Restrained Floor Beam

FEA studies of the slit RFB connection with a restrained floor beam under out-of-plane loading were conducted. In these studies, the floor beam section (FBS3) had a web depth of 26.5 inches and a web thickness of 1/2 inch, which provided the smallest web area below the rib among the floor beam sections that were studied previously. The deck plate and floor beam flange both had a thickness of 3/4 inch, resulting in an overall SOBD depth of 28 inches. The floor beam bottom flange was restrained using the truss system. The floor beam spacing is 20 feet, the recommended upper limit for floor beam spacing (Connor et al. 2012), to maximize the rib rotation and other effects from out-of-plane loads. The FEA results from the parametric slit geometry study above show that Slit 8 has relatively small values of the largest tension principal stress on both the south and north sides of the slit

RFB connection, and also has a moderate value of the largest compression principal stress on the north side. Also, the larger Radius 3 of the Slit 8 geometry was thought to be easier to fabricate and more practical. Therefore, the Slit 8 geometry, shown in Figure 56, was used in the slit RFB connection for the out-of-plane loading studies.

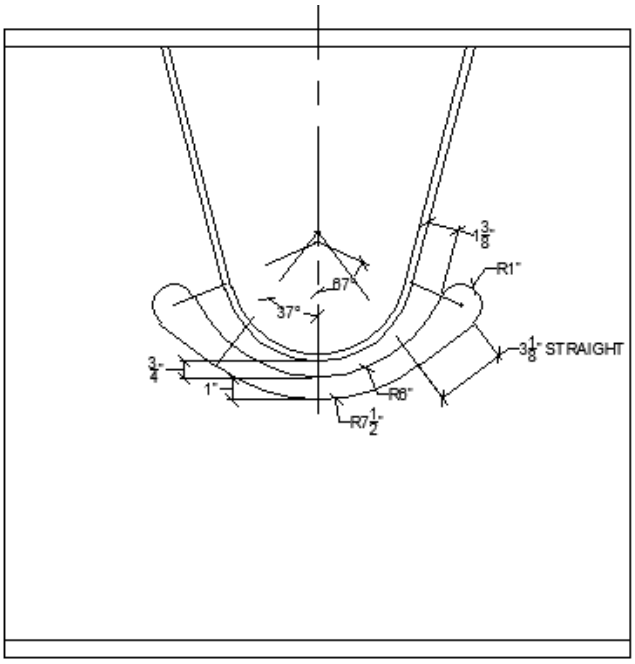

Figure 56. Illustration. Dimensioned Slit 8 RFB connection.

3.3.1 Half Tandem Loading to Determine Critical Longitudinal Load Positions

Initial FEA using MA were conducted to determine the out-of-plane load condition which created the most critical stresses for the slit RFB connection. To isolate the effect of out-of-plane rib rotation, half of the rear tandem axle loading was used and the half tandem was placed in a transverse load position with the load pads centered on Rib 6, as shown in Figure 51(a). Eleven different longitudinal positions of the half tandem were studied to

determine which position resulted in the most critical out-of-plane stresses. The center of the half tandem was moved in 2 foot increments from the center of Floor Beam 3 west towards Floor Beam 4 as shown in Figure 57; starting with tandem centered on Floor Beam 3 and ending with the tandem centered on Floor Beam 4.

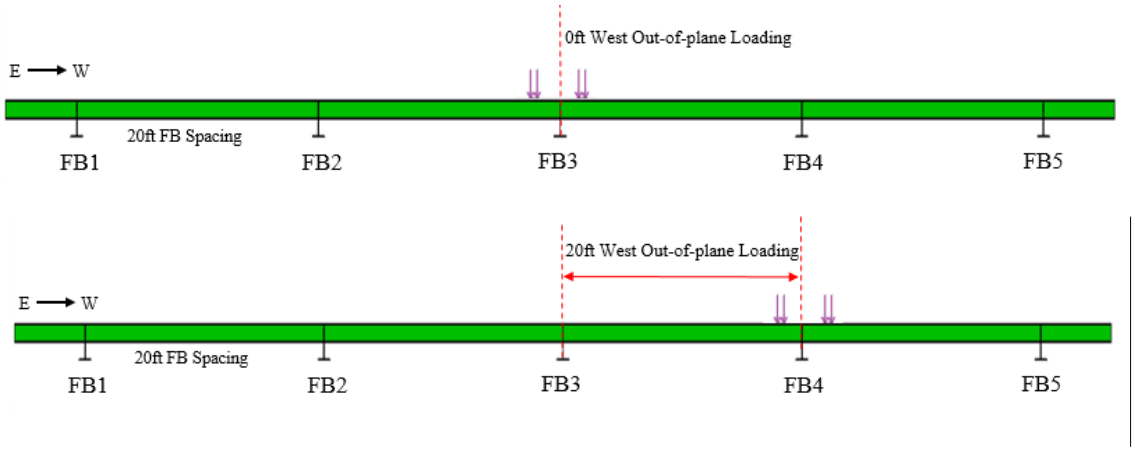

Figure 57. Illustration. Longitudinal load position variation for out-of-plane loading.

The large compression principal stress on the bottom north edge of the slit, found to be critical in the previous FEA studies of in-plane loading described above, was noted for each longitudinal load position. This stress value was at the mid-surface of the floor beam web, similar to the values presented for the studies of in-plane loading presented earlier. In addition, the stress values from the west face and east face of the floor beam web were also noted to reflect the effect of web plate bending which is the anticipated out-of-plane response to rib rotation. As the half tandem loading is moved from Floor Beam 3 toward Floor Beam 4 and the loading moves toward the mid span of the ribs, the ribs and deck plate deflect downward, resulting in rotation of the ribs into the span at the locations

where the ribs are supported by the floor beam. The web plate bending from compatibility with the rib rotation results in differences in the stresses on the west and east face of the floor beam web at the slit edge. This difference in the stresses on the west face and east face, is the portion of the stress from by out-of-plane bending. The stresses from these three locations for all eleven longitudinal load positions are shown in Figure 58 and summarized in Table 9.

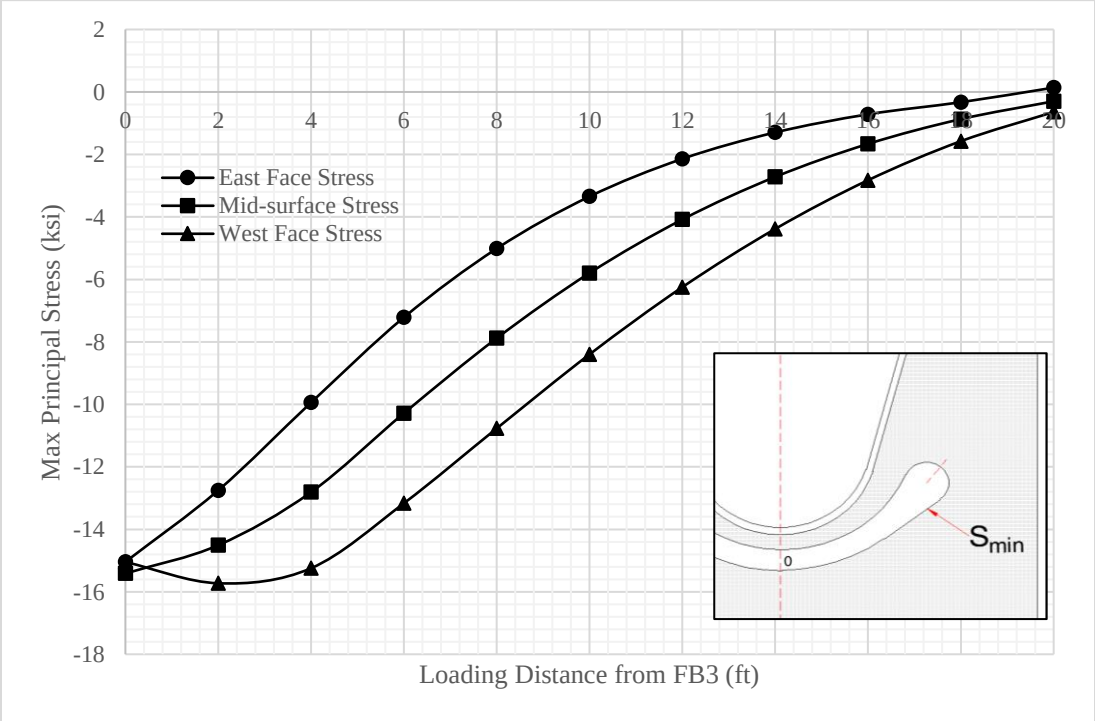

Figure 58. Graph. Largest compression principal stress at bottom north edge of slit RFB connection (Slit 8) of Rib 6 to truss-restrained floor beam (FBS3) on west face, east face, and mid-surface of web for various longitudinal load positions (MA).

Table 9. Largest compression principal stress at bottom north edge of slit RFB connection (Slit 8) of Rib 6 to truss-restrained floor beam (FBS3) on east and west face of web for various longitudinal load positions (MA).

Load Position (feet)	Stress on East Face (ksi)	Stress on West Face (ksi)	Difference (ksi)
0	-15.04	-15.05	0.01
2	-12.75	-15.73	2.98
4	-9.94	-15.25	5.31
6	-7.22	-13.17	5.95
8	-5.01	-10.77	5.76
10	-3.35	-8.40	5.05
12	-2.14	-6.25	4.11
14	-1.30	-4.38	3.08
16	-0.72	-2.83	2.11
18	-0.33	-1.58	1.25
20	0.14	-0.64	0.78

The study of longitudinal load position has two main results. First, the largest out-of-plane effect occurs when the half tandem is centered six feet west of Floor Beam 3, resulting in the maximum out-of-plane bending of the slit RFB connection. The difference in stress between the east and west faces was 5.95 ksi. Second, the longitudinal load position with the full tandem centered two feet west of Floor Beam 3 produces the largest compression stress. A compression principal stress of -15.73 ksi developed on the west face of the floor beam web at the slit edge which is slightly greater than the largest compression stress for in-plane loading (-15.05 ksi). In this longitudinal load position two feet west, one load pad of the half tandem is directly centered on Floor Beam 3, and the other load pad is four feet into the rib span between Floor Beam 3 and Floor Beam 4. This creates a large in-plane response at the slit edge like that seen previously, while also

introducing some out-of-plane loading response from rib rotation. Since the in-plane response was studied earlier and this FEA study focused on out-of-plane effects, the six foot longitudinal load position, which caused the largest out-of-plane stress component, was the focus of the out-of-plane studies.

3.3.2 Half Tandem Loading Away From Rib 1

Similar to the earlier FEA, two transverse positions were studied, namely the symmetric transverse load position in Figure 59(a), with the half tandem centered on Rib 6, and the eccentric transverse load position in Figure 59(b), with the half tandem centered between Rib 6 and Rib 7.

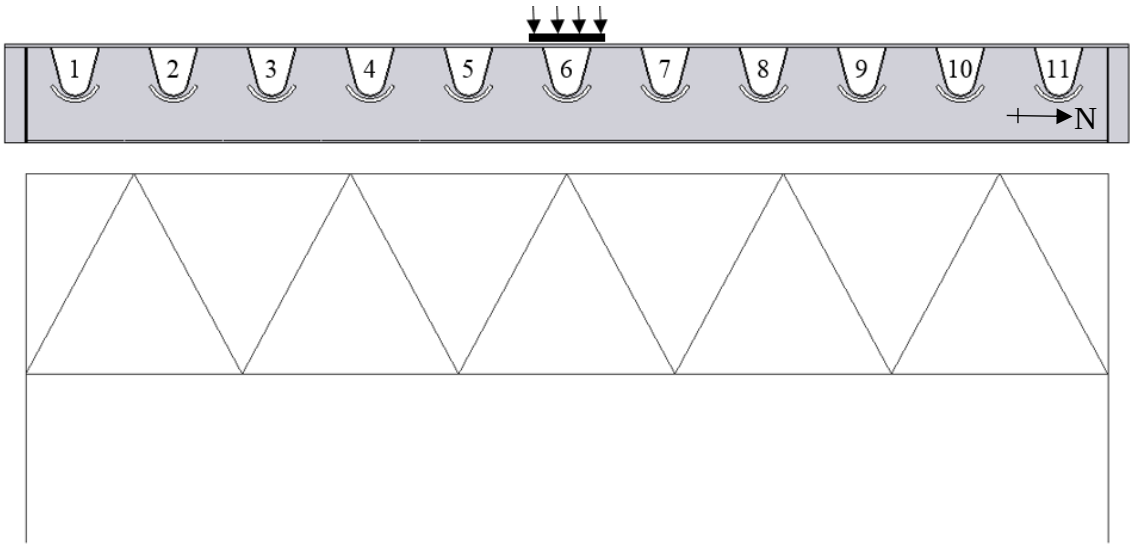

(a) Symmetric transverse load position with half tandem centered on Rib 6

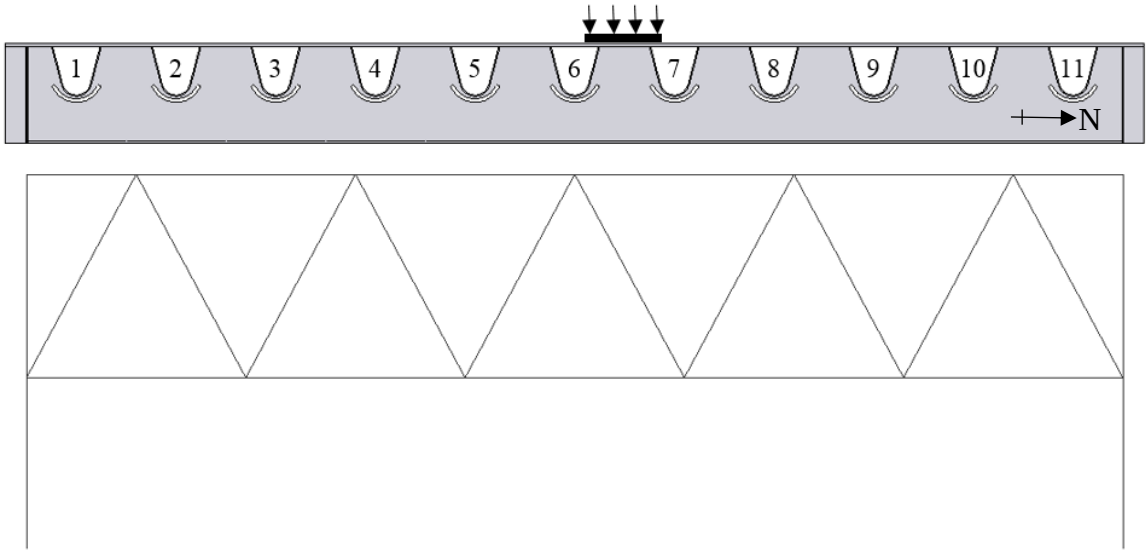

(b) Eccentric transverse load position with half tandem centered on Rib 6

Figure 59. Illustrations. Compound figure showing transverse load positions for slit RFB connection (Slit 8) of Rib 6 to truss-restrained floor beam (FBS3) under out-of-plane loading.

When the half tandem is located 6 feet west of Floor Beam 3 and the transverse load position is symmetric on Rib 6, the stresses on the east and west faces of the floor beam web from the FEA using SMB are shown in Figure 60 and Figure 61. The stresses are below the 24 ksi CAFL of AASHTO Category A, and the 6.65 ksi difference in stresses between the east and west faces on the bottom north side of the slit from out-of-plane bending of the web plate is the largest difference at the edge of the slit.

Figure 62 and Figure 63 show SMB stresses normal to the weld toes of the fillet weld of the slit RFB connection for the symmetric transverse load position on Rib 6, both on the rib wall and the floor beam web. The stresses normal to the rib wall fillet weld toe (Figure 62) are all compression stresses. On the east side of the floor beam at the bottom

of the rib, the largest compressive stress at the rib weld toe is -10.39 ksi. The magnitude of this stress is above the 10 ksi CAFL for AASHTO Fatigue Category C. Compression stresses are expected to contribute to fatigue damage only if tension stresses develop at the same location under a different fatigue loading condition. Since the full range of stresses that may occur at the bottom of the rib at the rib wall weld toe from different fatigue load conditions may include tension stresses, the large compression stresses could be critical. However, the addition of sustained loads such as the weight of the steel used in the SOBD or the wearing surface on the deck will likely create additional compression stresses at the weld toes of the slit RFB connection which may make the full stress range at the rib wall weld toe compressive.

The stresses normal to the floor beam fillet weld toe (Figure 63) are small. These stresses are well below the 10 ksi CAFL for AASHTO Fatigue Category C.

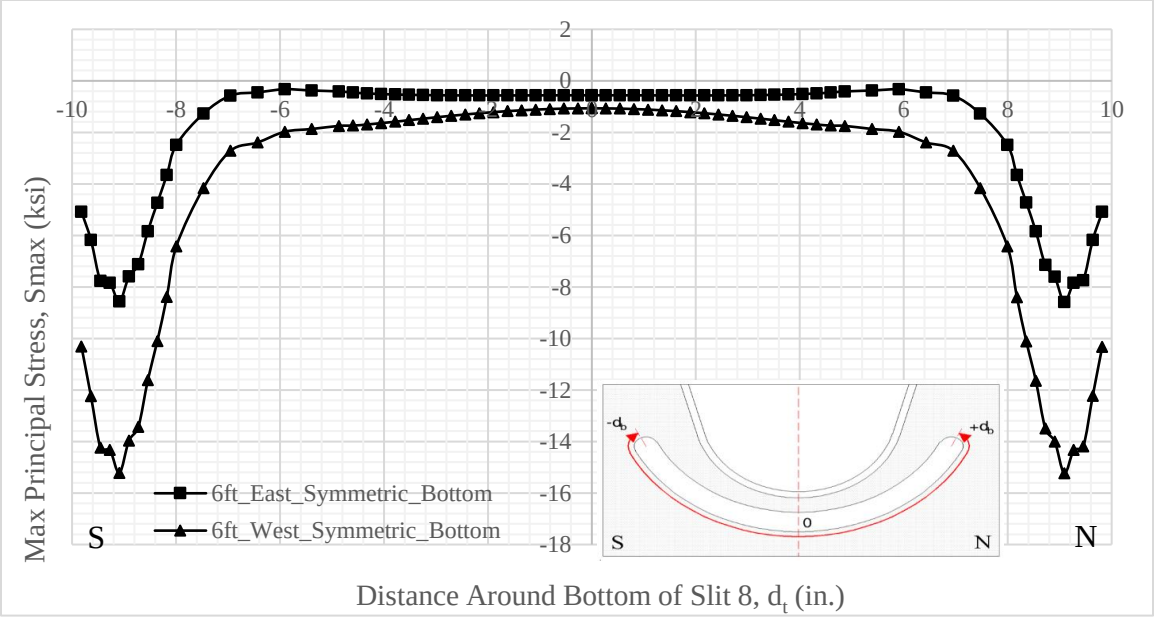

Figure 60. Graph. Variation in maximum principal stresses along bottom of slit RFB connection (Slit 8) of Rib 6 to truss-restrained floor beam (FBS3) on east and west faces of web under half tandem, symmetric out-of-plane loading (SMB).

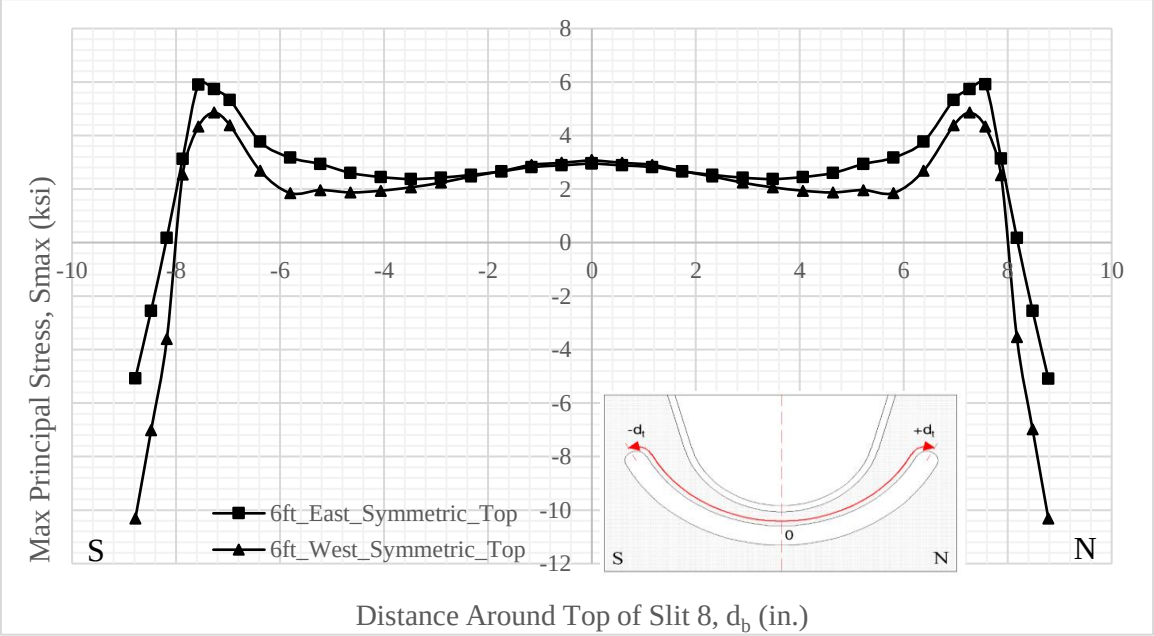

Figure 61. Graph. Variation in maximum principal stresses along top of slit RFB connection (Slit 8) of Rib 6 to truss-restrained floor beam (FBS3) on east and west faces of web under half tandem, symmetric out-of-plane loading (SMB).

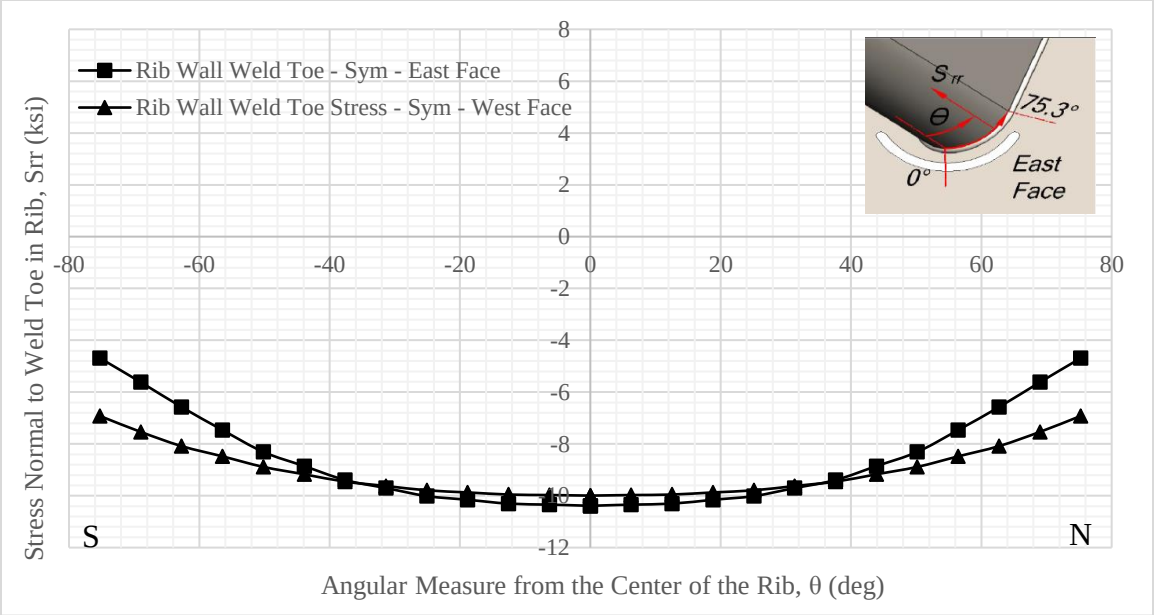

Figure 62. Graph. Variation in rib wall weld toe stress around rib bottom of slit RFB connection (Slit 8) of Rib 6 to truss-restrained floor beam (FBS3) on east and west faces of FB under half tandem, symmetric out-of-plane loading (SMB).

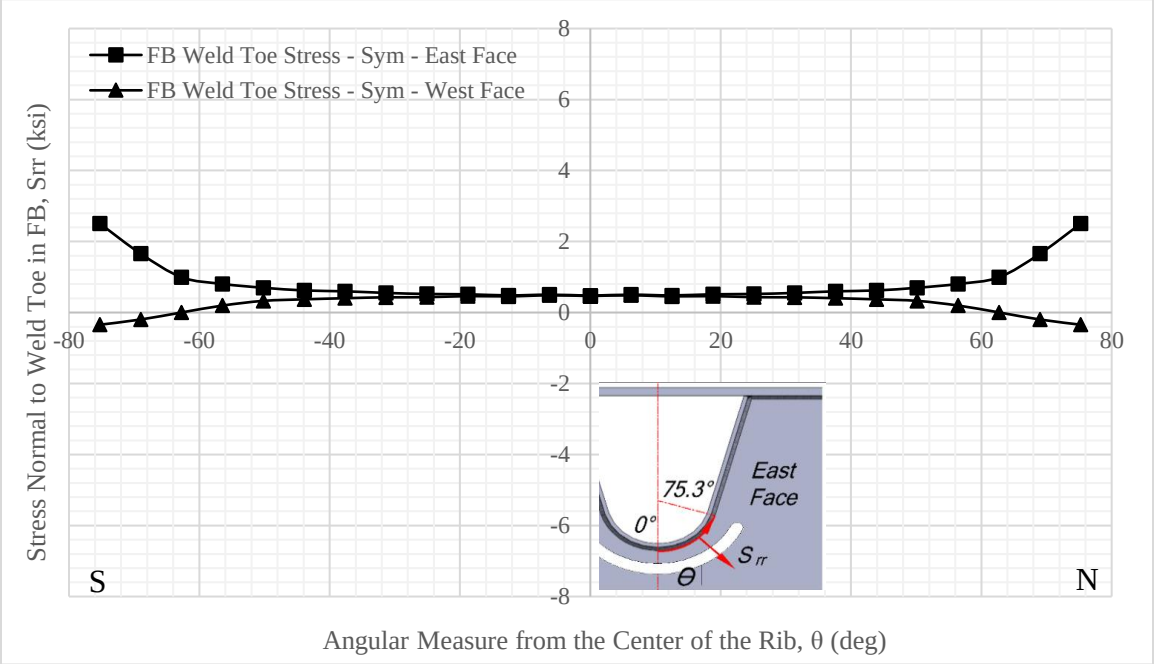

Figure 63. Graph. Variation in floor beam weld toe stress around rib bottom of slit RFB connection (Slit 8) of Rib 6 to truss-restrained floor beam (FBS3) on east and west faces of web under half tandem, symmetric out-of-plane loading (SMB).

When the half tandem is located 6 feet west of Floor Beam 3 and the transverse load position is eccentric on Rib 6, the stresses on the east and west faces of the floor beam web from the FEA using SMB are shown in Figure 64 and Figure 65. The stresses are below the 24 ksi CAFL of AASHTO Category A, and the 5.18 ksi difference in stresses between the east and west faces on the bottom north side of the slit from out-of-plane bending of the web plate is the largest difference at the edge of the slit. Eccentric loading introduces rib torsion and causes the stresses to increase compared to symmetric loading. The magnitudes of the stresses, however, are far below those from the in-plane loading because the shear forces in the rib walls are smaller, resulting in smaller reaction forces acting on the floor beam web, because the rear tandem axle loading is within the span between Floor Beam 3 and Floor Beam 4.

Figure 66 and Figure 67 show SMB stresses normal to the weld toes of the fillet weld of the slit RFB connection for the eccentric transverse load position on Rib 6, both on the rib wall and the floor beam web. The stresses normal to the rib wall fillet weld toe (Figure 66) are again all compression stresses, but unlike the symmetric load case, the magnitudes of these stresses are all well below the 10 ksi CAFL for AASHTO Fatigue Category C. The stresses normal to the floor beam fillet weld toe (Figure 67) are also well below the 10 ksi CAFL for AASHTO Fatigue Category C.

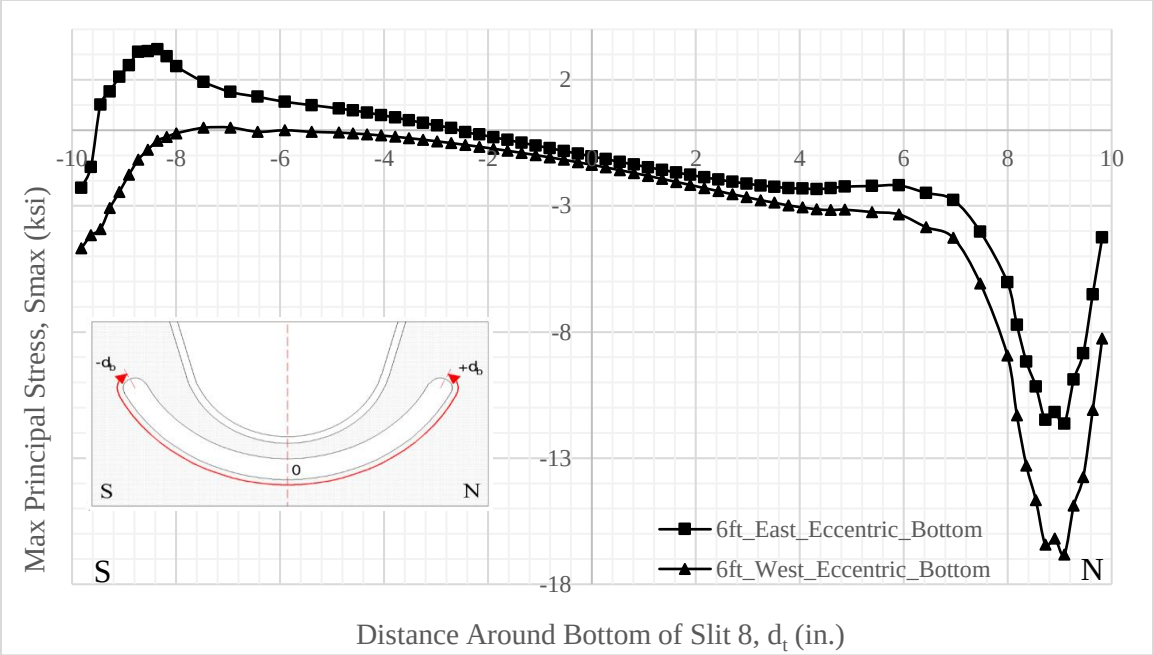

Figure 64. Graph. Variation in maximum principal stresses along bottom of slit RFB connection (Slit 8) of Rib 6 to truss-restrained floor beam (FBS3) on east and west faces of web under half tandem, eccentric out-of-plane loading (SMB).

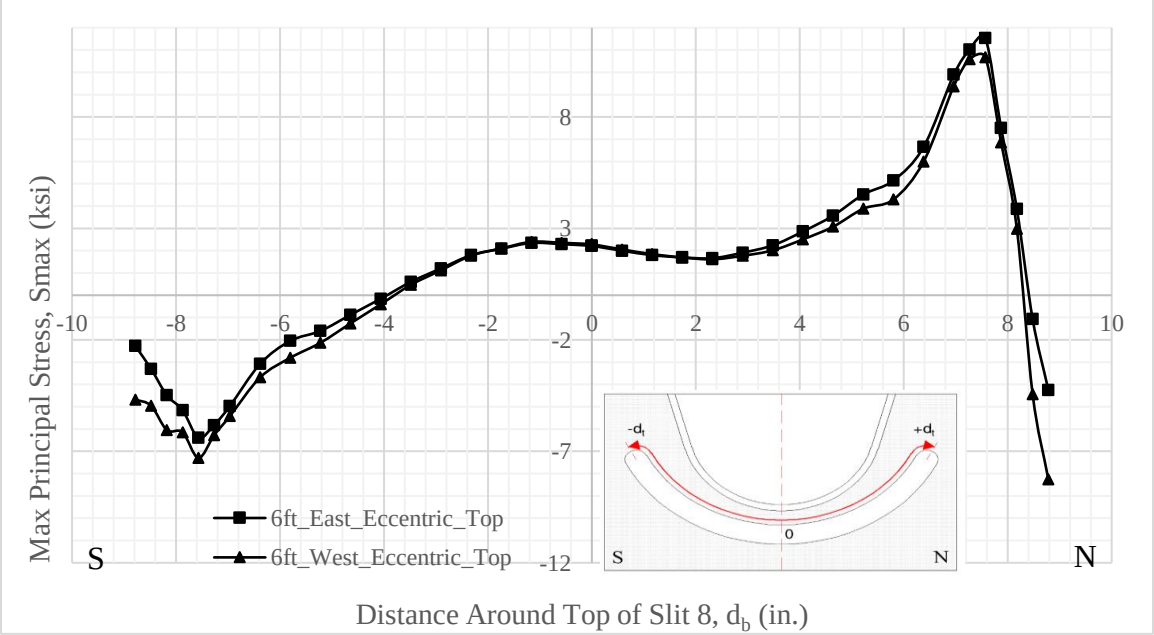

Figure 65. Graph. Variation in maximum principal stresses along top of slit RFB connection (Slit 8) of Rib 6 to truss-restrained floor beam (FBS3) on east and west faces of web under half tandem, eccentric out-of-plane loading (SMB).

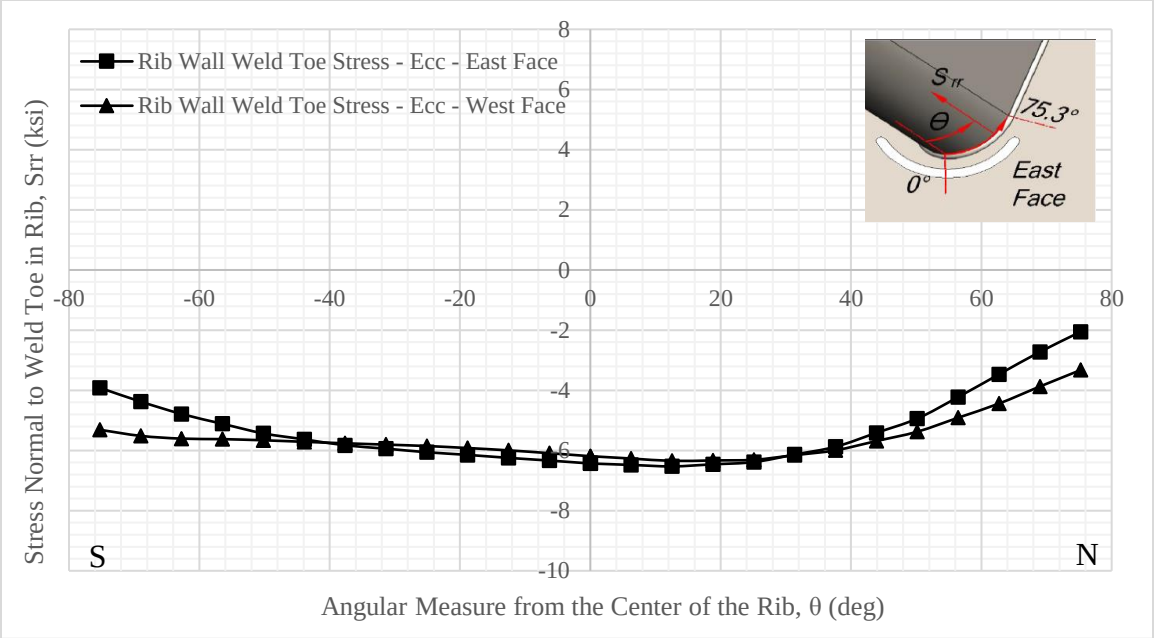

Figure 66. Graph. Variation in rib wall weld toe stress around rib bottom of slit RFB connection (Slit 8) of Rib 6 to truss-restrained floor beam (FBS3) on east and west faces of FB under half tandem, eccentric out-of-plane loading (SMB).

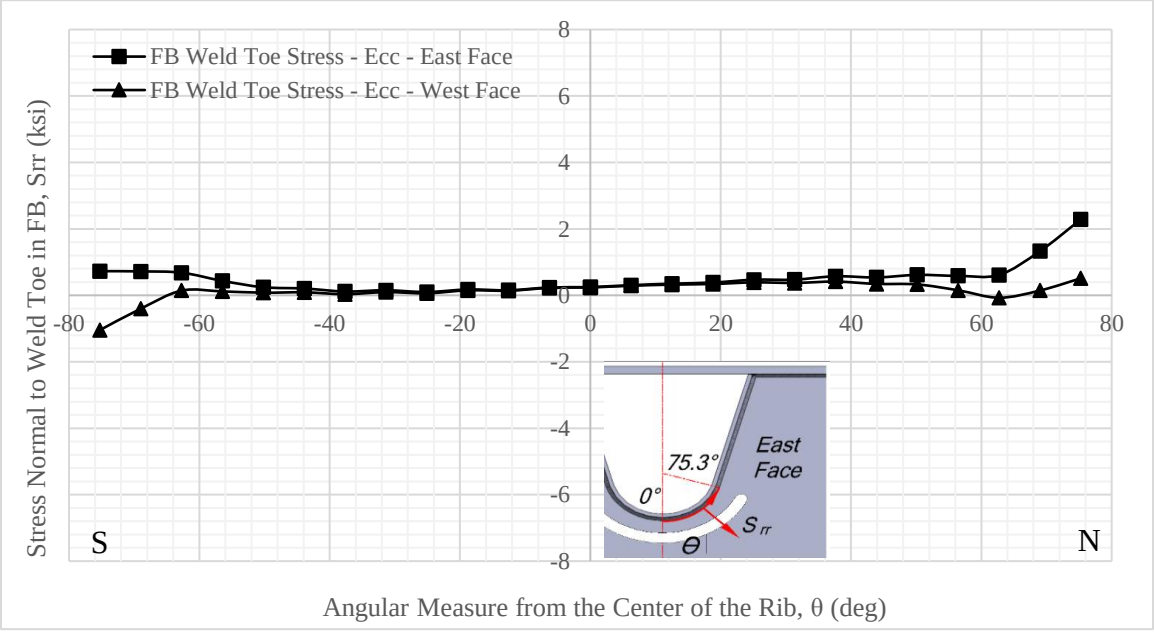

Figure 67. Graph. Variation in floor beam weld toe stress around rib bottom of slit RFB connection (Slit 8) of Rib 6 to truss-restrained floor beam (FBS3) on east and west faces of web under half tandem, eccentric out-of-plane loading (SMB).

4. SUMMARY, CONCLUSIONS, AND RECOMMENDATIONS

4.1 Summary

This study investigated a new type of rib-to-floor beam (RFB) connection for steel orthotropic bridge decks (SOBDs). In particular, the potential fatigue performance of the slit RFB connection as well as the potential for automated fabrication was studied. It was found that the slit RFB connection shows promise for both automated fabrication and good fatigue performance when it is used within a supported/restrained floor beam.

The slit RFB connection that was studied uses fillet welds for the entire connection which require no labor intensive joint preparation. Since the slit is located entirely within the floor beam web, the RFB fillet weld is uninterrupted around the bottom of the rib and can be made robotically while the SOBD panel is in the inverted position. Completing the RFB connection fillet weld in the inverted position eliminates the need to rotate the panel during fabrication, since the rib-to-deck plate (RDP) welds are made first with the SOBD panel in the inverted position. Good fit-up between the assembled rib-deck panel and the floor beam web is necessary for the robotic welding of the RFB connection. This fit-up can be achieved by using automated measuring techniques to measure the as fabricated profile of the assembled rib-deck panel followed by automated cutting of the floor beam web to match the measured rib-deck profile. The slit can be cut into the floor beam web at the same time. The slit RFB connection has no internal bulkheads or stiffeners within the rib, further increasing the manufacturability of the connection.

A finite element analysis parameter study was performed to evaluate the stress response and fatigue performance of several different variations on the slit RFB connection

considering various fatigue loading scenarios and two floor beam restraint conditions: independent floor beams and restrained/supported floor beams. Loading scenarios that introduced either dominant in-plane or dominant out-of-plane responses were studied using the rear tandem axle of the AASHTO fatigue truck (AASHTO 2016).

The stress response of the slit RFB connection is highly dependent on the magnitude of in-plane shear force carried by the floor beam. When the slit RFB connection was studied with an independent floor beam (which has no vertical support or horizontal restraint) large tension stresses developed along the edge of the slit when the in-plane shear force in the floor beam was large. These stresses developed in locations of high shear force in the floor beam web, such as adjacent to the edge plate girders of the bridge that was studied. The large tension stresses developed because the shear flow through the floor beam is interrupted by the slit. These stresses can be lowered slightly by changing the slit geometry or increasing the floor beam depth or floor beam thickness; however, a relatively deep floor beam would be needed to ensure good fatigue performance. For this reason, the slit RFB connection may not exhibit good fatigue performance if used with an independent floor beam.

When the floor beam is restrained/supported by a transverse structural member from the bridge superstructure such as a truss, the shear force carried by the floor beam web is significantly reduced, which reduces the large tension stresses that develop at the slit edge in areas near the edge plate girders. Instead, tension and compression stresses develop at the edge of the slit due to local in-plane deformation of the slit from reaction forces on the floor beam web that develop from shear forces in the rib walls, since the floor

beam provides vertical support to the ribs. Even with a shallow floor beam, the tension stresses that develop at the edge are below the AASHTO Category A CAFL. The largest magnitude stresses are compression stresses, which are expected to contribute to fatigue damage only if tension stresses develop at the same location under a different fatigue loading condition. Since the residual stress pattern at the slit edge from plasma-cutting the slit into the floor beam web is unknown, and the full range of fatigue loading stresses that may occur at the slit edge may include tension stresses, the large compression stresses could be important to fatigue performance. The stresses that develop at the fillet weld toe on the floor beam web and the fillet weld toe on the rib wall are low.

The stresses which develop due to in-plane response of the RFB connection are the dominant stress response. The slit in the floor beam web allows the rib to rotate with relative freedom as the rib deflects vertically when the tandem axle loads pass over the floor beam and into the adjacent rib span between floor beams. As a result, the stresses at the RFB connection caused by out-of-plane deformation of the floor beam web are relatively small. In-plane floor beam shear and in-plane deformation of the slit due to reaction forces from shear in the rib are the main causes of stress at the slit edge, even when the loading is out-of-plane.

4.2 Conclusions

The conclusions of this study of the slit RFB connection for SOBDs and its potential fatigue performance are:

(1) The slit RFB connection appears to be amenable to automated fabrication.

(2) For an independent floor beam (which has no vertical support within its span by a transverse structural member of the bridge superstructure), the stress response of the slit RFB connection is highly dependent on the magnitude of the in-plane shear force carried by the floor beam; large tension stresses may develop along the slit edge, and the fatigue performance may not be acceptable.

(3) When the floor beam is supported by a transverse structural member of the bridge superstructure, the stress response of the slit RFB connection is dominated by reaction forces on the floor beam web from shear forces in the rib walls; the resulting stresses along the slit edge are compressive, and are not excessive, and good fatigue performance is anticipated.

(4) The slit in the floor beam web allows the rib to rotate with relative freedom, resulting in small stresses in the slit RFB connection from out-of-plane deformation of the floor beam web; stresses at the fillet weld toes are relatively small.

(5) The slit RFB connection has the potential for good fatigue performance when used in deck replacement projects, when the floor beam is restrained/supported by existing transverse structural members of the bridge superstructure.

4.3 Recommendations for Future Work

This study investigated the stress response and fatigue performance of the slit RFB connection under various fatigue loading scenarios and connection configurations. Critical stress locations were determined to occur around the edge of the slit, away from the fillet weld toes. The critical stresses were primarily compression stresses which are considered to contribute to fatigue damage if tension stresses develop at these locations under different fatigue loading conditions. However, locations which remain in compression under all fatigue loading conditions (in combination with dead load stress) are not usually considered when assessing fatigue performance (AASHTO 2016). Since the residual stress pattern at the edge from plasma-cutting the slit into the floor beam web is unknown, and the full range of stresses that may occur at the slit edge may include tension stresses, these critical compression stresses could be important to fatigue performance. Limited research exists on the fatigue resistance of plasma-cut edges, especially when the dominant stress is in compression. Further work is needed to define the fatigue resistance of the slit edge and to understand how compression stresses contribute to fatigue of the slit edge.

Various slit geometries were studied to determine how the geometry affects the stress response of the slit RFB connection. The variations in geometry were not exhaustive, and optimization of the slit geometry could be performed to improve the slit RFB connection fatigue performance.

REFERENCES

AASHTO. 2016. *AASHTO LRFD Bridge Design Specifications.* 7th Edition with 2015 and 2016 Interims, Washington, DC: American Association of State Highway and Transportation Officials.

Connor et al. 2012. *FHWA Manual for Design, Construction, and Maintenance of Orthotropic Steel Deck Bridges.* Washington, D.C.: US Department of Transportation Federal Highway Administration.

Connor, R., and J. Fisher. 2006. "Consistent Approach to Calculating Stresses for Fatigue Design of Welded Rib-to-Web Connections in Steel Orthotropic Bridge Decks." *Journal of Bridge Engineering* (ASCE) 517-525.

Dassault Systemes Simulia Corp. 2016. *ABAQUS/Standard Documentation, Version 16.* Providence, RI: Dassault Systemes, Inc.

Fisher, J. W., and S Roy. 2010. "Fatigue of Steel Bridge Infrastructure." *Structure and Infrastructure Engineering* 7 (7-8): 457-475.

HNTB. 2015. *Cost-Effective Orthotropic Bridge Decks (An Evaluation of Optional Welding Processes).* New York: HNTB Corporation.

IIW. 2007. *Recommendations for Fatigue Design of Welded Joints and Components.* Paris, France: International Institute of Welding.

Kitner, Katelyn. 2016. *A Study of Manufacturable Rib-to-Floor Beam Connections in Steel Orthotropic Bridge Decks.* MS Thesis, Lehigh University, Bethlehem, PA.

Marks, J., J. Saunders, Y. Chen, R. Sause, and I. Hodgson. 2018. *Fatigue Resistant Rib-to-floor Beam Connections for Steel Orthotropic Bridge Decks with Potential for*

Automated Fabrication. ATLSS Report No. 18-01, Bethlehem, PA: ATLSS Engineering Research Center, Lehigh University.

Mukherjee, Soham. 2016. *Laboratory Fatigue Evaluation of a Full Scale Steel Orthotropic Bridge Deck with Round Bottom Ribs and Fitted Floor Beams.* MS Thesis, Lehigh University, Bethlehem, PA.

AUTHOR BIOGRAPHY

Jayne Ann Marks, the daughter of Mary Marks and the late Alfred Marks, was born on October 20th, 1994 in Pittsburgh, PA. Jayne received her Bachelors of Science degree in Civil Engineering from the University of Pittsburgh in April 2016. Jayne joined the ATLSS Engineering Research Center at Lehigh University as a Graduate Research Assistant in July 2016 where she worked on a number of projects. Jayne began graduate studies in the Department of Civil and Environmental Engineering at Lehigh University in Bethlehem, PA in September 2016. She will receive her Master of Science in Structural Engineering from Lehigh University in May 2018.